MOLECULAR MECHANISMS OF CELLULAR RESPONSE TO PARTICULATE FORM OF THE BIOMATERIAL COBALT CHROMIUM ALLOY: AN INVESTIGATIVE STUDY USING *IN VIVO* AND *IN VITRO* MODELS

Bernadette K. Madathil

PhD THESIS – April 2007

SREE CHITRA TIRUNAL INSTITUTE FOR
MEDICAL SCIENCES AND TECHNOLOGY
THIRUVANANTHAPURAM – 695 011

MOLECULAR MECHANISMS OF CELLULAR RESPONSE TO PARTICULATE FORM OF THE BIOMATERIAL COBALT CHROMIUM ALLOY: AN INVESTIGATIVE STUDY USING *IN VIVO* AND *IN VITRO* MODELS

A THESIS PRESENTED

BY

BERNADETTE K. MADATHIL

TO

THE DIVISION OF IMPLANT BIOLOGY

IN PARTIAL FULFILLMENT OF THE REQUIREMENTS

FOR THE DEGREE OF

DOCTOR OF PHILOSOPHY

SREE CHITRA TIRUNAL INSTITUTE FOR
MEDICAL SCIENCES AND TECHNOLOGY
THIRUVANANTHAPURAM – 695 011

The thesis

titled

MOLECULAR MECHANISMS OF CELLULAR RESPONSE TO PARTICULATE FORM OF THE BIOMATERIAL COBALT CHROMIUM ALLOY: AN INVESTIGATIVE STUDY USING IN VIVO AND IN VITRO MODELS

Submitted by

Bernadette K.Madathil

for

The Doctor of Philosophy

of

Sree Chitra Tirunal Institute
For Medical Sciences and Technology
Thiruvananthapuram – 695 011

Evaluated and approved

By

Mira Mohanty 12.4.08

Name of the Guide

(Mira Mohanty)

B. Murali Manohar 12.4.8

Name of Thesis Examiner

(B. MURALI MANOHAR)

DECLARATION

I, Bernadette K. Madathil, hereby declare that I had personally carried out the work depicted in the thesis entitled **"Molecular mechanisms of cellular response to particulate form of the biomaterial cobalt chromium alloy: An investigative study using *in vivo* and *in vitro* models"** under the direct supervision of Dr. Mira Mohanty, Scientist G, Division of Implant Biology, Biomedical Technology Wing, Sree Chitra Tirunal Institute for Medical Sciences and Technology, Thiruvananthapuram, Kerala, India, except where external help sought and acknowledged.

Bernadette K. Madathil

Dr. Mira Mohanty
Scientist G

Histopathology Laboratory
Division of Implant Biology
Biomedical Technology Wing
Sree Chitra Tirunal Institute for Medical Sciences & Technology
Poojappura, Thiruvananthapuram, Kerala

CERTIFICATE

This is to certify that Ms. Bernadette K. Madathil, in the Division of Implant Biology of this institute, has fulfilled the requirements of the regulations relating to the nature and prescribed period of research for the PhD degree of the Sree Chitra Tirunal Institute for Medical Sciences and Technology, Thiruvananthapuram. The work relating to her thesis entitled **"MOLECULAR MECHANISMS OF CELLULAR RESPONSE TO PARTICULATE FORM OF THE BIOMATERIAL COBALT CHROMIUM ALLOY: AN INVESTIGATIVE STUDY USING *IN VIVO* AND *IN VITRO* MODELS"** was carried out under my direct supervision.

Mira Mohanty.

Dr. Mira Mohanty

If HE has brought you to it .....

.....HE will get you through it

CONTENTS

Acknowledgements i

List of figures ii

List of tables v

Abbreviations vi

Synopsis viii

Chapter 1 Introduction 1

1.1. Architecture of the Articulatio Coxæ 1

1.2. Diseases of the Joint 2

1.3. The Artificial Hip Prosthesis 2

1.4. Host Response to the Hip Prosthesis 4

1.5. Asceptic Loosening- Primary reason for failure of the Hip prosthesis 7

Chapter 2 Review of Literature 9

2.1. WEAR DEBRI 9

2.1.1. Source and morphology of particulate debri 9

2.2. BIOLOGICAL RESPONSE TO WEAR DEBRI 11

2.2.1. Local effects 12

2.2.1.1. Cells 12

2.2.1.2. The Cytokine Web 17

2.2.1.3. NF-κB Signaling pathway 21

2.2.1.4. Reactive oxygen species (ROS) in asceptic loosening 23

2.2.1.5. Necrosis and Apoptosis 24

2.2.1.6. Proteomics in relation to biomaterials 25

2.2.2. Systemic effects 27

2.3. PHARMACOLOGICAL MODULATION OF DEBRI INDUCED OSTEOLYSIS. 28

2.4. AIMS & OBJECTIVES OF THE WORK 30

Chapter 3 Materials and Methods **32**

3.1. Material Particles 32

3.2. Characterization of size and shape of material particles by SEM, TEM and LM. 32

3.3. Endotoxin test 33

3.4. *In vivo* experiments 33

3.4.1. Implantation and retrieval of CoCr alloy particles. 33

3.4.2. Histopathological Analysis 34

3.4.2.1. Sample Processing 34

3.4.2.2. Embedding 34

3.4.2.3. Sectioning 35

3.4.2.4. Staining 35

3.4.2.5. Light microscopy 36

3.4.3. Immunohistochemical Analysis 36

3.4.4. Transmission Electron Microscopic analysis 38

3.4.4.1. Sample Processing 38

3.4.4.2. Staining for Light Microscopy (LM) 40

3.4.4.3. Staining for TEM 40

3.5. *In vitro* Studies 41

3.5.1. Cytoskeletal rearrangments and cytokine profile in L929 fibroblasts cultured with CoCr alloy particles. 41

3.5.1.1. Cell lines and culture conditions 41

3.5.1.2. Phase contrast and Scanning electron microscopy studies 41

3.5.1.3. Cytoskeletal rearrangements in L929 fibroblasts grown with CoCr particles 42

3.5.1.4. Expression profile the cytokines IL-6 and IL-1α 43

3.5.2. Proteomic profile of human fibroblasts cultured with Cobalt Chromium alloy particles and effect of the conditioned media on human monocyte cultures. 44

3.5.2.1. Cell lines and culture conditions 44

3.5.2.2. Particle preparation for culture with Fibroblast 44

3.5.2.3. Fibroblast viability response to CoCr particles 44

3.5.2.4. Study design and proteomic analysis of fibroblast cultured with CoCr particles 45

3.5.2.5. Effect of conditioned media on monocyte U-937 45

3.5.2.6. Protein Extraction 46

3.5.2.7. 2D gel electrophoresis (2DGE) 46

3.5.2.8. Computer Assisted Image analysis of 2D Gels 48

3.5.2.9. Spot excision and In-gel proteolytic digestion 48

3.5.2.10. Protein identification via MALDI TOF TOF MS and data base searching 49

Chapter 4 Results and Discussion 50

4.1. Characterization of size and shape of material particles by SEM 50

4.2. Endotoxin test 50

4.3. *In vivo* experimentation 51

4.3.1. Histological analysis by Light microscopy 51

4.3.2. Transmission Electron microscopic evaluation 53

4.3.3. Immunohistochemical analysis 55

4.4. *In vitro* experiments 79

4.4.1. Cytoskeletal rearrangements and cytokine profile in murine L929 fibroblasts cultured with CoCr alloy particles. 79

4.4.1.1. Phase contrast and scanning electron microscopic studies 79

4.4.1.2. Cytoskeletal rearrangement in L929 fibroblasts grown with CoCr alloy particles. 80

4.4.1.3. Expression profile of IL-6 and IL-1α. 81

4.4.2. Proteomic profile of human fibroblasts cultured with CoCr alloy particles and effect of the conditioned media on human monocyte cultures. 93

4.4.2.1. Effect of CoCr particles on fibroblast viability 93

4.4.2.2. Proteomic analysis of fibroblast cultured with CoCr particles 95

4.4.2.3. Proteomic analysis of monocytes cultured in 40% conditioned medium 96

4.4.2.4. PDQuest analysis 96

4.4.2.5. Protein identification by MALDI-TOF TOF MS and Mascot protein database search engine 96

Chapter 5 Summary, Conclusions & Future directives 115

5.1. Summary 115

5.2. Conclusions 118

5.3. Future directives 118

Chapter 6 BIBLIOGRAPHY 120

Chapter 7 APPENDIX 132

ACKNOWLEDGEMENTS

I would like to place on record my sincere and profound gratitude to my guide and mentor Dr. Mira Mohanty for her indelible support and guidance throughout this work.

I express my sincere thanks to my Doctoral Advisory Committee members Mr CV Muraleedharan, Dr. TV Kumary and Dr RV Omkumar for their constructive suggestions and timely advice which has brought this work to successful completion.

The Director and The Registrar, SCTIMST and The Head, BMT Wing are duly acknowledged.

I wish to acknowledge the CSIR, INDIA for funding this doctoral study. I am grateful to the Jawaharlal Nehru Memorial Fund for awarding me the JNMF Doctoral Scholarship. The scholarship was instrumental in enabling me to undertake the proteomics work in this thesis at the National University of Singapore.

I am thankful to Prof CL Hew, Head, Department of Biological Sciences, NUS for accepting me as an intern student to work at The Protein and Proteomics Center (PPC), NUS. Thanks and gratitude are due to Dr Lin Qing Song, for supervising my work and for giving me the freedom to pursue my research ideas. Heartfelt thanks to all staff and students of the PPC, especially Ms. Wu Shihui, who taught me the *in vitro* cell culture techniques and Ms. Wang Xian Hui for her technical assistance in Mass spectrometry.

Smith & Nephew, Memphis, USA are acknowledged for donating the CoCr alloy particles, which is the mainstay of this work.

I express my sincere gratitude to Dr TV Kumary for permitting me to use the facilities of the Tissue Culture Laboratory. The technical assistance and support provided by the staff and students of the TIC, Mrs. Usha Vasudev, Chitra, Tilak and Viji, is sincerely and thankfully acknowledged.

Special thanks are due to Dr. Annie John and staff of the TEM laboratory for the unwavering tenacity shown in achieving the TEM work presented in this thesis. Dr H K Verma and Mr. R Sreekumar are sincerely acknowledged for the technical assistance in SEM and Dr TV Anil Kumar for help in the confocal microscopy.

Dr PV Mohannan and the staff at the Division of Toxicology for all the *in vivo* experiments and Dr AC Fernandez and his team at the Division of Laboratory Animal Sciences for the timely provision and maintenance of the experimental animals are gratefully acknowledged.

Thanks and gratitude goes without measure to Ms. Sulekha Baby for instructing me on the techniques of histopathology and to all my colleagues at the Histopathology Laboratory.

Heartfelt thanks to all the PhD students of the campus for their fraternity and especially to my colleague and roommate Asha S Mathew. Special thanks are due to my senior colleague Anil Kumar PR for his timely advice, suggestions and computer expertise.

Last but most importantly to family and friends, for always being the bridge over troubled waters.

Bernadette K Madathil

LIST OF FIGURES

Figure 1 : A is the Cross sectional view of the hip-joint and B is the posterior view of the hip joint. (Williams PL *et al*, 1989) 2

Figure 2: Schematic representation of the Total Hip prosthesis 4

Figure 3: Light photmicrograph (A), Transmission electron micrograph (B) and Scanning Electron Micrograph (C) of the CoCr alloy particles 50

Figure 4: Light micrographs of H&E stained sections of 1day (A, B); 3 days (C, D) and 5 days (E, F) muscle with CoCr alloy particles. 58

Figure 5: Light micrographs of H&E stained sections of 7days (A, B); 10 days (C); 15 days (D,E) and 20 days (F) muscle with CoCr alloy particles. 59

Figure 6: Light micrographs of H&E stained sections of 30 days (A, B, C); 45 days (D) and 60 days (E, F) muscle with CoCr alloy particles. 60

Figure 7: Light micrographs of H&E stained sections of 75 days (A); 90 days (B); 120 days (C, D) and 150 days (E, F) muscle with CoCr alloy particles. 61

Figure 8: Light micrographs of toluidine blue stained sections of 5 days (A) muscle with CoCr alloy particles. Transmission electron micrographs showing ultrastructural details of tissue response around CoCr alloy particles (B, C, D, E, F) at 5 days. X ray diffraction pattern of the CoCr alloy particles in tissue (G). 62

Figure 9: Light micrographs of toluidine blue stained sections of 45 days (A, B) muscle with CoCr alloy particles. Transmission electron micrographs showing ultrastructural details of tissue response around CoCr alloy particles (C, D, E, F) at 45 days. 63

Figure 10: Light micrographs of toluidine blue stained sections of 90 days (A, B) muscle with CoCr alloy particles. Transmission electron micrographs showing ultrastructural details of tissue response around CoCr alloy particles (C, D, E, F) at 90 days. 64

Figure 11: Light micrographs of toluidine blue stained sections of 120 days (A, B) muscle with CoCr alloy particles. Transmission electron micrographs showing ultrastructural details of tissue response around CoCr alloy particles (C, D, E, F) at 120 days. 65

Figure 12: Light micrographs of IHC, ED1 stained sections of 5 days (A); 45 days (B); 90 days (C); 120 days (D); 150 days (E) and negative control (F). 66

Figure 13: Light micrographs of IHC, ED2 stained sections of 5 days (A); 45 days (B); 90 days (C); 120 days (D); 150 days (E) and negative control (F). 67

Figure 14: Light micrographs of IHC, IL-1β stained sections of 5 days (A); 45 days (B); 90 days (C); 120 days (D); 150 days (E) and negative control (F). 68

Figure 15: Light micrographs of IHC, IL-1α stained sections of 5 days (A); 45 days (B); 90 days (C); 120 days (D); 150 days (E) and negative control (F). 69

Figure 16: Light micrographs of IHC, IL-6 stained sections of 5 days (A); 45 days (B); 90 days (C); 120 days (D); 150 days (E) and negative control (F). 70

Figure 17: Light micrographs of IHC, TNF-α stained sections of 5 days (A); 45 days (B); 90 days (C); 120 days (D); 150 days (E) and negative control (F). 71

Figure 18: Light micrographs of IHC, smooth muscle-actin, stained sections of 5 days (A); 45 days (B); 90 days (C); 120 days (D); 150 days (E) and negative control (F). 72

Figure 19: Light micrographs of IHC, vimentin, stained sections of 5 days (A); 45 days (B); 90 days (C); 120 days (D); 150 days (E) and negative control (F). 73

Figure 20: L929 fibroblasts were cultured with CoCr particles at varying concentrations (as indicated in the graph) for 72 hours. Culture medium was harvested and analyzed for released IL-6 by ELISA. 82

Figure 21: L929 fibroblasts were cultured with CoCr particles at varying concentrations (as indicated in the graph) for 72 hours. Culture medium was harvested and analyzed for released IL-1 α by ELISA. 82

Figure 22: Phase contrast images of murine L929 fibroblasts following 72 hours culture with CoCr alloy particles at concentrations of 0.3mg/cm^2 (B), 0.5mg/cm^2 (C), 1.0mg/cm^2 (D), 5mg/cm^2 (E)and 8mg/cm^2 (F). Cultures without particles served as control (A). 83

Figure 23: Environmental Scanning Electron micrographs of murine L929 fibroblasts following 72 hours culture with CoCr alloy particles at concentrations of 0.5mg/cm2 (B, C), 1.0mg/cm2 (D, E). Cultures without particles served as control (A, B). 84

Figure 24: Confocal micrographs of control L929 fibroblasts, stained for F-actin with Phalloidin-TRITC conjugate, following 72 hours culture (A) and Z stack images of the cells (B). 85

Figure 25: Confocal micrographs of L929 fibroblasts, stained for F-actin with Phalloidin-TRITC conjugate, following 72 hours culture with 0.5mg/cm^2 of CoCr alloy particles (A) and Z stack images of the cells (B). 86

Figure 26: Confocal micrographs of L929 fibroblasts, stained for F-actin with Phalloidin-TRITC conjugate, following 72 hours culture with 1mg/cm^2 of CoCr alloy particles (A) and Z stack images of the cells (B). 87

Figure 27: Confocal micrographs of control L929 fibroblasts, stained for α-actinin, following 72 hours culture (A) and Z stack images of the cells (B). 88

Figure 28: Confocal micrographs of L929 fibroblasts, stained for α-actinin, following 72 hours culture with 0.5mg/cm^2 of CoCr alloy particles (A) and Z stack images of the cells (B). 89

Figure 29: Confocal micrographs of L929 fibroblasts, stained for α-actinin, following 72 hours culture with 1mg/cm^2 of CoCr alloy particles (A) and Z stack images of the cells (B). 90

Figure 30: MRC-5 fibroblasts were cultured with CoCr particles at varying concentrations (as indicated in the graph) for 24 hours (Series 1) and 72 hours (Series 2). Viability of MRC-5 fibroblasts was studied via MTS assay. 95

Figure 31: Light micrographs of human MRC-5 fibroblasts following 24 hours culture with CoCr alloy particles at concentrations of 0.05mg/cm^2 (B), 0.5mg/cm^2 (C), 1mg/cm^2 (D) and 5mg/cm^2 (E). Cultures without particles served as control (A). 97

Figure 32: Light micrographs of human MRC-5 fibroblasts following 72 hours culture with CoCr alloy particles at concentrations of 0.05mg/cm^2 (B), 0.5mg/cm^2 (C), 1mg/cm^2 (D) and 5mg/cm^2 (E). Cultures without particles served as control (A). 98

Figure 33: Representative analytical 2D maps of total fibroblast cellular proteins, 72 hours after culture with (A) and without (B) 0.5mg/cm^2 of CoCr particles. 100μg of proteins were loaded onto each 17cm IPG strip of pH 3-10. 99

Figure 34: Representative analytical 2D maps of total fibroblast cellular proteins, 72 hours after culture with (A) and without (B) 0.5mg/cm^2 of CoCr particles. 100μg of proteins were loaded onto each 17cm IPG strip of pH 4-7. 99

Figure 35: Gel images comparing analytical 2D maps of total monocytes cellular proteins, 48 hours after culture with (A) and without (B) 40% conditioned medium from fibroblast-CoCr cultures. 100μg of proteins were loaded onto each 17cm IPG strip of pH 4-7. 100

Figure 36: Representative 2D map of total fibroblast cellular proteins, 72 hours after culture with 0.5mg/cm^2 of CoCr particles. 100μg of proteins were loaded onto each 17cm IPG strip pH4-7. Protein spots identified by MALDI TOF TOF MS are represented on the gel image by their serial number. 100

Figure 37: Peptide Mass Fingerprint of Spot 1 102

Figure 38: Peptide Mass Fingerprint of Spot 2 104

Figure 39: Peptide Mass Fingerprint of Spot 3 106

Figure 40: Peptide Mass Fingerprint of Spot 4 108

LIST OF TABLES

Table 1: Biomaterials used in total joint replacements. (Adapted from "Biomaterials". Sujata V. Bhatt. 2002. Narosa Publishing House).....6

Table 2: Human MRC-5 fibroblast cellular proteins, identified by MALDI TOF TOF MS, which were found to have two fold increase in expression following a 72 hour culture with CoCr particles. 101

ABBREVIATIONS

2D-GE	Two Dimensional Gel Electrophoresis
CLSM	Confocal Laser Scanning Microscope
CoCr	Cobalt chromium
COX	Cyclo Oxygenase
DAB	Di Amino Benzidine
DNA	Deoxy ribo Nucleic Acid
ECM	Extra cellular Matrix
ELISA	Enzyme Linked Immunosorbent Assay
FBGC	Foreign Body Giant Cells
Fkn	Fractalkine
GM-CSF	Granulocyte Monocyte-Colony Stimulating Factor
GSSG	Oxidized glutathione
HA	Hydroxy Apatite
HDPE	High Density Polyethylene
IFN	Interferon
IL	Interleukin
IM	Interfacial Membrane
iNOS	inducible Nitric Oxide Synthase
LPS	Lipo Poly Saccharide
LTB4	Leukotriene B4
MALDI	Matrix Assisted Laser Desorption Ionisation
MCP	Macrophage Chemotactic Protein
M-CSF	Macrophage-Colony Stimulating Factor
MDA	Malon Di Aldehyde
MIP	Macrophage Inhibitory Protein
MOM	Metal on Metal

mRNA	messenger Ribo Nuclei Acid
MS	Mass Spectrometer
NF-κB	Nuclear Factor-Kappa B
PAGE	Poly Acrylamide Gel Electrophoresis
PBS	Phosphate Buffered Saline
PGE_2	Prostaglandin E_2
PMMA	Poly Methyl Meth Acrylate
PTFE	Poly Tetra Fluoro Ethylene
ROS	Reactive Oxygen Species
SDS	Sodium Dodecyl Sulphate
SEM	Scanning Electron Microscopy
TCP	Tri Calcium Phosphate
TEM	Transmission Electron Microscopy
THA	Total Hip Arthroplasty
THR	Total Hip Replacement
TiAlVa	Titanium Aluminium Vanadium
TJA	Total Joint Arthroplasty
TNF	Tumour Necrosis Factor
TOF-MS	Time Of Flight- Mass Spectrometer
UHMWPE	Ultra High Molecular Weight Polyethylene

SYNOPSIS

Human joints are prone to inflammatory and degenerative diseases. In extremes of such diseases, wherein the very function of the joint is compromised, the only alternative available is to replace the natural joint with an artificial prosthesis. The artificial joint implants are designed to emulate the shape of the natural joint. Although successful initially, asceptic loosening of the prosthesis 10-15 years post surgery continues to be the primary cause for long term failure of artificial joint replacements. Much research initiatives are being undertaken to delineate the mechanisms of asceptic loosening, so as to devise means of controlling and mitigating the same.

Chapter 1 in the thesis introduces the topic. The area of this research is focused mainly on the artificial hip prosthesis. A brief description of the normal hip joint begins the chapter, which is followed by an account of diseases that affect the human joint. In extremes of such diseases the natural joint is replaced by an artificial prosthesis, which comprises of a femoral and an acetabular component. An update of materials that are used to fabricate the artificial prosthesis and the different combinations for femoral and acetabular component available in the market has been summarized. The chapter details out the normal biological response seen around the implant and goes on to introduce the topic of asceptic loosening, the primal reason for long term failure of artificial hip replacements.

Chapter 2 reviews the scientific literature published in relation to asceptic loosening and long term failure of total hip replacements. Investigations to understand the cause of asceptic loosening were initially centered on studies of tissues surrounding clinically failed prosthesis. Such studies have revealed the presence of a chronic

inflammatory response of the host to particulate debri that emanate from the surface of the prosthesis. The chapter summarizes data published on the source and morphology of particulate debris retrieved from clinical tissue samples and those obtained from *in vitro* experiments using joint simulators. The biological responses to these debri have been detailed out under the broad classification of local effects and systemic effects. The major cell types found in the interfacial membrane around failed implants are macrophages and fibroblasts. The pathological findings around failed implants are a result of a continuous cellular response to an ongoing release of wear debri into the original fibrous capsule formed around the implant. Literature reported on results obtained from *in vivo* and *in vitro* experiments reveal that the particulate debri emanating from the implant surfaces incites an inflammatory response. The inflammatory cells and the cytokines that they produce modulate resorption of host bone adjacent to the implant. This periprosthetic osteolysis culminates in asceptic loosening and failure of the prosthesis. An account of data published on the cell types, cytokine profile and signaling pathways associated with asceptic loosening has been detailed in this chapter. Data published on the systemic effect of metal ions that leach out from the wear particles, have also been reviewed. Elevated levels of metal ions have been reported in serum and urine of patients with hip replacements. The migration of particulate debri to lymph nodes, liver and spleen have also been reported. The current pharmacological strategies adopted to mitigate periprosthetic bone loss that leads to asceptic loosening are also included. However, to date the exact pathomechanisms of wear debri induced inflammation leading to periprosthetic osteolysis is still not delineated. In the present study we aim to study the cellular response to particulate materials of the orthopedic biomaterial CoCr alloy (ASTM-

F75) in soft tissue using an *in vivo* model and elucidate the molecular changes in specific cell types in response to these particles using *in vitro* models.

Chapter 3 details out the materials used and methodology adopted in this study. The methodology has been broadly categorized under three main subheadings: - (i) Characterization of the CoCr alloy particles (ii) *In vivo* experiments and (iii) *In vitro* experiments.

Particulate form of CoCr alloy obtained from a commercial source was characterized for size and surface morphology by SEM, TEM and Light microscopy.

In vivo responses to CoCr alloy particles were evaluated using a rat animal model. CoCr alloy particles were injected into the gluteus muscle of rats using 0.9% sterile saline as carrier. 0.9% saline alone served as control. The tissue response to CoCr alloy particles over fourteen different time periods, ranging from one to 150 days, have been evaluated using the techniques of histology, light microscopy and transmission electron microscopy (TEM). Cellular and cytokine profile have also been examined via immunohistochemistry (IHC).

The fibroblasts were chosen as the specific cell type for study of cell-particle interaction. *In vitro* experiments to study cytoskeletal reorganization and cytokine production in murine L929 fibroblast cultured with CoCr alloy particles were also carried out. L929 fibroblasts were grown with varying concentrations of CoCr alloy particles and morphological changes characterized via phase contrast microscopy and SEM. Cytoskeletal reorganization of F-actin filaments, and focal adhesion rearrangements of α actinin molecules, of the fibroblasts in association with CoCr alloy particles were examined by immunofluorescence labeling and observed via confocal laser scanning microscopy. Expression profile of the proinflammatory cytokines IL-1α

and IL-6 secreted by the fibroblasts into the culture medium was analyzed by commercially available ELIZA kits.

In the present study, a proteomic approach to elucidate the initial signals that are expressed to particulate material, using an *in vitro* cell culture system, has also been adopted. Human fibroblasts cell line MRC-5 was cultured with CoCr alloy particles, at varying concentrations. Morphology of these cells were examined after 24 and 72 hours via light microscopy. Viability of these cells were assayed after 24 and 72 hours via MTS assay. MRC-5 fibroblasts were cultured with CoCr alloy particles at a non toxic concentration, for 72 hours and changes in total cellular proteins were analyzed using Two dimensional polyacrylamide gel electrophoresis (2-DGE) in conjunction with mass spectrometry (MS), which is the technique currently most used for studying expression levels of cellular proteins. The effect of conditioned medium from these fibroblast-CoCr cultures on protein expression profile of human monocytes U-937 have also been studied using the 2DGE and MS.

Chapter 4 presents the results obtained from the experiments conducted and reviews and discusses these results vis-à-vis scientific data already published. SEM, TEM and Light microscopical examination revealed the CoCr alloy particles to be of a spherical shape with a smooth surface morphology. The metal particles were found to be in the size range of 1-7μm.

Histopathological examination of tissue sections obtained from *in vivo* experiments reveals the persistence of a chronic inflammatory response to the CoCr particles, with time. This inflammatory response is characterised by the presence of macrophages, fibroblasts and numerous new blood vessels. A characteristic difference in host response to the CoCr particles implanted within the muscle fibres and within

the endomysium was noted. In muscle fibres inflammatory response to the CoCr particles was mild but persistent even at longer time periods. In endomysium the inflammatory response was more pronounced. With time excessive fibrosis with scant macrophages and presence of numerous new blood vessels was noted. At longer time periods clumping of particles within the fibrous tissue was observed. The difference in response could be attributed to the difference in cellular constitution, with the endomysium having more of fibroblasts and connective tissue. These results were also substantiated in the IHC and TEM micrographs. Immunohistochemical analyses showed a positive staining for cytokine IL-6, TNF-α and IL-1α at early time periods. IL-1β was not detected at any time period. Macrophage markers ED1 and ED2 for newly recruited and resident cells were stained positive at early time periods. Cells that stained positive for macrophage markers were also positive for the cytokines, suggesting that it is the macrophages in early time periods that are responsible for the secretion of proinflammatory cytokines.

Interactions of CoCr particles with fibroblasts cells were studied using an *in vitro* model of murine L929 fibroblasts. Phase contrast microscopy had revealed the CoCr alloy particles to be toxic at higher concentrations. At low concentrations the morphology of the fibroblasts were similar to that of control. It was observed that the CoCr particles tend to cluster and adhere to the fibroblast cells. This was substantiated in the SEM micrographs which showed the metal particles to align along the cellular margins of the fibroblasts. Confocal laser scanning microscopy had also revealed a characteristic difference in F-actin and α actinin arrangements along areas of cellular association with the CoCr alloy particles. ELISA analyses did not show a significant change in expression of IL-1α and IL-6 between the control and test cultures.

Downstream proteomic analysis of total cellular proteins of MRC-5 fibroblasts cultured with CoCr alloy particles revealed thirteen protein spots that showed greater than two fold increase. Four of these proteins were identified by tandem mass spectrometry. These were Annexin II, Pyruvate kinase, Triose phosphate isomerase and N-myc downstream regulated gene 1 protein. Cobalt is a hypoxia mimicking agent and N-myc downstream regulated gene 1 protein, Triose phosphate isomerase, Pyruvate kinase and Annexin II are important hypoxia regulated gene products that are found to be over expressed in cellular oxidative stress response. Our data indicates that exposure of fibroblast to CoCr induces the transition of these cells into a state of hypoxia and oxidative stress even in normoxic culture conditions. The study reflects the possibility of a hypoxic environment in the periprosthetic tissue surrounding metallic implants. The conditioned media from the fibroblast-CoCr cultures however did not effect an increase in the expression of intracellular proteins of the U937monocytes, which indicate that the activation of monocytes might not be directly influenced by the fibroblasts and suggest the requirement of other chemokines like M-CSF or other cell types probably endothelial cells.

Chapter 5 summarizes the salient findings in this work and concludes the thesis. Data obtained from the *in vivo* studies, show with time the presence of an excessive fibrotic response to cobalt chromium alloy particles in the endomysium and a mild but persistent chronic inflammatory response in muscle fibre. The endomysium comprises of fibroblasts and connective tissue. It would in its cellular constituents mimic the interfacial membrane around implants and hence reflect the initial sequence of response once material particles are released into the biological milieu. *In vitro* interactions of murine and human fibroblasts with the CoCr alloy particles indicate a toxic nature of the metal particles with increase in concentration. A close association

between the cellular membrane and particles which required a rearrangement of F-actin and α-actinin moieties was observed. Data obtained from this study also strongly reflect the transition of fibroblasts to a state of hypoxia even at low concentrations of metal particles and suggest the possibility of a hypoxic environment in the periprosthetic tissue. Hypoxia is a known potent inducer of fibrogenesis and angiogenesis and could be responsible for the excessive fibrosis seen at later time periods in our *in vivo* studies. The chapter concludes with a brief note on future prospects in relation to this work. The insights revealed through this work highlight the importance of studying the role of fibroblasts in asceptic loosening. More in-depth studies regarding the role of hypoxic fibroblasts in the induction and promotion of osteoclastogenesis need to be addressed. The role of endothelial cells in the downstream activation of fibroblasts and macrophages in relation to material particle induced inflammation also needs to be extensively probed.

The generation of osteolysis and implant loosening is complex and involves many proteins and cell types. Identifying the key regulatory signals that are expressed to particulate material would help in devising biological means of controlling and ameliorating the inflammatory response to particulate material. This work draws significance in view of the recent comeback of metal on metal total hip replacements into the orthopaedic market.

Chapter 1

INTRODUCTION

1.1. ARCHITECTURE OF THE ARTICULATIO COXÆ

The Coxal articulation or the hip joint is a ball and socket type of synovial joint, formed by the reception of the head of the femur into the cup-shaped cavity of the acetabulum (Figure 1). The articular cartilage covers the head of the femur and is thicker at the center than at the circumference. The cartilage on the acetabulum forms an incomplete marginal ring, the lunate surface. Within the lunate surface there is a circular depression devoid of cartilage, occupied in the fresh state by a mass of fat and is covered by the synovial membrane (Williams PL *et al*, 1989). The joint is completely enclosed by the capsular ligament which holds the joint together and helps to contain the synovial fluid. The capsular ligament is also lined with a synovial membrane. This membrane secretes the synovial fluid into the synovial cavity. The synovial fluid helps lubricate the joint and provides nourishment to the articular cartilage.

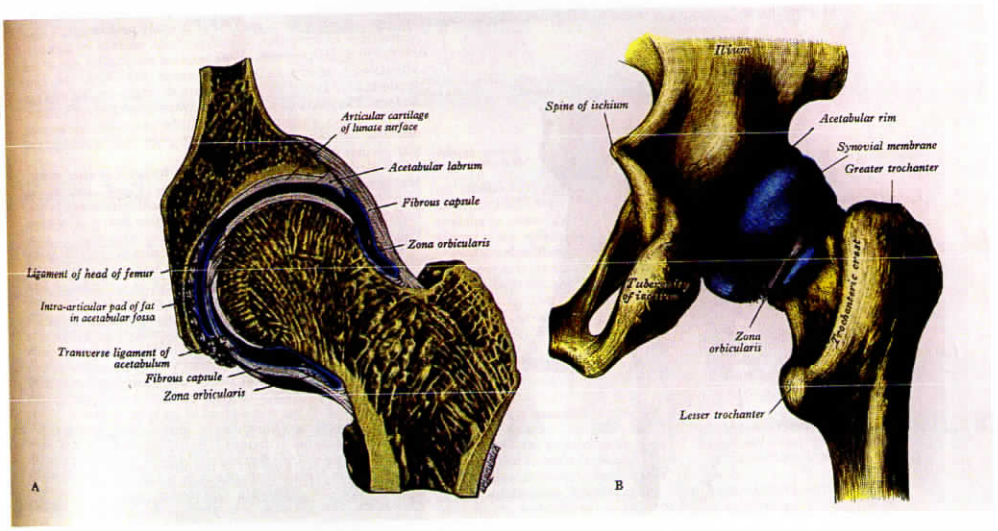

Figure 1 : A is the Cross sectional view of the hip-joint and B is the posterior view of the hip joint. (Williams PL *et al*, 1989)

1.2. DISEASES OF THE JOINT

Human joints are prone to inflammatory and degenerative diseases. Joints vary in structure and function and also in their predisposition to diseases. The most common diseases that affect the hip joint are osteoarthritis, rheumatoid arthritis, infective arthritis, metabolic arthritis, avascular necrosis and bone tumours. In extremes of such diseases, wherein the very function of the joint is compromised, the only alternative available to alleviate pain and make the patient ambulant is to replace the natural joint with an artificial prosthesis. If the surgical procedure is a "hemi-arthroplasty" then the acetabulum is left intact and the femoral head is replaced with an artificial prosthesis. In cases where both the femoral head and the acetabulum have been severely affected, a total hip arthroplasty is performed.

1.3. THE ARTIFICIAL HIP PROSTHESIS

Artificial hip implants are designed to emulate the shape of the natural joint and comprise of a femoral component that is made to articulate against an acetabular component (Figure 2). The femoral components are mainly comprised from metals

like Co-Cr alloy, TiAlVaa alloy or ceramics like alumina while the acetabular components are made from polymers mainly UHMWPE or metals like Co-Cr alloy, TiAlVaa alloy (Table 1). Materials that are intended to interface with the biological systems to evaluate, treat, augment or replace any tissue, organ or function of the body are termed as 'Biomaterials'.

A prerequisite for orthopedic biomaterials is an ability to withstand cyclic load bearing applications, for which material properties of high strength, ductility, fracture toughness, hardness, corrosion resistance and biocompatibility are desirable. Fixation of the prosthesis into the host bone is mediated via cement or press fit. PMMA is the cement routinely used for fixation and combinations of a cementless acetabular component with a cemented femoral component are frequently used. With press fit implants, the implant is fitted compactly into the bone. Press fit implants may have special porous surface coatings. Surface coating of the femoral stem with irregular particles, etchings and beads of ceramic, metal, polymer or a combination of these allows for bone ingrowth into the pores enabling bonding of the implant to bony tissue.

Charnley's introduction of Ultra high olecular weight polyethylene (UHMWPE) as the acetabular component of the total joint replacement, in the early 1960's had revolutionized the field of arthroplasty and introduced the concept of low-frictional arthroplasy. While metal on polyethylene hip prosthesis still form a large part of the TJA market, failure of these prosthesis, due to elevated volumetric wear rate of the polyethylene components have been reported. To reduce wear and particle generation, the last decade has seen the introduction of second generation metal on metal (MOM) prostheses. These prosthesis are made from different Cobalt Chromium alloys. The design and material properties of these prosthesis differ from first

generation MOM prosthesis in many parameters like modularity, alloy type, ball diameter, diametrical clearance, contact areas, surface finish etc... (Anissian HL *et al*; 2001)

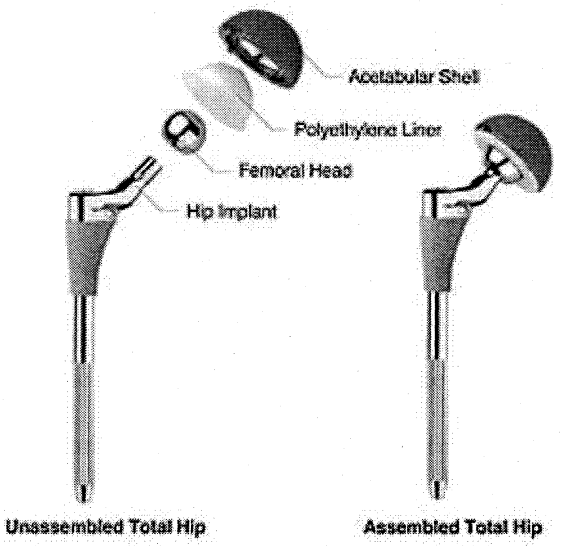

Figure 2: Schematic representation of the Total Hip prosthesis

1.4. HOST RESPONSE TO THE HIP PROSTHESIS

The introduction of any inert implant into the body elicits a response of wound healing and repair, which culminates in the formation of a thin fibrous capsule around the implant. Alternatively bioactive implants like ceramics, elicits the formation of normal tissue at its surface, by eliciting a controlled action and reaction in the physiological environment. The presence of Hydroxyapatite coatings leads to osteoconduction in which bone grows along the coating forming a mechanically strong interface. The third group of biomaterials, termed as resorbable, exhibit a clinically relevant controlled chemical breakdown and resorption, with the foreign material being ultimately replaced by regenerating tissue, there being no discernable difference between the implant site and host tissue.

Although this is the general scheme of events, the initial interaction that occurs when an implant is placed in the body is the adsorption of proteins, from the biological fluids and ECM, onto the implant surface. The types of proteins adsorbed depend on the surface characteristics of the implant, such as hydrophobicity, energy, roughness, charge and chemical composition. Hence, the cells of the body essentially recognize not the surface of the implant but rather a surface that has been translated by proteins into a biological language (Wilson CJ *et al*, 2005). It is to this biological language that the cells respond. In effect, it is the interfacially adsorbed proteins that determine the body's response to an implant and ultimately the fate of the implant. A fibrous tissue layer containing few cells or vessels develops in relation to most non bioactive implants while normal tissue forms on the surface of bioactive implants.

Table 1: Biomaterials used in total joint replacements. (Adapted from "Biomaterials". Sujata V. Bhatt. 2002. Narosa Publishing House)

MATERIALS	APPLICATIONS
Metals	
Stainless steels 316 L	Femoral
Cobalt based alloys	Porous coatings, femoral stems, heads, tibial and
Cast Co-Cr-Mo	femoral components.
Wrought Co-Ni-Cr-MO	
Wrought Co-Cr-W-Ni	
Titanium based materials	
Ti-6Al-4V	Femoral stems, Heads, Porous coatings
Ti-5Al-2.5Fe	Femoral stems, Heads
Ti-Al-Nb	Femoral stems, Heads
Ceramics	
Bioinert Carbon	Coatings on metallic femoral stems, second phase in composites and bone cement.
Alumina	Femoral stems, heads and ace tabular cups
Zirconia	Femoral heads, acetabular cups
Bioactive calcium phosphates	Coatings on metallic and ceramic femoral stems, scaffold materials, second phase in PMMA and UHMWPE composites.
Bioglasses	Coatings on metallic and ceramic femoral stems
Polymers	
PMMA	Bone cement
UHMWPE/HDPE	Acetabular cups, Porous coatings on metallic and ceramic femoral stems.
Pulysulfolene	Femoral stems, porous coatings on metallic femoral stems.
PTFE	Femoral stems, porous coatings on metallic femoral stems.
Composites	Femoral Stems
Polysulfone-carbon	
Polycarbonate-carbon	
Polysulfone-Kevlar	

1.5. ASCEPTIC LOOSENING- PRIMARY REASON FOR FAILURE OF THE HIP PROSTHESIS

Although artificial joint replacements are successful initially, asceptic loosening of the prosthesis 10-15 years post surgery continues to be the most vexing problem (Ratner BD *et al*, 2004). Radiographic studies of such loosened prosthesis have shown the presence of diffuse cortical thinning and focal osteolytic lesions in areas of host bone adjacent to the implant. As a result of this periprosthetic osteolysis the bond between the prosthesis and the host bone is greatly reduced, causing the loosening of the prosthesis and failure of the implant. Such cases necessitate a revision surgery wherein the failed prosthesis is replaced with a new one.

Examination of the periprosthetic tissue around failed implants have shown the presence of a large amount of particulate material and a vascular granulation tissue comprising of a heavy cellular infiltrate of inflammatory cells like macrophages, fibroblasts and FBGC. These particles are generated as a result of wear between the component parts of the prosthesis. Histological observations of the periprosthetic tissue have shown a thickened fibrous capsule characterized by the presence of a large number of macrophages actively engaged in the phagocytosis of these particles, new blood vessels and few fibroblasts. It has been identified that such particle stimulated macrophages produce a myriad of cytokines, inclusive of bone resorbing factors like PGE2, TNF-α and collagenase, which modulate periprosthetic osteolysis of host bone (Archibeck MJ *et al*, 2000 and Horowitz SM *et al*, 1994). Periprosthetic osteolysis can also result as an outcome of stress- shielding, due to a reduction in the load transmitted to the host bone. Progressive loss of host bone disrupts the bond between the implant and the host bone, culminating in the loosening of the prosthesis necessitating a reoperation which is a definite measure of the clinical failure of the joint prosthesis.

The enormous volumes of polyethylene wear from conventional metal-polyethylene THR have been perpetrated to be the main cause of periprosthetic osteolyis. This piloted the introduction of second generation MOM THRs, into the market. The improved design and material properties of these prosthesis have been propounded to reduced wear and particle generation. However early osteolysis in MOM THRs are also being reported (Park YS *et al*, 2005). The nature and mechanism of host response to these orthopedic metal particles are only being evaluated.

However to date the exact pathomechanisms of wear debri induced inflammation leading to periprosthetic osteolysis is still not delineated. We aim to use a proteomic and molecular pathological approach to study the cellular response to particulate materials of the orthopedic biomaterial CoCr alloy (ASTM-F75) in soft tissue using an *in vivo* model and to elucidate the molecular changes in specific cell types in response to these particles using *in vitro* models. Understanding the initial signals that are expressed to particulate material would help in devising biological means of controlling the inflammatory response to particulate material. This work draws significance in view of the recent comeback of metal on metal total hip replacements into the orthopaedic market.

Chapter 2

REVIEW OF LITERATURE

Though joint replacements are successful initially, the problem of asceptic loosening sets in 10 to 15 years postoperative. Periprosthetic osteolysis leading to asceptic loosening continues to date to be the primal reason for failure of joint replacements, after long term implantation.

Investigations to understand the cause of asceptic loosening were initially centered on studies of tissues surrounding failed prosthesis. Such studies have revealed the presence of a chronic inflammatory response of the host to implant debri. The main inflammatory cells present were macrophages, foreign body giant cells along with fibroblasts, neutrophils and occasional T lymphocytes. A notable feature throughout these studies was the presence of phagocytosed implant debri within the macrophages and FBGC (Boss JH *et al*, 1996).

2.1. WEAR DEBRI

2.1.1. Source and morphology of particulate debri

Research into the nature and source of particulate debris have revealed these debri to emanate from the hip prosthesis as result of either wear or corrosion of the component parts. Wear involves the physical removal of material from the surface of

the prosthesis. The mechanisms of wear processes being abrasive, adhesive, surface fatigue or third body wear. Corrosion is an electrochemical process in which metal ions are released from an implant surface. The particles are metal salt precipitates of these ions, which form in the surrounding aqueous environment (Archiebeck MJ *et al*, 2000) .

Early investigations into the size and morphology of wear particles centered on the digestion of periprosthetic tissue with proteolytic enzymes and subsequent isolation, separation and characterization of the particles, the characterization of the particles being performed by SEM, TEM or particle size analyzers. Most of the particles retrieved comprised of UHMWPE, PMMA, cobalt or titanium alloys. The concentration of wear particles can extend into billions per gram of periprosthetic tissues (Schmalzried TP *et al*, 1999). The size of the debris recorded range from submicron to as large as 200μm for UHWMPE, from less than one micron to 25μm for metals like Ti-Al-Va, while the reported size ranges for Co-Cr alloy are submicron to 100μm (Savio JA *et al*, 1994). CoCr particles have been reported to be present *in vivo* in the synovial fluid, acetabular cup, within bone and in the surrounding muscle and fascial tissue. CoCr particles in the size range of 1-5μm are most reported and have been described variously as needles, splinters or rods. CoCr particles of size 5-25μm are reported to morphologically be of irregular shape, fragments, clusters and globules suggesting that many of these may be aggregates of smaller particles. Observations of CoCr particles in the size range 100μm to 1mm have been reported, but on the whole very few particles >25μm occur *in vivo* (Schmalzried TP *et al*, 1999). Hirakawa *et al,* (1996) had reported that submicrometer granules are prevalent in specimens obtained from the tissues around both total knee replacements and total hip replacements. Larger flake-shaped particles, measuring several micrometers in length and width, are

relatively common in association with total knee replacements than in association with total hip replacements. The overall average area of particles generated by total knee replacements has been reported to be about twice that of particles generated by total hip replacements.

Doorn *et al*, (1998) had enzymatically digested periprosthetic tissue from MOM THRs. CoCr alloy particles obtained appeared as round, oval or irregular spike shaped. Majority of the particles were rounded with irregular border and a particle size range of 19 to 79nm. Particles were observed to exist individually and as agglomerates.

Ichinose *et al*, (2003) had examined the size and distribution of the fine particles that were released from Co-Cr-Mo and Ti-Al-V alloy types of knee prosthesis. TEM observations had revealed large CoCrMo alloy particles of length 30-35nm and width 20-25nm.

Catelas *et al*, (2004) was the first to systematically compare particles isolated from a hip simulator with particles isolated from similar implants *in vivo*. TEM micrographs revealed the *in vitro* generated particles to have a rounded or oval morphology with a size of 53-43nm diameter. The *in vivo* particles also exhibited a similar morphology and an average size range of 57nm. These results substantiate the suitability of using hip simulators to generate wear particles that can be used for *in vitro* and *in vivo* experimentations to study cellular response to these particles.

2.2. BIOLOGICAL RESPONSE TO WEAR DEBRI

Periprosthetic osteolysis is usually visualized as focal lesions of reduced bone mineral density. These focal losses of bone are usually detected at multiple points along the length of the prosthesis and are seen in conjunction with an inflammatory

response to implant derived polymeric and metallic wear debri. Research, using both *in vitro* and *in vivo* techniques, have been directed in understanding the many ramifications involved in the cascade of events that ensue from the release of implant debri and culminate in periprosthetic osteolysis and asceptic loosening of the prosthesis.

2.2.1. Local effects

2.2.1.1. Cells

The central role in periprosthetic osteolysis is played by the synovial like interfacial membrane (IM) that forms the periprosthetic tissue. Early research publications centered on the examination of the IM retrieved from clinically failed prostheses. To further the understanding of the mechanisms of wear debri induced inflammation, numerous *in vivo* and *in vitro* studies have been performed over the last decade.

Lalor *et al*, in 1993 had used immunohistochemical techniques to study the bone-implant interface in samples retrieved from 23 patients who had revision surgery of total hip arthroplasty and 6 patients of total knee replacements. All implants apart from one were comprised of Cobalt-Chrome (CoCr) alloy articulating with High density polyethylene (HDP). Data obtained demonstrated the presence of two distinct cell types, those which labeled with macrophage markers and those which stained positive for markers of type B synoviocytes indicating a synovial like structure of the interfacial membrane.

Boss *et al*, (1996) had histologically evaluated the interfacial membrane of cemented hip arthroplasties retrieved after 6-15 and 16-22 years implantation. Results of their study suggest an outer predominately fibrous layer and an inner synovial like

aspect to the IM. A midzone containing prosthetic debri induced granulomas and macrophages were noted. Fibrotic tissue was more dominant in the 16-22 years time group while macrophagic sheets and giant celled granulomas were more common in the 6-15 years time group. Goodman *et al*, (1996) had analyzed tissue surrounding nine revised hip prosthesis. The results published from the study demonstrate a heterogeneity in cellular and cytokine profile in tissue harvested at different locations along the interface surrounding a hip prosthesis. This heterogeneity being attributed to variable anatomy, vascularity and exposure to distinct mechanical forces and levels of wear debris in different areas. In the same year Kadoya *et al*, (1996) had published data obtained from the examination of bone adjacent to the interfacial membrane obtained from eleven hip and six knee revision operations. Immunohistochemical analysis of areas of host bone that showed radiographical evidence of osteolysis, exhibited the presence of osteoclasts and macrophages and foreign body giant cells. The remaining areas of bone were osteogenic, identified by the presence of an osteoid layer or positive staining for alkaline phosphatase activity. Al-Saffar, (1999) had also reported on the osteogenic potential of the interfacial membrane, following a histological evaluation of periprosthetic tissue from sixty patients undergoing revision surgery. Lynne *et al*, (1999) had immunohistochemically evaluated the interface membranes from cemented and uncemented acetabular components. While macrophages were present in both groups a predominance of fibroblastic connective tissue was noted around failed cementless implants.

The role of T lymphocytes in asceptic loosening is still debatable. Li TF *et al*, (2001) had evaluated interfacial membrane from ten patients undergoing revision hip arthroplasty. Results obtained from their study were negative for T cell activation marker interleukin-2 receptor (IL-2R) suggesting that T-cell mediated immune

response was not involved in asceptic loosening of THR. Hercus *et al*, (2001) had examined the interfacial membranes from revision cases, for CD3. Of the fifteen cases studied twelve had stained positive. The group had also reported in 2002 on the expression profile of IL-17, fractalkine (Fkn), IFN-γ and IL-10. Results published by the group suggest that a Th1 response characterized by the production of IFN-γ, IL-17 and Fkn predominates over Th2, IL-10 mediated response (Hercus B *et al.*, 2002).

To better understand data obtained from clinically retrieved samples a number of *in vivo* experiments have been performed. Rae T, (1986 a) had reported on the tissue response to titanium and TiAlVa following injection of these particles into the knee joint of mice. Neither type of particles produced a chronic inflammatory response at 2, 4, 8, 16, 26 and 52 weeks. Data published by Jiranek *et al*, (1995) from *in vivo* experiments conducted using immunocompetant and lymphocyte dysfunctional mice, reveal the tissue response to subcutaneously injected PMMA particles is characterized by granuloma formation. The foreign body response appears to be macrophage initiated and mediated by a lymphocyte independent pathway.

Immunohistochemical evaluation for resident (ED2) and recruited (ED1) macrophages, around different biomaterials implanted subcutaneously and in abdominal muscles of rats was conducted by Rosengren *et al*, (1998) and later by Hagerty *et al*, (2000). Hooper *et al*, (2000) had characterized the foreign body response to different biomaterials using a rodent air pouch model. Two days post implantation macrophages appeared to be the main cell type (60-75%) followed by granulocytes (20-25%) and lymphocytes (10%). The inflammatory response specifically to orthopaedic biomaterials i.e, TiAlVa, UHMWPE, CoCr and PMMA particles implanted *in vivo* using a murine air pouch model, was evaluated by Wooley

et al, (2002). Histological and immunohistochemical evaluation revealed a variation in tissue response with material compositon. TiAlVa induced the maximum membrane thickness, while UHMWPE induced maximum number of macrophages. A further difference in tissue response was noted when materials where implanted in combinations, suggesting a synergistic effect in the level of inflammatory response.

A large number of *in vitro* studies have been documented in relation to particle stimulated macrophages and osteoblasts but very few in relation to fibroblasts. As early as 1986, Rae *et al* (1986, b) had investigated the ability of particulate forms of titanium and its alloy TiAlVa to induce the release of lactate dehydrogenase in human synovial fibroblasts and mouse peritoneal macrophages, cultured *in vitro*, highlighting the inflammatory potential of these particles. Horowitz *et al*, (1994) had experimentally proved the ability of conditioned medium from macrophage cultures that were stimulated with bone cements to induce prostaglandin PGE_2 production in osteoblasts. This induction was possible only if the macrophages had phagocytosed the particles of bone cements. The group had later published data in 1995, which demonstrate the release of TNF by PMMA stimulated macrophages and the ability of conditioned media from such cultures to induce IL-6, GM-CSF and PGE_2 production in osteoblasts (Horowitz SM *et al*, 1995). Further studies demonstrate the potential of polyethylene particles to stimulate the release of PGE_2 from macrophages in *in vitro*, and the propensity of conditioned media from such cultures to induce bone resorption in rat calvarial organ cultures. The resorptive effect could however be inhibited via palmidronate incubation (Horowitz SA *et al*, 1997).

The macrophage response is dependent on the composition, size and concentration of the particles as demonstrated by the work of Shanbhag *et al*, (1994)

wherein macrophages were challenged with different titanium, titaniumdioxide and polystyrene particles. These macrophages were reported to secrete cytokines and prostaglandins that were able to modulate fibroblasts proliferation and bone resportion *in vitro*.

Published data have also demonstrated that wear particle associated macrophages are capable of differentiating into multinucleated cells that exhibit all the phenotypes of osteoclasts, the bone resorbing cells. Udagawa *et al*, (1990) first demonstrated in mice that mononuclear phagocytes were capable of differentiating into osteoclasts in the presence of bone marrow-derived stromal cells. They showed that the differentiation of osteoclasts from mononuclear cell progenitors or tissue derived macrophages *in vitro* required physical contact with stromal cells derived from bone marrow or osteoblasts. It has also been shown that monocytes and macrophages that have phagocytosed implant derived polymeric or metallic biomaterial wear particles, when cocultured in the presence of osteoblast like cells and 1,25-dihydroxyvitamin D3 are capable of differentiating into osteoclasts, which have the ability to resorb bone (Pandey R *et al*, 1996) .

To investigate the effect of metal particles on the fibrous capsule formation Thomas *et al*, (1986) had measured the effect of cobalt-chromium-molybdenum powder on collagen production by fibroblasts *in vitro*, while Maloney *et al*, (1993) examined the effects of metallic particles on cellular proliferation and enzyme induction of isolated fibroblasts of connective tissue origin. The effect of particles on cellular viability of macrophage and fibroblast has also been looked into in detail (Germain MA *et al*, 2003 and Oliver V *et al*, 2003). Reno *et al*, (2003) had reported on the activation of the apoptosis marker, caspase-8 in fibroblast like cells in the

periprosthetic tissue around asceptically loosened cemented prosthesis. Cell-cell interactions have been studied to a lesser extent. These studies have employed the use of either conditioned medium or coculture systems. The effect of secretory mediators from particle stimulated macrophages on fibroblast activation was studied by Lind *et al*, 1998 using a coculture system. While the supporting role of granulation fibroblasts in osteoclast differentiation is just being looked into (Sakai H *et al*, 2002), researchers are also demonstrating the ability of fibroblast like cells from tissue surrounding aseptically loosened prosthesis, to directly resorb bone without the help of osteolclasts (Pap T *et al*, 2003).

2.2.1.2. The Cytokine Web

Histological studies have shown the interfacial membrane to be composed of a fibrous stroma laden with macrophages, giant cells, fibroblasts and particulate debris. *In vivo* studies have indicated this tissue to produce metalloproteinases, prostaglandins and cytokines, which are implicated in periprosthetic bone resorption.

The cytokines are a family of low molecular weight proteins, produced by many cell types and are the master regulators of the immune response, tissue remodeling and cell differentiation. One cytokine can regulate the synthesis and release of a myriad of cytokines culminating in a highly intricate web of interacting molecules. Cytokines can be either pro-inflammatory or anti-inflammatory and act via either an autocrine or paracrine function that is under strict control in the physiological conditions. Several studies have accumulated direct evidence, both *in vitro* and *in vivo*, that phagocytosis of prosthetic wear particles by macrophages induces the release of bone resorbing cytokines. These cytokines include IL-1β, IL-1α, IL-6 and

TNF-α. As a result osteoclast differentiation and maturation is accelerated, leading to osteolysis at the bone implant interface.

Al-Saffar *et al*, (1994) had evaluated the bone implant interface obtained from ten revision THRs. Positive staining for IL-1β was noted in seven cases, with most of the positively stained cells being macrophages. The group had also demonstrated the presence of GM-CSF, IL-6 and absence of TNF-α in the periprosthetic tissue (Al-Saffar N *et al*, 1995). Absence of IL-1α but presence of TNF-α along with IL-β and the chemokines MIP-1α, MIP-1β, MCP-1, in interface tissue was reported by Ishiguro *et al*, (1997).

In vivo experiments using Ti and PTFE chambers implanted in the abdominal wall of rats have shown the presence of leukotriene B4 and interleukin-1 in the exudates. The amount of LTB4 and IL-1 being higher for PTFE as compared to Ti (Eriksson AS *et al*, 1991). The ability of anti-inflammatory cytokine IL-10 in suppressing polyethylene wear debri induced inflammation and promoting bone ingrowth in a rabbit model using a drug test chamber was demonstrated by Goodman *et al*, (2003). Subcutaneous implantation of Ti and Cu coated Ti disks in rats showed an early transient response to Ti as characterized by production of IL-1α and TNF-α. Enhanced and prolonged production of IL-α was observed around Cu coated Ti disks. These results reflect on the role of underlying chemical composition and properties of the material in dictating inflammatory response (Suska F *et al*, 2003). Warne *et al*, (2004) had implanted intramedullary rods into mice femurs along with titanium particles. Femurs were harvested at 2, 10 and 26 weeks following surgery and organ cultures maintained. ELISA analysis of the culture medium showed an increase of cytokines MCP-1, IL-6 and M-CSF at two weeks, but not at later time periods. Masui

et al, (2005) had implanted TiAlVa, CoCr, and HDP into murine calvaria. Explants were used for organ culture and medium from the same was evaluated for TNF-α and IL-1β via ELISA. An increase in TNF-α and IL-1β production around Ti implants as compared to CoCr, HDP and control was noted.

The ability of particulate forms of implant materials to stimulate the production of cytokines IL-6 and TNF-α *in vitro* in human monocytes and osteoblasts have been extensively documented. *In vitro* experiments by Wang *et al*, (1996) using LPS stimulated U937 monocytes and human blood monocytes exposed to Ti, Co and Cr ions at varying concentration have shown an increase in the secretion of IL-β to all metal ions. TNF-α production was increased in presence of Ti and Cr ions only, while IL-6 production increased on exposure to Ti ions only. It was interesting to note that in the absence of LPS stimulation none of the metal ions stimulated cytokine production. Algan *et al*, (1996) had reported on the ability of PMMA particles to stimulate production of TNF-α in J774 mouse macrophages. PGE_2, IL-1α and IL-1β levels were however found not to be increased compared to control. The conditioned medium induced PGE_2 production and bone resorption in calvaria organ cultures. Bone resorption but not PGE_2 production was inhibited by administration of anti TNF-α antibodies into the culture medium. Liu *et al*, (1999) had incubated human peripheral leukocytes with various concentrations of Co^{2+}, Cr^{3+} and Ti^{3+} ions. TNF-α, IL-6 and PGE_2 were reported to increase following exposure to Co^{2+}ions. Cr^{3+} ions stimulated an increase of IL-6 and PGE_2 release while Ti^{3+} ions caused a decrease in TNF-α and PGE2 release. Im *et al*, (2001) had experimentally demonstrated the ability of IL-4 and IL-10 to decrease the levels of proinflammatory cytokines IL-6 and TNF-α from human monocytes cultured with TiAlVa. PMMA (Miyaguchi M *et al*, 2002 and Mitchell W *et al*, 2003), Hydroxyapatite (Laquerriere P *et al*, 2003) and alumina

(Hatton A *et al*, 2003) have been reported to induce TNF-α and IL-6 production in human monocyte cultures. The responses varying on the size, shape and surface morphology of the particles. Similar results showing increased release of IL-6 and PGE_2 in human osteoblasts following exposure to CoCrMo alloy, TiAlVa, TiAlNb and CpTi was reported by Schmidt *et al,* (2003).

Intermediary cells such as fibroblasts are abundant in the periprosthetic membrane and have been shown to phagocytose particles and produce cytokines and protease that are associated with bone resorption and degradation of the extracellular matrix. Manlapaz *et al*, (1996) had directly stimulated human dermal and foreskin derived fibroblasts with varying concentrations of TiAlVa particles. A dose dependent increase in both IL-6 and PGE_2 secretion was noted. Presence of IL-1β and TNF-α was not detected. Ninomiya *et al*, (2001) had compared IL-6, IL-1β and TNF-α production in human neonatal fibroblasts following stimulation with HA, Ti, CoCr and HA/TCP. Bukata *et al*, (2004) had demonstrated through immunohistochemical evaluation of retrieved interfacial membrane and *in vitro* experiments on fibroblasts derived from knock out mice, the role of cyclooxygenase-2 pathway in the release of PGE_2 and IL-6 following Ti particle stimulation.

Using DNA microarrays, gene expression profile studies of cells grown with metallic particles have also been published. Pioletti *et al*, (2002) had investigated the response of human MG-63 osteoblast like cells to Ti particles using Genefilters. Results obtained indicate an upregulation of inflammatory cytokines IL-1α, IL-1β, TGF-β following four hours incubation with Ti particles. Similar results were also reported by Garrigues *et al*, (2005) who had examined gene expression changes in human macrophages cultured with TiAlVa and UHMWPE using a nylon membrane

based cDNA microarray. Following thirty minutes incubation genes for the cytokines IL-6, RANTES and MIP-1 and their receptors were found to be upregulated. In addition genes for IL-1α, IL-3 and IL-5 were found to be upregulated after four hours of incubation.

2.2.1.3. NF-κB Signaling pathway

Genes involved in inflammation and immune responses are regulated by the inducible transcription factor, nuclear factor- kappa B (NF-κB). NF- κB transcription factors are a family of four proteins (p50, p52, p65 and cRel), that dimerize at specific consensus sequences in target gene promoters. In the cytoplasm they are present in the inactive form bound to the inhibitor protein IκB. In response to an extracellular inducer, a protein kinase is activated that phosphorylates IκB resulting in its dissociation from NF-κB. The release and activation of NF-κB leads to its migration to the nucleus where it regulates the expression of genes coding pro-inflammatory cytokines, adhesion molecules, chemokines, inducible enzymes such as cyclo-oxygenase 2 (COX2) and inducible nitric oxide synthase, iNOS (Tripathi P *et al*, 2006).

Recent research initiatives have reported on the involvement of NF- κB signaling pathways in wear debri induced periprosthetic osteolysis. Nakashima *et al*, in 1999 had reported on the induction and activation of the transcription factor NF-κB in isolated human macrophages following thirty minutes incubation with titanium particles (Nakashima *et al*, 1999). The data published suggest that release of TNF-α and IL-6 by macrophage does not require phagocytosis of the titanium particles, contact of particles with cell surface membrane proteins itself being a sufficient signal. Proinflammatory cytokine release is however dependent on tyrosine and

serine/threonine kinase activity culminating in the activation of the transcription factor NF- κB.

Schwarz *et al*, (2000) had detected an increase of NF-κB in mouse macrophages J774 cells thirty minutes after stimulation with titanium particles, and also reported on a decrease in bone resorption induced by titanium particles in genetically engineered mice deficient in NF-κB(-/-). Data published by Soloviev *et al*, (2002) demonstrates the rapid induction of TNF-α by titanium particles in an ANA-1 murine macrophage cell lines. Electrophoretic mobility shift assays prove the activation of NF-κB signaling and its association with p105 (a precursor of p50) degradation. Data obtained from their study suggests that TNF-α induction is mediated in part by NF- κB binding to the κB2a site of the TNFα promoter.

A recent study by Clohisy *et al*, (2004) has shown that NF-KB inhibition via TPCK (N-tosyl-L-phenylalanine chloromethyl ketone), CPI (Calpain Inhibitor I) and TAT:IκB (TAT bound, mutant IκB) abolishes osteoclastogenesis induced by PMMA-particles in all three cases. Ren *et al*, (2004) had experimentally proved the ability of erythromycin, a macrolide antibiotic, to significantly inhibit mRNA expression of NF-κB, IL-1β, cathepsin K and TNF-α in mouse RAW 264.7 macrophages that had been stimulated with wear debris. Baumann *et al*, (2005) had exposed differentiated THP-1 macrophages to increasing number of TiAlVa and polyethylene particles for 0, 60,180 and 360 minutes. NF-κB activation, examined by electrophoretic mobility shift assay (EMSA), showed an increase in activity at 180 minutes. Experimental data published by Fritz *et al*, (2005) suggest that titanium particles induce IL-8 and MCP-1 chemokine expression in osteoblasts via NF- κB mediated transcriptional activation, which in turn is controlled by the MAPK signal transduction pathway. These results together

indicate the induction of NF-κB signal transduction pathway in mediating the inflammatory response to periprosthetic osteolysis.

Contrary reports have also been published that fail to detect a significant increase in NF- κB production by metal ions using both *in vivo* and *in vitro* models. Akisue *et al*, (2002) had reported on the absence of NF- κB activation in differentiated THP-1 cells following a one hour incubation with titanium wear debri obtained from periprosthetic tissue around a failed THR. Lewis *et al*, (2003) also had failed to detect a significant change in basal levels of NF- κB, in THP-1 monocytes following 24 hours exposure to sublethal concentrations of metal ions, Co^{2+}, Hg^{2+}, Ni^{2+} and Cu^{2+}. Suska *et al*, (2005) had reported on the decreased amounts of activated NF- κB around copper disks as compared to titanium disks following 12 and 48 hour implantation in rats. The reason for decreased production being the induction of apoptosis in adjacent cells due to the toxic nature of copper.

2.2.1.4. Reactive Oxygen Species (ROS) in asceptic loosening

High oxidative stress has been proposed to be a causative factor in many inflammatory diseases with tissue damage and fibrosis. It has been hypothesized that excessive production of ROS exacerbates the inflammatory response to wear particles and promotes bone resportion. ROS are also known to stimulate the production of cytokines (Becker S *et al*, 1996). However there is much dearth in literature on particle mediated ROS and its role in asceptic loosening of TJR. Work published by Wang *et al*, have demonstrated the synergistic effect of particle and cell activation on the release ROS by THP-1 macrophages and HD-11EM avian osteoclasts (Wang *ML et al*, 2002). Western blot analysis of macrophage cultures exposed to Co^{2+} and Cr^{3+} ions revealed the presence of protein carbonyls, which are products of protein

oxidation. The protein oxidation was noted to vary in a time and dose dependent manner, reaching a maximum of 6.5 and 2.9 times the control, after 72 hours, for Co^{2+} and Cr^{3+} ions respectively. These results reflect the possibility of metal ions from MOM prosthesis to modify the redox state of macrophages in the periprosthetic tissue (Petit A *et al*, 2005). The group had also reported similar results in human MG-63 osteoblast cell lines that had been exposed to Co^{2+} and Cr^{3+} ions (Fleury C *et al*, 2006). Kinov *et al*, (2006) had reported on increased levels of the levels of oxidized glutathione (GSSG) and malondialdehyde (MDA) and decreased GSH/GSSG ratio in periprosthetic tissue obtained from forty different patients undergoing revision arthroplasty, as compared to control. Results from the study suggest that elevated production of ROS, which are known to cause tissue fibrosis may play a role in the fibrous pseudocapsule formation around hip implants.

2.2.1.5. Necrosis and Apoptosis

The two distinct forms of cell death are necrosis and apoptosis. Necrosis is a passive form of cell death characterized by the disruption of the integrity of the cell membrane, leakage of cellular contents into the peri-cellular area and uncontrolled DNA fragmentation. Apoptosis or programmed cell death, is an active form of cell death which is under the control of positive and negative genetic regulation. Apoptosis is characterized by cell shrinkage, surface blebbing, organized DNA fragmentation and release of apoptotic bodies. Both necrosis and apoptotsis can occur in response to a toxic stimulus. Unlike necrosis, elimination of the apoptotic bodies does not induce an inflammatory response. Recent research initiatives have been directed to ferret the role of apoptosis in aseptic loosening of joint prosthesis.

Schelde *et al*, (1995) had reported on the absence of apoptosis in L929 cells following exposure to metal ions of Cr, Co, Ni and Mo. Prabhu *et al*, later in 1998 had also reported on the absence of apoptosis in J774A.1 murine macrophages on exposure to particles of Co-Cr and bone cement (Prabhu A *et al*, 1998) .

Stea *et al*, (2000) examined 54 biopsies of the peri-implant tissue from 30 patients who underwent revision surgery for aseptically loosened hip joint prosthesis. Data obtained revealed a higher percentage of apoptotic cells in samples containing metal particles as compared to those with plastic or ceramic debri. In 2001, Huk *et al,* have demonstrated the presence of apoptotic cells in the periprosthetic tissue surrounding aseptically loosened THA (Huk OL *et al*, 2001). The group had also conducted *in vitro* studies and demonstrated the apoptotic response of macrophages following 24 hour exposure to cobalt and chromium ions. They suggest that the modulation of the expression of proteins from the bcl-2 and the caspase families of proteins are implicated in the induction of macrophage apoptosis by Co^{2+} and Cr^{3+} ions (Catelas I *et al*, 2001 and Petit A *et al*, 2004). The group had further analyzed the effect of prolonged exposure time (48hours) of cobalt and chromium ions on macrophage mortality and TNF-α secretion. Both Co^{2+} and Cr^{3+} ions induce macrophage mortality in a dose and time dependent manner. At higher concentrations of ions and longer exposure periods necrosis rather than apoptosis was the major mode of cell death (Catelas I *et al*, 2003 and Catelas I *et al*, 2005).

2.2.1.6. Proteomics in relation to biomaterials

Recent research initiatives, to better elucidate biocompatibility at the molecular level, have been directed in understanding protein adsorption onto biomaterials. The initial presentation of the implant to the cells is as a layer of spontaneously adsorbed

proteins, whose composition and bioactivity provide a biological interpretation of the underlying physicochemical properties. Cells interact with these adsorbed protein layer via surface receptor molecules like the integrins and respond through the synthesis of proteins and organization of extracellular proteins via various intracellular signaling pathways. Studies of these adsorbed proteins have mainly employed the techniques of SDS-PAGE, western blotting, 2D-Electrophoresis and MALDI-TOF MS. Most of these works have been done using *in vitro* models.

The pathomechanisms of wear debri-induced inflammation that leads to asceptic loosening involves the interaction of particulate material with the phagocytic cells of the immune system leading to cellular activation. Elucidation of the mechanisms of asceptic loosening via a proteomic approach has only recently been initiated. Interaction between particles and adsorbed proteins occur as an opsonistion process which plays a pivotal role in recognition and uptake of foreign material by these phagocytic cells. Sun *et al*, 2003 had shown in their study that distinct particulate materials exhibited selective affinity for specific serum proteins and particle opsonization with serum albumin significantly increased particle-induced macrophage activation. Hallab *et al*, (2003) had studied the distribution of titanium [Ti] and chromium [Cr] in serum protein fractions of patients with and without total joint replacements containing Cr and Ti. Two molecular weight ranges were found to bind Cr (at »70 and »180 kDa) in patients with CoCr alloy prostheses, whereas a single molecular weight range (at »70 kDa) was found to bind Ti in patients with Ti alloy implants. The group had also used an *in vitro* model to study the differential biofilm composition of human serum proteins adsorbed onto Co-Cr-Mo and Ti- based implant alloy bead surfaces and the lymphocyte response to serum protein complexed with the metal (Hallab NJ *et al*, 2001 and Hallab NJ *et al*, 2003).

2.2.2. Systemic effects

Elevated levels of cobalt and chromium have been reported in serum and urine samples of patients with THR. Dobbs *et al,* (1980) had used neutron activation analysis of peri-prosthetic tissue from an autopsy case. They reported on elevated levels of Co and Cr in lung, kidney, liver and spleen. Co ions also predominated in the urine samples. In a follow up study of 30 patients, six months post implantation with metal-on metal bearings, 2 fold and 1.5 fold increases of Co and Cr respectively in the blood, while a 10 fold and 3 fold increase of cobalt and chromium in urine was reported (Masse A *et al*, 2003). Savarino *et al*, in 2002 also reported on the higher systemic release of cobalt and chromium in patients with metal-on-metal components compared to those with metal-on polyethylene (Savrino L *et al*, 2002).

The dissemination of wear debri to distant organs of the body have been reported only since the early 1990's. Majority of the data obtained have been from pathological examination of autopsy and biopsy samples while few data from animal experimentations have also been reported.

Langkamer *et al*, (1992) have reported through histological and electron microscopic evidence the presence of metallic debris in the lymph nodes, liver and spleen in autoposy samples from two patients with joint arthroplasties. Their work having suggested that wear debris may be cleared to distant sites by the lymphoreticular system.

In 1996, Basle *et al*, also had reported on the migration of wear particles from the prosthetic site to the regional lymph nodes and the subsequent induction of an intense lymph node histiocytic reaction. In some of the clinical cases that the group

had observed, lymph node histiocytosis was found to mimic pseudo malignant lymphadenopathy (Basle MF *et al*, 1996).

Urban *et al,* (2000) examined post mortem samples and biopsy samples from patients with joint arthroplasties to study the prevalence and histopathological characteristics of disseminated debris in the liver, spleen and abdominal para-aortic lymph nodes. 68% of the clinical cases exhibited the presence of metallic and polyethylene debri in the para-aortic lymph nodes. The group has also reported a prevalence of metallic debri in the liver and spleen of patients with failed hip arthroplasty as compared to patients with primary hip or knee replacements.

In addition, experimental studies on rats by Olmedo *et al*, (2002) had shown the dissemination of intraperitoneally injected titanium and zirconium particles to organs like lungs and liver, five months post implantation. Additional data published by the group in 1993, revealed presence of monocytes containing titanium particles, suggesting the role of the blood cells and the vasculature in the dissemination of titanium particles. These data spring concern, more so, in view of younger patients where the resident life of the implant spans the entire lifetime of the individual reflecting a proportional period of exposure to the wear debri (Olmedo DG *et al*, 2003).

2.3. PHARMACOLOGICAL MODULATION OF DEBRI INDUCED OSTEOLYSIS.

Prospects for pharmacological inhibition in wear debri induced inflammation have also been looked into. Anti osteolytic agents like bisphosphonates have classically been used for the treatment of Pagets disease, osteoporosis and metastatic bone disease, which are associated with accelerated bone resorption. Bisphoshonates

have been shown to disrupt osteoclast morphology at the cellular level and prevent the dissolution of hydroxyapatite crystals from mineralized bone. Horowitz *et al*, (1996) demonstrated that bisphosphonates may also be effective in reducing particle mediated osteolysis, reporting a reversal in bone resorption in macrophage/osteoblast co-cultures in response to Ti and PMMA particles, following treatment with pamidronate. In addition, Shanbhag *et al*, (1997) reported reduced periprosthetic osteolysis following treatment with alendronate in a canine THA model. Using the murine clavier osteolysis model and polyethylene particles, Knoch *et al*, (2005) have reported a marked decrease in bone resorption following a single dose of the third generation bisphosphonates zolendronic acid. Using the same model, the group had also shown that simvastatin could decrease UHMWPE particle induced osteolysis (Knoch FV *et al*, 2005).

It has been well established that macrophages take up wear debri and cytokinetically stimulate osteoclasts to resorb host bone. Many research groups have investigated the potential role of anti inflammatory agents in modulating the inflammatory response to wear debri. Blaine *et al*, (1997) demonstrated that the production of cytokines by Ti-stimulated monocytes could be modulated by pharmacologic agents, reporting decreased levels of TNF-α following treatment with cAMP agonists. Schwarz *et al*, (2000) suggested that future clinical intervention strategies for wear-mediated osteolysis may include anti–TNF-α gene therapy, as a possible treatment for controlling excessive inflammation, osteolysis, and osteoclastogenesis at the bone-implant interface.

Several antioxidant agents have been shown to be potent scavengers of ROS, including the bioflavonoid pyconogenol (PYC), ascorbic acid, N-acetylcysteine,

pyrrolidinedithiocarbamic acid, and nitrosoprocainamide. PYC has been reported to decrease the gene expression and production of the proinflammatory cytokines IL-1β and IL-2 in addition to scavenging ROS, suggesting that an antioxidant, such as PYC, may be effective in controlling ROS-mediated osteolysis and inflammation (Wang ML *et al*, 2004).

2.4. AIMS & OBJECTIVES OF THE WORK

Therapeutic modulations of cytokines to control inflammatory diseases like arthritis are recently being explored. The four major approaches being: inhibition of cytokine synthesis, inhibition of cytokine release, inhibition of cytokine action and inhibition of cytokine intracellular signaling pathways (Henderson B, 1995).

The exact pathomechanisms of wear debri induced inflammation leading to periprosthetic osteolysis have still not been delineated. We aim to study the cellular response to particulate material of the orthopedic biomaterial CoCr alloy (ASTM-F75) in soft tissue using an *in vivo* model and to elucidate the molecular changes in specific cell types in response to these particles using *in vitro* models.

We hypothesised that the initial stages of asceptic loosening would involve the release of implant particles into the fibrous capsule that surrounds the implant. This fibrous capsule is mainly comprised of collagen and few cells like the fibrocytes and fibroblasts. On release of wear debri into the biological mileu, the fibroblasts would be the first type of cells they come in contact with. The macrophages, which are key players in the inflammatory response, come into the scenario only at a later stage. Research has already established that these particle-stimulated macrophages release cytokines that play a role in periprosthetic osteolysis (Ingham E *et al*, 2005). However

the initial interactions of particles with fibroblast and the cytokines that they release have been studied only to a lesser extent.

In the present study the sequence of *in vivo* cellular responses to CoCr alloy particles have been evaluated using a rat model. The tissue response to CoCr alloy particles over different time periods have been evaluated using the techniques of immunohistochemistry, light microscopy and transmission electron microscopy. In this study we have also adopted a proteomic approach to elucidate the initial signals that are expressed to particulate material, using an *in vitro* cell culture system. Two dimensional polyacrylamide gel electrophoresis (2-DGE) in conjunction with mass spectrometry is the technique currently most used for studying expression levels of cellular proteins. Cytoskeletal reorganization and cytokine production have also been examined by confocal laser scanning microscopy (CLSM) and ELIZA.

The generation of osteolysis and implant loosening is complex and involves many proteins and cell types. Studying the mechanisms of debri induced inflammation leading to osteolysis would provide a basis for devising methods to mitigate and inhibit the biological response to particulate debris.

Chapter 3

MATERIALS AND METHODS

3.1. MATERIAL PARTICLES

The CoCr alloy (ASTM-F75) particles were donated by Smith & Nephew (Memphis TN, USA), a leading manufacturer of orthopedic joint prosthesis. ASTM F-75 is of medical grade and is a common material used in the fabrication of joint prosthesis.

3.2. CHARACTERIZATION OF SIZE AND SHAPE OF MATERIAL PARTICLES BY SEM, TEM AND LM.

Suspension of CoCr particles in methanol was pipetted onto the aluminum stub and copper grids and examined using SEM (Hitachi S2500) and TEM (Hitachi-600), respectively. The particles were also placed on glass slides and examined via light microscopy using a trinocular microscope (Nikon Eclipse Model E600, Japan) and images captured using a digital camera (Nikon model DXM1200F, Japan) with ACT-1 software.

3.3. ENDOTOXIN TEST

The presence of endotoxin on the CoCr particles was tested using the Sigma E-TOXATE kit (ET 0200). The test was repeated twice.

3.4. *IN VIVO* EXPERIMENTS

3.4.1. Implantation and retrieval of CoCr alloy particles.

All animal experiments were conducted with prior approval of the Institute Animal Ethics Committee (IAEC). Male Wistar rats of age 2.5-3 months and weight 200-250 grams were used as the animal model. Animals were divided into fourteen time groups, with six animals per group. The gluteus muscle was chosen as the site of implantation, because it resembles the soft tissue found at the tissue-implant interface.

Animals were anaesthetized via intramuscular injection of xylazine (5mg/kg body weight) and ketamine (100mg/kg body weight). The fur on both legs of the animal was clipped and skin swabbed with disinfectant, 70% alcohol. An incision was made in the skin and approximately 0.03 grams of CoCr alloy particles were injected into the gluteus muscle using 0.9% sterile saline as the carrier. 0.9% sterile saline alone served as sham. The particles were sterilized via autoclaving prior to implantation. Animals were fed food and water *ad libitium* and taken care of in the animal house.

Animals were sacrificed over different time periods of 1, 3, 5, 10, 15, 20, 30, 45, 60, 75, 90, 120 and 150 days. Gluteus muscle with implanted particles was harvested and fixed in 3% gluteraldehyde for TEM, 10% neutral buffered formalin for paraffin embedding and snap frozen in liquid nitrogen cooled isopentane for cryosectioning for immunohistochemistry.

3.4.2. Histopathological Analysis

3.4.2.1. Sample Processing

Muscles with the implanted particles were grossed. Cross section of the muscle with implanted particles were processed in tissue capsules. Tissues were dehydrated in isopropyl alcohol in ascending grades of dilution, cleared in chloroform and impregnated in paraffin wax. This processing was done using the Automatic Tissue Processor (LEICA TP 1020). The following protocol was followed:

1. 10% neutral buffered formalin -10 minutes
2. 80% alcohol - 2 hours
3. 95% alcohol I -2 hours
4. 95% alcohol II - 2 hours
5. 100% alcohol I - 2 hours
6. 100% alcohol II - 1 hour
7. 100% alcohol III - 1 hour
8. 100% chloroform I - 1 hour
9. 100% chloroform II - 1 hour
10. 100% chloroform III -2 hours
11. Paraffin wax I - 2 hours
12. Paraffin wax II -2 hours

3.4.2.2. Embedding

Processed tissues were embedded into paraffin blocks using the Paraffin Embedder (LEICA EG 1160). Tissue samples were removed from the cassettes with

warmed pointed forceps. Each tissue samples was oriented and placed in a mould filled with warm paraffin, in such a way that the cutting surface would include a cross section of the implant/implant area with surrounding tissue. The embedding ring was filled with warm paraffin and the entire mould placed along with the ring on a cold plate. Once the wax had cooled, the blocks with the embedding ring were removed from the mould and stored till sectioning.

3.4.2.3. Sectioning

Sides of the blocks were trimmed and shaped using a wax cutter. Opposite edges of the block were maintained parallel. Blocks were sectioned using the Automatic Microtome (LEICA RM 2155). The paraffin blocks were initially trimmed till the tissue surface was completely exposed. The exposed surface of the block was cooled with ice cubes and 7μm thick sections were cut. To help expand the tissue sections, they were floated onto water in a flotation bath (LABINDIA HISTOBATH HI-1210). Sections were picked up onto glass slides coated with Meyers Egg Albumin.

3.4.2.4. Staining

Paraffin sections of samples from all the 14 time periods were stained with Harri's Heamatoxylin and Eosin using the Automatic Stainer (LEICA AUTOSTAINER XL) using the following protocol:

1. Glass slides with sections were placed in slide racks and kept in the autostainer oven for 1 hour at 50°C.
2. Xylene I - 10 minutes
3. Xylene II - 5 minutes
4. 90% alcohol - 3 to 5 minutes
5. 70% alcohol - 3 to 5 minutes
6. Tap water - 1 to 5 minutes

7. Harris Haematoxylin - 5 to 20 minutes
8. Tap water - 1 to 3 minutes
9. Acid Alcohol - 10 sec to 1 minutes
10. Tap water - 1 to 5 minutes
11. Scotts tap water - 1 to 5 minutes
12. Tap water - 1 to 5 minutes
13. 1% Eosin(water soluable) - 5 to 20 minutes
14. Tap water - 10 sec to 30 sec
15. 70% alcohol - 2 to 5 minutes
16. 100% alcohol I - 2 to 5 minutes
17. 100% alcohol II - 2 to 5 minutes
18. Xylene III - 10 minutes
19. Xylene IV - 10 minutes

Slides were air dried and mounted with Cytoseal ™ 60 (Electron Microscopic Sciences, USA) and cover slipped.

3.4.2.5. Light microscopy

Histological analysis of the sections were performed via light microscopy using a trinocular microscope (Nikon Eclipse Model E600, Japan) and images captured using a digital camera (Nikon model DXM1200F, Japan) with ACT-1 software.

3.4.3. Immunohistochemical Analysis

Retrieved tissues with implant were grossed and snap frozen in liquid nitrogen cooled isopentane (SD Fine Chemicals Ltd, India) and stored in liquid nitrogen overnight. The samples were subsequently stored at -80°C. Cryosections (7µm thick) of the 5, 45, 90, 120 and 150 day samples were taken using the Leica Cryostat Model CM 3050S. Sections were taken onto Poly-L-Lysine (1:10 dilution, SIGMA) coated glass slides, air dried and stored at -80°C till further evaluation. The sections were stained for the Macrophage markers CD 68 (ED1, Serotec, UK), CD 163 (ED2, Serotec, UK), cytoskeletal components vimentin (Santa cruz biotechnology, Inc USA)

and smooth muscle actin (Santa cruz biotechnology, Inc USA), and cytokines IL-6 (Santa cruz biotechnology, Inc USA), IL-1α (Santa cruz biotechnology, Inc USA), IL-1β (Serotec, UK) and TNF-α (Santa cruz biotechnology, Inc USA). Specific staining was detected using the Streptavidin-Biotin Universal Detection System [UltraTech HRP (DAB), Immunotech, Beckman Coulter, France]. Immunohistochemistry was performed using the following protocol:

1. Sections were allowed to thaw to room temperature in a desiccator for at least one hour.
2. Sections were fixed in cold acetone (-20°C) for ten minutes.
3. Slides were placed into a coupling jar containing PBS for ten minutes.
4. Area around each section was demarcated using the DAKO PEN for immunohistochemistry (S2002, DAKO).
5. Sections were treated with 3% hydrogen peroxide for ten minutes at room temperature.
6. Washed in PBS buffer for two minutes.
7. Removed slides from buffer, wiped gently around each section and covered each section with Protein Blocking Agent (PBA). Allowed to incubate for five minutes at room temperature.
8. It was ensured that the slides were not washed.
9. Poured off PBA, wiped gently around each section and covered the section with primary antibody. Incubated in a humidity chamber at room temperature for 60 minutes.
10. Washed in PBS buffer for two minutes.
11. Wiped gently around each section and covered each section with biotinylated secondary antibody. Incubated for ten minutes at room temperature.
12. Washed in PBS buffer for two minutes.
13. Wiped around sections and covered each section with Streptavidin-peroxidase reagent. Incubated for ten minutes at room temperature.
14. Washed in PBS buffer for two minutes.

15. Wiped around each section and covered each section with freshly prepared DAB chromogen solution. Incubated at room temperature for one minute.
16. Washed slides in distilled water for two minutes
17. Counter stained the sections with Harris haematoxylin (one minute)
18. Washed with tap water.
19. Bluing of haematoxylin was done with scotts tap water.
20. Washed with tap water.
21. Sections were air dried and mounted with Cytoseal ™ 60 (Electron Microscopic Sciences, USA) and cover slipped. .

Each immunohistochemical experiment was repeated at least twice. Primary antibodies for macrophage markers CD 68 (ED1), CD 163 (ED2), cytoskeletal components vimentin and smooth muscle actin, and cyokines IL-6, IL-1α, IL-1β and TNF-α were used in the dilutions 1:150, 1:100, 1:200, 1:200, 1:500, 1:500, 1:250 and 1:500 respectively. A positive reaction was indicated by a brown coloured precipitate at sites of specific cellular antigen localization. For negative controls incubation with primary antibody was substituted with PBS alone, and all other procedures followed as with test samples. Slides were analysed via light microscopy using a trinocular microscope (Nikon Eclipse Model E600, Japan) and images captured using a digital camera (Nikon model DXM1200F, Japan) with ACT-1 software.

3.4.4. Transmission Electron Microscopic analysis

3.4.4.1. Sample Processing

Tissue samples harvested at 5, 45, 90 and 120 days were grossed into $1mm^3$ size and fixed in 3% gluteraldehyde in phosphate buffer. The 8% gluteraldehyde (Polyscience, USA) stock was diluted to 3% using Sorenson's phosphate buffer (0.1 M, pH 7.4). 40.5ml of 0.2M disodiumhydrogen phosphate was mixed with 0.2M of sodium dihydrogen phosphate to obtain 0.1 M Sorensons phosphate buffer, pH 7.4.

3.4.4.1.1 Fixation

Gluteraldehyde was discarded and samples were washed with cold phosphate buffer (pH 7.4), 4 changes, for 10 minutes each, with sample vials standing in an ice bath. Samples were then placed in 1% OsO_4 for 2 hours and thereafter washed with phosphate buffer, 4 changes for 15 minutes each, in an ice bath. Samples were then rinsed in distilled water for five minutes.

3.4.4.1.2 Dehydration

The samples were dehydrated in ascending grades of acetone using the following protocol:

i. 50% acetone, 10 minutes (2 changes) in cold.
ii. 70% acetone, 10 minutes in cold. (stored overnight in refrigerator)
iii. 70% acetone, 10 minutes at room temperature (RT).
iv. 90% acetone, 10 minutes (2 changes) at room temperature
v. 100% acetone, 15 minutes (4 changes) at room temperature
vi. 100% dry acetone, 15 minutes at room temperature

3.4.4.1.3 Infiltration

Samples were placed in two changes of propylene oxide for five minutes each and then transferred into propylene oxide-resin mixtures of ratio 3:1 for two hours, 1:1 for two hours and finally kept overnight in vacuum in a propylene: epoxy resin mixture of ratio of 1:3. Final infiltration was carried out in pure resin prior to embedding.

3.4.4.1.4 Embedding

The samples were embedded in molds containing the epoxy resin - Polybed 812 mixed with dodecenyl succinic anhydride (DDSA – Hardener), Nadic methyl anhydride (NMA – Hardener), Dimethylaminomethyl phenol (DMP – Accelerator) in appropriate ratios as per the kit instructions (Polysciences Inc, USA) and polymerized at 60°C in an oven for three days.

3.4.4.1.5 Sectioning

For light microscopy semithin sections (~ 1μm) were cut using a glass knife in an ultramicrotome. Once the area of interest was identified, the remaining areas of the block were trimmed off. Ultrathin sections (50-70nm) were cut using a diamond knife (Diatome®) and collected onto the shiny side of copper grids of 300 mesh size.

3.4.4.2. Staining for Light Microscopy (LM)

The semithin sections were stained with Toludine blue.

i. Sections were taken onto a few drops of water on a slide and a drop of toludine blue was added.
ii. Sections were heated on a hot plate for a few seconds.
iii. The sections were washed well in distilled water and air dried.
iv. The sections were mounted using DPX and the photographs were taken using the trinocular microscope (Nikon Eclipse Model E600, Japan) and images captured using a digital camera (Nikon model DXM1200F, Japan) with ACT-1 software.

3.4.4.3. Staining for TEM

i. All grids were made wet by dipping in distilled water.
ii. The grids were immersed in filtered Uranyl Acetate for two hours with the section side up.
iii. The grids were washed in methanol series (100%, 80%, 50%), and then washed with distilled water.
iv. The grids were placed on a filter paper to dry.
v. 0.025g of Lead Citrate was dissolved in 10ml 0.1N NaOH and centrifuged for 10 minutes.
vi. Sodium hydroxide pellets were placed in a Petri dish to eliminate carbon dioxide. The grids were then floated onto the drop of lead citrate on a parafilm placed in the carbon dioxide-free petri dish, with section side facing down and incubated for 10 minutes.
vii. The grids were washed in four changes of distilled water collected in beakers. The first two beakers contained two drops of NaOH solution.

3.4.4.1.5 Sectioning

For light microscopy semithin sections (~ 1μm) were cut using a glass knife in an ultramicrotome. Once the area of interest was identified, the remaining areas of the block were trimmed off. Ultrathin sections (50-70nm) were cut using a diamond knife (Diatome®) and collected onto the shiny side of copper grids of 300 mesh size.

3.4.4.2. Staining for Light Microscopy (LM)

The semithin sections were stained with Toludine blue.

i. Sections were taken onto a few drops of water on a slide and a drop of toludine blue was added.
ii. Sections were heated on a hot plate for a few seconds.
iii. The sections were washed well in distilled water and air dried.
iv. The sections were mounted using DPX and the photographs were taken using the trinocular microscope (Nikon Eclipse Model E600, Japan) and images captured using a digital camera (Nikon model DXM1200F, Japan) with ACT-1 software.

3.4.4.3. Staining for TEM

i. All grids were made wet by dipping in distilled water.
ii. The grids were immersed in filtered Uranyl Acetate for two hours with the section side up.
iii. The grids were washed in methanol series (100%, 80%, 50%), and then washed with distilled water.
iv. The grids were placed on a filter paper to dry.
v. 0.025g of Lead Citrate was dissolved in 10ml 0.1N NaOH and centrifuged for 10 minutes.
vi. Sodium hydroxide pellets were placed in a Petri dish to eliminate carbon dioxide. The grids were then floated onto the drop of lead citrate on a parafilm placed in the carbon dioxide-free petri dish, with section side facing down and incubated for 10 minutes.
vii. The grids were washed in four changes of distilled water collected in beakers. The first two beakers contained two drops of NaOH solution.

viii. The grids were then dried and viewed under the Transmission Electron Microscope (Hitachi H-600) at an accelerating voltage of 75kV and photographs (Kodak Illford film) were taken.

3.5. *IN VITRO* STUDIES

3.5.1. Cytoskeletal rearrangments and cytokine profile in L929 fibroblasts cultured with CoCr alloy particles.

3.5.1.1. Cell lines and culture conditions

Murine connective tissue fibroblasts, L929 (ATCC Number CCL1, ATCC, Virginia, USA) were maintained in Minimum Essential Medium (MEM, Sigma) supplemented with 10% Fetal bovine serum (GIBCO), 2mM L-Glutamine (SIGMA), Sodium bicarbonate (SIGMA) and 1% Penicillin-streptomycin (SIGMA). Cells were grown in a humidified incubator at 37°C with 5% CO_2.

Murine L929 fibroblasts at a density of 4 x 10^3 were seeded onto glass coverslips inserted into 24 well tissue culture plates. Cells were grown overnight in MEM medium, following which they were fed with fresh medium containing CoCr alloy particles at varying concentrations of 0.3 mg/cm^2, 0.5 mg/cm^2, 1 mg/cm^2, 5 mg/cm^2 and 8 mg/cm^2. Cells without any metal particles served as control.

3.5.1.2. Phase contrast and Scanning electron microscopy studies

Following 72 hours culture of L929 fibroblasts with CoCr alloy particles at varying concentrations of 0.3 mg/cm^2, 0.5 mg/cm^2, 1 mg/cm^2, 5 mg/cm^2 and 8 mg/cm^2, cells were viewed directly using a Phase contract microscope (Leica DMIL, Germany) and images captured using the digital camera (Leica DFC 280).

For SEM analysis, cells were washed thrice with PBS and fixed overnight in 3% gluteraldehyde. Cells were dehydrated in increasing concentrations of alcohol using the following protocol:

i) 30% ethanol, two changes – 15 minutes each

ii) 50% ethanol, two changes – 15 minutes each

iii) 70% ethanol, two changes – 15 minutes each

Samples were kept in 70% ethanol till viewing. Samples were viewed using the E-SEM, Quanta 200 (FEI, Netherlands) under low vacuum conditions.

3.5.1.3. Cytoskeletal rearrangements in L929 fibroblasts grown with CoCr particles

Murine L929 fibroblasts cultured with and without CoCr alloy particles at concentrations of 0.3 mg/cm^2, 0.5 mg/cm^2 and 1 mg/cm^2, were washed thrice with PBS and fixed overnight in 4% paraformaldehyde. Cytoskeletal rearrangement of F-actin filaments were studied by fluorescent labeling with Phalloidin-TRITC conjugate (SIGMA). Changes in focal adhesion organization was studied by immunofluorescent labeling of α-actinin (Santa cruz biotechnology, Inc USA). The following methodology for specific staining was adopted:

i) Washed cells with PBS, two changes, five minutes each.

ii) Incubated cells with Triton X100 (0.1% in PBS) for ten minutes.

iii) Non specific binding sites were blocked using BSA (1% in PBS) for fifteen minutes.

iv) Incubated cells with Triton X100 (0.1% in PBS) for two minutes.

v) Incubated cells with primary antibody, goat anti mouse α-actinin (at 1:100 dilution) for one hour.

vi) Washed cells with PBS, three changes, five minutes each.

vii) Incubated cells with secondary antibody FITC conjugated rabbit anti goat (PIERCE, USA, at 1:50 dilution) for one hour.

viii) Washed cells with PBS, three changes, five minutes each.

ix) Incubated cells with Phalloidin-TRITC conjugate, for twenty minutes.

x) Washed cells with PBS, three changes, five minutes each.

xi) Mounted in fluorescent mounting medium S3023 (Dakocytomation) and coverslipped.

All steps from vii – xi were performed in dark. Cells were viewed under confocal laser scanning microscope (Carl Zeiss, LSCM 510 Meta, Germany) using 543, 488nm excitation filters and Band Pass (BP) 560-615nm, Long Pass (LP) 505nm emission filters. Images were obtained in z stack to view cytoskeletal and focal adhesion rearrangements in three dimension.

3.5.1.4. Expression profile the cytokines IL-6 and IL-1α

L929 fibroblasts were cultured with CoCr alloy particles at varying concentrations of 0.3 mg/cm^2, 0.5 mg/cm^2, 1 mg/cm^2, 5 mg/cm^2 and 8 mg/cm^2. Following 72 hours incubation, medium was harvested and stored at -80°C till further downstream analysis of the cytokines IL-6 and IL-1α. The expressions of these proinflammatory cytokines were studied using the commercially available ELISA kits from Biosource International Inc, USA. Readings were obtained at 450nm using a automated microplate reader TECAN infinite F200 (Austria) with the software Magellan version 6.1 and results compared with standard concentrations read on the same plate. The experiment was performed in duplicate and repeated twice. Statistical analysis of the data was done using the Students t test. Probability (P) values < 0.05 were considered significant.

3.5.2. Proteomic profile of human fibroblasts cultured with CoCr alloy particles and effect of the conditioned media on human monocyte cultures.

3.5.2.1. Cell lines and culture conditions

Human lung fibroblast cell line MRC-5 (ATCC Number CCL-171, ATCC, Virginia, USA) was maintained in Minimum Essential Medium (MEM 5650, Sigma) supplemented with 10% Fetal bovine serum (GIBCO), 2mM L-Glutamine (GIBCO), 1mM Sodium Pyruvate (SIGMA) and 1% Penicillin-streptomycin (GIBCO).

Human monocyte cell line U-937 (ATCC Number CRL-1593.2, ATCC, Virginia, USA) were cultured in RPMI 1640 medium (GIBCO) supplemented with L-Glutamine, 25mM HEPES (GIBCO) and adjusted to contain 10% Fetal bovine serum (GIBCO), 1.0mM Sodium Pyruvate (SIGMA), 1.5g/L of Sodium bicarbonate (SIGMA), 4.5g/L glucose (SIGMA), and 1% Penicillin-streptomycin (GIBCO).

Both cells were grown in a humidified incubator at 37°C with 5% CO_2.

3.5.2.2. Particle preparation for culture with fibroblast

The CoCr alloy particles (ASTM F75) were weighed into centrifuge tubes and autoclaved at 121°C for 30 minutes, before introduction into the cell culture system.

3.5.2.3. Fibroblast viability response to CoCr particles

3.5.2.3.1 Microscopic evaluation

Fibroblast were grown in T-25 flasks with medium for 24 hours, following which the cells were fed with fresh medium containing CoCr alloy particles in varying concentrations of 0.05mg/cm^2, 0.5mg/cm^2, 1mg/cm^2 and 5mg/cm^2. The cells were examined microscopically after 24 and 72 hours. Fibroblasts not exposed to CoCr particles served as controls. Each test was done in duplicate.

3.5.2.3.2 MTS-assay

Fibroblasts were seeded onto 96 well plates at a density of 1 x 10^4 and grown in medium for 24 hours, following which they were fed with fresh medium containing CoCr alloy particles in varying concentrations of 0.3mg/cm^2, 0.5mg/cm^2, 1mg/cm^2, 2mg/cm^2, 5mg/cm^2 and 8mg/cm^2. Fibroblasts not exposed to CoCr particles served as controls. The viability of the fibroblasts was assayed after 24 and 72 hours using the MTS-Assay (Promega CellTiter 96® AQueous One Solution Cell Proliferation Assay). Supernatant was read at 490nm using an Eliza plate reader (BioRad Micro plate reader, Model 680). The experiment was repeated thrice. Each set of experiment had four wells per metal concentration. Statistical analysis of the data was done using the Students t test. Probability (P) values <0.05 were considered significant.

3.5.2.4. Study design and proteomic analysis of fibroblast cultured with CoCr particles

Fibroblasts were subcultured into T-175 flasks and grown in medium for 24 hours following which they were fed with fresh medium containing CoCr alloy particles at a concentration of 0.5mg/cm^2. Fibroblasts not exposed to CoCr particles served as controls. After 72 hours, cells along with the particles were harvested, centrifuged at 800 rpm and the medium discarded. Cells were washed twice in PBS, lysed via sonication and incubated in 40mM Tris HCl pH8. Proteins were extracted and analyzed using 2D gel electrophoresis and MALDI-TOF TOF MS. Biological replicates of the culture system were used.

3.5.2.5. Effect of conditioned media on monocyte U-937

Fibroblasts were sub-cultured into T-175 flasks and grown in 50% MEM and 50% RPMI-1640 medium for 24 hours following which they were grown in RPMI-1640 alone for a further 24 hour period. The fibroblasts cultures were then fed with

fresh RPMI-1640 medium containing CoCr particles at a concentration of 0.5mg/cm^2 and grown for 72 hours, following which the conditioned media from fibroblast-CoCr culture was collected. Fresh cultures of monocytes were initiated and grown in 40% conditioned medium from the fibroblast-CoCr cultures. Monocytes grown in RPMI-1640 alone served as controls. These cells were harvested after a 48 hour period, centrifuged at 800 rpm and the medium discarded. Cells were washed twice in PBS, lysed via sonication and incubated in 40mM Tris HCl pH8. Total cellular proteins were extracted for downstream analysis using 2D electrophoresis and MALDI-TOF TOF MS.

3.5.2.6. Protein extraction

Proteins were extracted using a buffer containing, 7M Urea, 2M Thiourea, 4% CHAPS (3-[(3-cholamidopropyl) dimethylammonio]-1-propane-sulfonate), 2mM Tributyl phosphine (TBP), together with protease inhibitor (HALT protease inhibitor cocktail, PIERCE) and endonuclease (SIGMA). The extract was ultra centrifuged at 81,000 rpm for 1 hour at 20°C to remove cellular fragments and/or debri. Supernatant obtained was aliquoted and stored at −80°C until analysis.

3.5.2.7. 2D gel electrophoresis (2DGE)

Amount of proteins in the samples were estimated using the RcDc protein assay kit (BioRad, Hercules, CA). For analytical gels, 100µg of sample was loaded onto each 17cm IPG strip. Protein samples were made up to 300µl, with 0.2% ampholytes, 20mM DTT (Dithiothreitol), extraction buffer and bromophenol blue. Isoelectric focusing was carried out with IPG strips of pH 3-10 (linear) and/or pH 4-7 (linear) (BioRad, Hercules, CA) using the PROTEAN IEF cell (BioRad, Hercules, CA). Strips were focused overnight using the following programme

250V for fifteen minutes

500V for one hour

1000V for one hour

10,000V for three hours

10,000V for 60,000Vhrs

500V for 24 hours

Since IEF was performed overnight the strips were refocused at 10,000V for fifteen minutes. The focused IPG strips were equilibrated and simultaneously reduction-alkylation performed using dithiothreitiol and iodoacetamide. The IPG strips were then embedded onto 12% SDS-PAGE gels. The second dimension SDS-PAGE was run using the PROTEAN II xi Cell (BioRad, Hercules, CA). Each gel was run at 15mA for 30 minutes and 30mA for a maximum of 5 hours. The proteins after separation by 2D Electrophoresis where visualized by silver staining of the gels. Silver staining was performed as per the modified protocol of Blum *et al*, 1987 (Improved silver staining of plant proteins, RNA and DNA in polyacrylamide gels. Electrophoresis 1987;8:93-99) described below:

i) Washed gels in distilled water for one minute.

ii) Gels were fixed in fixative (50% methanol and 10% acetic acid) for at least one hour.

iii) Washed with distilled water for ten minutes.

iv) Washed with 30% ethanol for ten minutes.

v) Sensitized for one minute with 0.02% Sodium thiosulfate ($Na_2S_2O_3$).

vi) Rinsed with distilled water for one minute.

vii) Impregnated with silver nitrate for twenty five minutes.

viii) Washed with distilled water three times for thirty seconds each.

ix) Developed image in developer (3% sodium carbonate, 0.05% formaldehyde (37%), 0.0005%sodium thiosulfate).

x) Washed with distilled water for twenty seconds.

xi) Stoped development using 1.4% EDTA-Na_2, for ten minutes.

xii) Rinsed with distilled water three times, one minute each, prior to drying or imaging.

3.5.2.8. Computer assisted image analysis of 2D Gels

Image acquisition and analysis were performed with an image scanner, GS 710 densitometer (BioRad) and image software PDQuest version 7.3 (BioRad Laboratories). Spot assignment was checked individually by visually inspecting each spot detected by the program and eliminating incorrectly assigned ones (caused by artifacts like specks, bubbles, streaks). Individual spot intensities where normalized against total density in gel image. Match sets for each time period were created. Each match set comprised of two replicate groups, control and experiment with each replicate group consisting of three replicate gels. The software performed an automatic Boolean analysis between the replicate groups using the criterion of 2 fold increase with a statistical significance of 90%.

3.5.2.9. Spot excision and In-gel proteolytic digestion

Spots in the experimental gels that changed consistently and significantly (greater than two fold increase) were manually excised and in-gel digestion performed along with sample desalting and cleaning using a Zip-Plate micro SPE Plate (Millipore, Bedford, MA, US). The peptides were eluted and spotted for further analysis onto MALDI TOF TOF MS target plates, using α-Cyano-4-hydroxycinnamic acid matrix.

Chapter 4

RESULTS AND DISCUSSION

4.1. CHARACTERIZATION OF SIZE AND SHAPE OF MATERIAL PARTICLES BY SEM

The CoCr alloy (ASTM-F75) particles were examined via light microscopy, TEM and SEM. All three analyses revealed the CoCr particles to be of a spherical shape with a smooth surface morphology (Figure 3). The metal particles were found to be in the size range of 1-7μm.

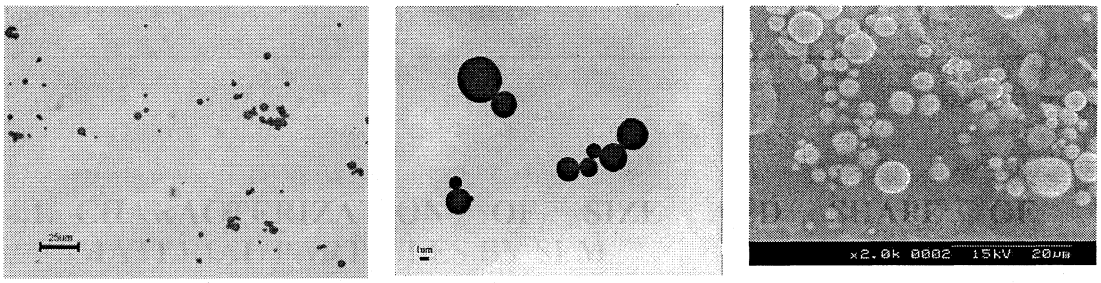

A B C

Figure 3: Light photmicrograph (A), Transmission electron micrograph (B) and Scanning Electron Micrograph (C) of the CoCr alloy particles

4.2. ENDOTOXIN TEST

The E-toxate kit found the CoCr particles to be endotoxin free.

4.3. *IN VIVO* EXPERIMENTATION

4.3.1. Histological analysis by Light microscopy

Cellular response at 14 time periods i.e, 1, 3, 5, 10, 15, 20, 30, 45, 60, 75, 90, 120 and 150 days was assessed by light microscopy.

Neutrophils and macrophages were seen adjacent to the CoCr alloy particles, as early as twenty four hours post implantation (Figure 4A & Figure 4B). The presence of these cell types indicates the host response to be that of acute inflammation.

Histological examination of three day samples revealed the CoCr alloy particles in both muscle and endomysium (connective tissue that encloses a muscle fibre) to be lined by a large number of inflammatory cells (Figure 4C). The inflammatory cells were also noted among the metal particles. The cellular profile was predominantly one of fibroblasts and fibrocytes. In and among these fibroblasts, numerous macrophages and isolated neutrophils were also noted (Figure 4D). The presence of these cell types suggests the transition into a late acute inflammatory stage. The histology was quite similar at five days also. Presence of numerous macrophages and numerous fibroblasts was observed adjacent along the metal particles (Figure 4E & Figure 4F).

One week post implantation the presence of numerous fibroblasts, macrophages and occasional formation of multinucleated foreign body giant cells (FBGC) were observed (Figure 5A). The presence of macrophages was more in and among the particles, while fibroblasts were located along the periphery (Figure 5B). Numerous small new blood vessels in the vicinity were also noted. These histological observations are indicative of the progression from an acute to a chronic inflammatory phase. This response persisted even at ten days post implantation, were chronic

inflammation with presence of fibrocytes, fibroblasts and macrophages was observed (Figure 5C).

As early as fifteen days, aggregation of the metal particles into distinct clumps was observed. These clumps appeared to be surrounded by spindle shaped cells (Figure 5D). Onset of fibrosis with presence of numerous fibroblasts, macrophages and few fibrocytes was noted (Figure 5E).

The presence of moderate number of macrophages and spindle shaped cells was observed at the implant site even at twenty days, indicating a persistent chronic inflammatory response to the CoCr alloy particles (Figure 5F). At thirty days differences in host response to particles located in muscle fibre and endomysium could clearly be observed (Figure 6A). Excessive fibrosis characterised by the presence of large numbers of fibroblasts, fibrocytes, new blood vessels was noted around particles located in the endomysium (Figure 6B). In and among the metal particles few macrophages were also observed. The tissue response around CoCr alloy particles located in muscle fibre was mild and comprised predominantly of few fibroblasts and macrophages (Figure 6C).

At forty five days post implantation, the inflammatory cell type comprised largely of macrophages with fibroblasts; indicating the persistence of the chronic inflammatory response (Figure 6D). The chronic inflammatory response continued at sixty days. Clumping of particles with excessive fibrosis, presence of numerous blood vessels, fibroblasts and fibrocytes was noted in the endomysium (Figure 6E). In muscle fibre, macrophages and fewer spindle shaped cells were observed adjacent to the metal particles (Figure 6F).

Light microscopic evaluation revealed the persistence of a chronic inflammatory response to the CoCr particles, at seventy five (Figure 7A) and ninety days (Figure 7B) post implantation. The cellular profile being one of a large number of macrophages and few spindle shaped cells. At later time periods of four (Figure 7C & Figure 7D) and five (Figure 7E & Figure 7F) months, excessive fibrosis was noted near particles in the endomysium. The particles appeared clumped into groups that were neatly surrounded by fibrous capsule like structures. Presence of few fibroblasts and fibrocytes and large number of blood vessels were noted. These results suggest the host response to be a walling of the implanted CoCr alloy particles. The inflammatory response at these time periods in muscle fibre was mild and was characterised by the presence of scant macrophages.

4.3.2. Transmission Electron Microscopic evaluation

The cellular response was further investigated at the ultrastructural level at specific time periods.

Light micrographs of the toluidine blue stained semi thin sections revealed the presence of inflammatory cells adjacent to the cobalt chromium (CoCr) particles as early as five days (Figure 8A). Most of these cells appeared to be macrophages and plump fibroblasts. These results were substantiated in the electron micrographs. Figure 8B shows the presence of a macrophage as identified by their large indented or bean shaped euchromatic nuclei, the cytoplasm of the cell is not visible probably due to the plane of cutting. CoCr alloy particles in the vicinity are also noted. The area appears to be highly regenerative as evidenced by the presence of a large number of blood vessels Figure 8C. Presence of CoCr alloy particles and short strands of collagen in the vicinity are also noted on close observation. These collagen strands are

short and randomly dispersed. In Figure 8D a portion of fibroblast cell is seen, the amount of heterochromatin is reduced and distributed along the periphery of the cell. Figure 8E shows collagen in the implantation site. The characteristic periodic striations of the collagen bundles is clearly visible. In this context it was interesting to note that the long collagen fibrils are arranged in parallel bundles while the short collagen strands are randomly dispersed. Figure 8F shows the presence of many metal particles. Among these particles collagen bundles are observed. The identity of metal particles were confirmed by X ray diffraction (Figure 8G).

Light microscopical analysis of toulidine blue stained sections of fortyfive day samples, revealed the presence of inflammatory cells and new blood vessels (Figure 9A & Figure 9B). TEM analysis of fortyfive day samples showed the presence of mast cells and macrophages most of latter coalescing probably in an attempt to form foreign body giant cells (Figure 9C). Figure 9D is a higher magnification of the FBGC. The presence of four nuclei can be clearly seen. The nuclei appear to be enclosed by a common cytoplasmic membrane that is highly ruffled indicating an active state. Presence of short strands of collagen is also visible in the vicinity of the FBGC. Figure 9E is a higher magnification of the mast cell. The characteristic presence of a highly granulated cytoplasm is clearly visible. Large numbers of short strands of collagen are observed near the mast cell. In Figure 9F, macrophages with their characteristic large indented nuclei are observed. Cells with long spindle shaped nuclei and highly ruffled cytoplasm are also seen.

At 90 days the presence of few spindle shaped cells and sparse collagen deposition was noted in the light micrographs of toluidine blue stained sections (Figure 10A & Figure 10B). These results were confirmed in the TEM micrographs.

Figure 10C shows the presence of a fibroblast, with the characteristic large oval nuclei and sparce cytoplasm. The chromatin appears to be thickened and distributed along the margins of the nucleus. The presence of collagen adjacent to the cell is noted. Figure 10D also shows the presence of collagen in transverse section that appears to be arranged as small parallel bundles. Scattered fragments of small fibrils of collagen are also observed. Figure 10E reveals a highly activated fibroblast. The presence of many secretory bodies in the cytoplasm is clearly evident in Figure 10F.

At longer time periods of 120 days, light micrographs reveal the presence of excessive fibrosis adjacent to the metal particles (Figure 11A & Figure 11B). In Figure 11C, presence of both fibrocytes and fibroblasts adjacent to the collagen bundles were observed. Figure 11D is a higher magnification, of the fibrocyte. A prominent oval shaped nucleus, and presence of vacuoles was noted. Adjacent to the cell, large amounts of collagen arranged in parallel bundles were observed. The characteristic banding pattern of collagen bundles was visible. In Figure 11E the presence of collagen as short fibrils and short bundles that are randomly arranged was also noted. Figure 11F shows the presence of blood vessels and numerous inflammatory cells adjacent to these vessels indicating the persistence of a chronic inflammatory response to CoCr alloy particles.

4.3.3. Immunohistochemical analysis

Immunohistochemical evaluation for the macrophage markers ED1, ED2, cytokines IL-6, IL-1β, IL-1α, TNF-α and cytoskeletal elements smooth muscle actin and vimentin were performed on cryosections of 5, 45, 90, 120 and 150 days sample.

Positive staining for the macrophage marker ED1 (CD68) and ED2 (CD163) was observed at five days (Figure 12A & Figure 13A), fourty five days (Figure 12B &

Figure 13B) and ninety days (Figure 12C & Figure 13C). The expression of ED1 is mainly localized on newly recruited macrophages while ED2 expression is more predominant on resident macrophages. Later time periods of four months (Figure 12D & Figure 13D) and five months (Figure 12E & Figure 13E) did not show the presence of either ED1 or ED2.

IL-1β was found to be absent at all the five time periods of five days (Figure 14A), fourty five days (Figure 14B), ninety days (Figure 14C), four months (Figure 14D) and five months (Figure 14E). These results suggest the non involvement of the cytokine IL-1β in mediating the inflammatory response to implanted CoCr alloy particles. The presence of IL-1α was detected at five (Figure 15A), fourty five (Figure 15B) and ninety days (Figure 15C). Most of the positively stained cells were found in and among the metal particles. Immunohistochemical evaluation of 120 days (Figure 15D) and 150 days (Figure 15E) sample did not show the presence of IL-1α. Positive staining for IL-6 was found to be present at early time periods of five days (Figure 16A) and fourty five days (Figure 16B) only. Expression of IL-6 was found to be absent at later time periods of 90 days (Figure 16C), 120 days (Figure 16D) and 150 (Figure 16E) days The expression pattern of TNF- α mirrored that of IL-6 with positive staining observed at five days (Figure 17A) and fourty five days (Figure 17B) only. Immunohistochemical evaluation of 90 days (Figure 17C), 120 days (Figure 17D) and 150 days (Figure 17E) sample did not show the presence of TNF-α.

The imunohistochemical markers of myofibroblasts smooth muscle α-actin and vimentin were also analysed. The expression for smooth muscle actin was detected at time periods of five (Figure 18A), forty five (Figure 18B) and ninety days (Figure 18C). The expression was absent at longer time periods of four months

(Figure 18D) and five months (Figure 18E). A similar trend was noted in the expression profile of vimentin. Positive staining was noted at five (Figure 19A), forty five (Figure 19B) and ninety days (Figure 19C) and an absence of staining noted at longer time periods of 120 days (Figure 19D) and 150 days (Figure 19E).

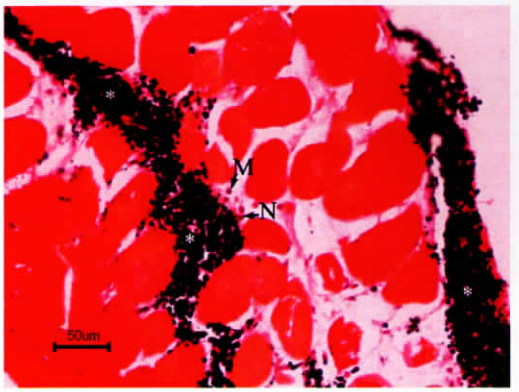

A (1 day)

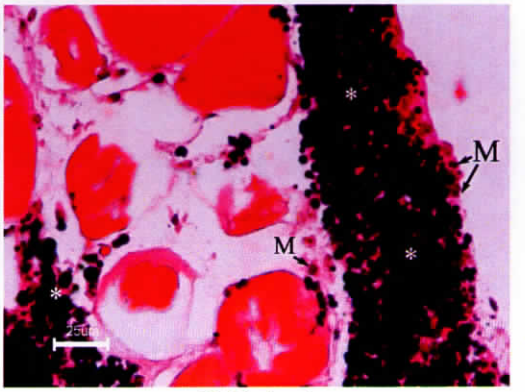

B (1 day)

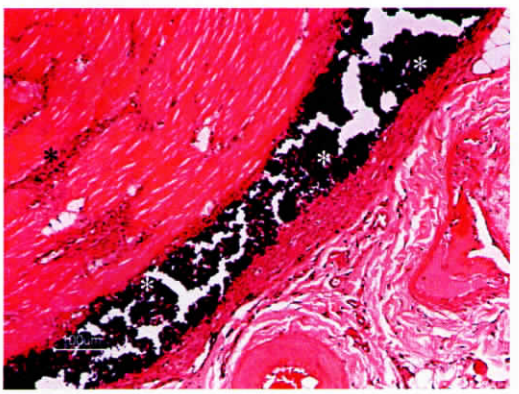

C (3 days)

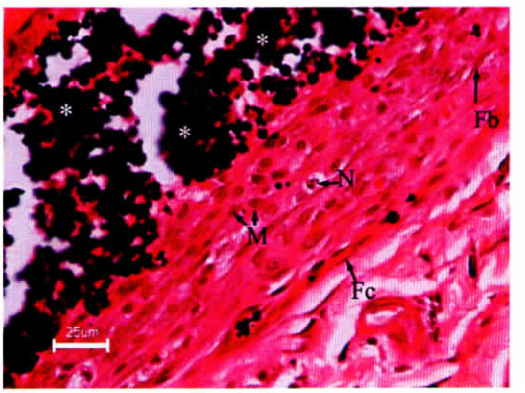

D (3 days)

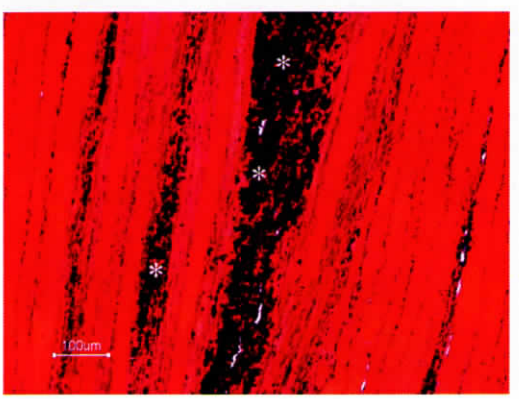

E (5 days)

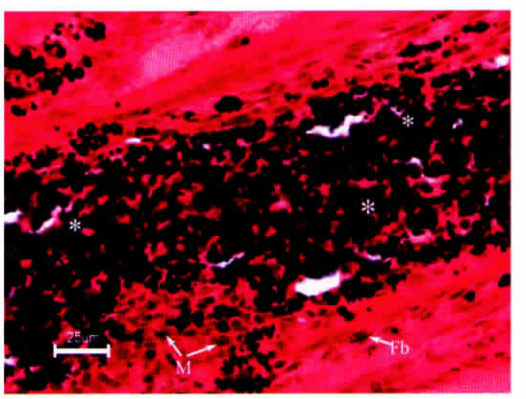

F (5 days)

Figure 4: Light micrographs of H&E stained sections of 1day (A, B); 3 days (C, D) and 5 days (E, F) muscle with CoCr alloy particles.

(M- macrophage, N- Neutrophils, Fb- Fibroblasts, Fc- Fibrocytes, FBGC- Foreign Body Giant Cells, * - CoCr alloy particles)

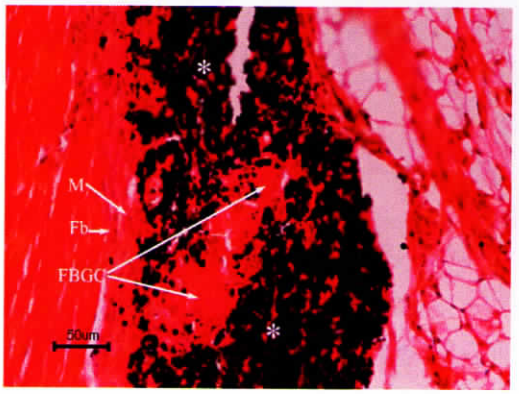

A (7 days)

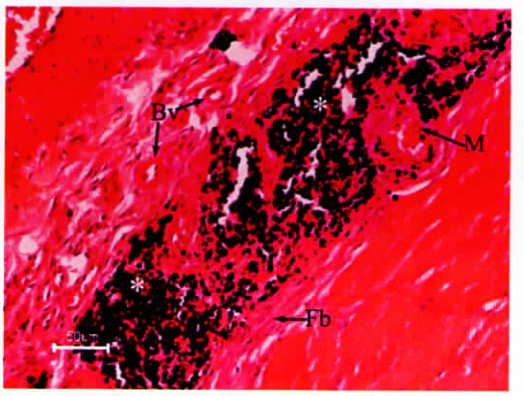

B (7 days)

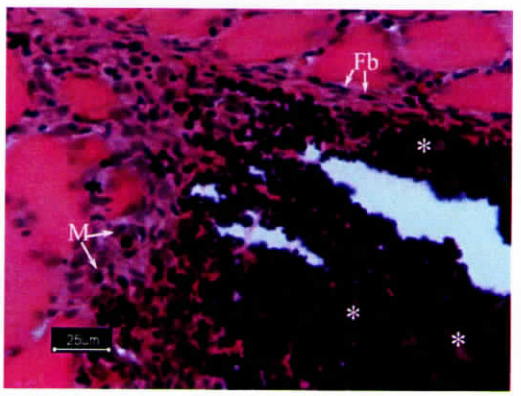

C (10 days)

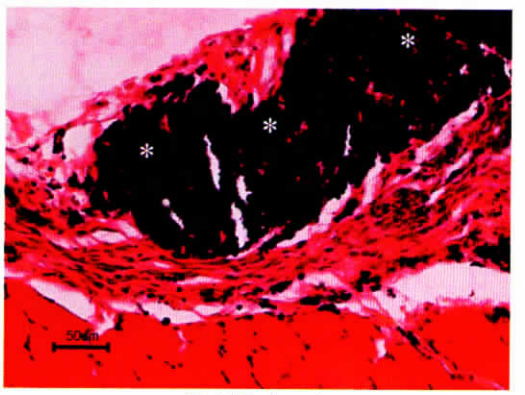

D (15 days)

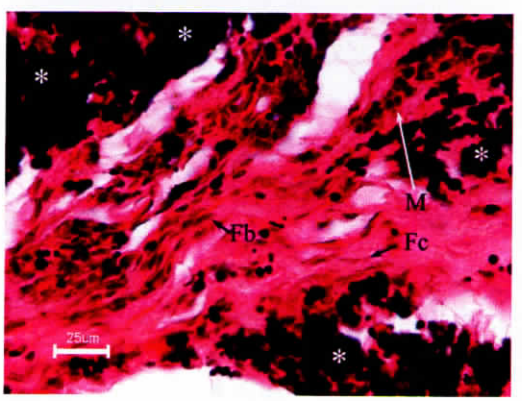

E (15 days)

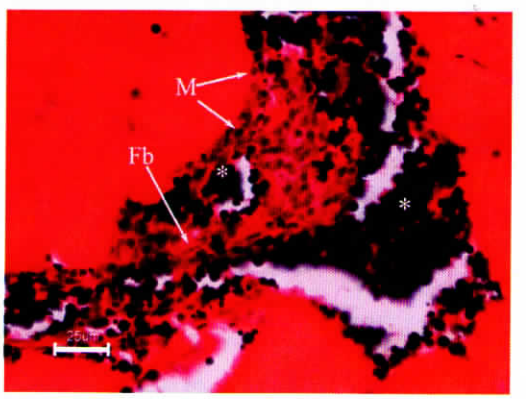

F (20 days)

Figure 5: Light micrographs of H&E stained sections of 7days (A, B); 10 days (C); 15 days (D,E) and 20 days (F) muscle with CoCr alloy particles.

(M- macrophage, N- Neutrophils, Fb- Fibroblasts, Fc- Fibrocytes, FBGC- Foreign Body Giant Cells, * - CoCr alloy particles)

A (30 days)

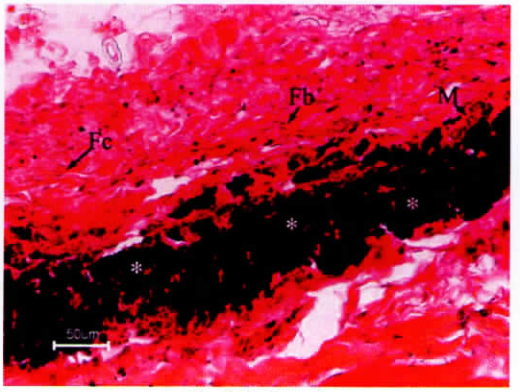

B (30 days)

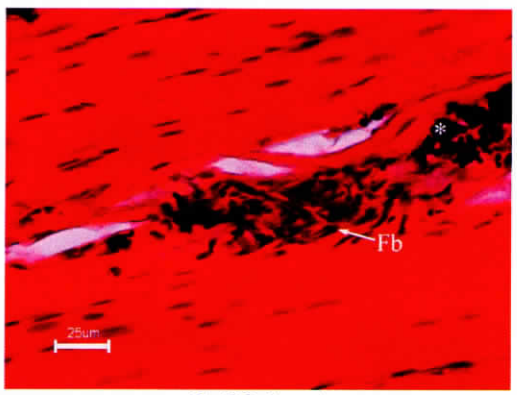

C (30 days)

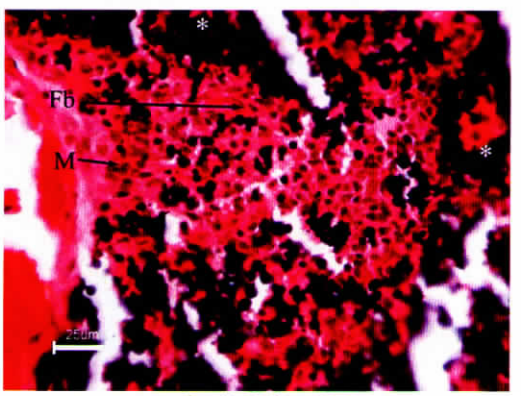

D (45 days)

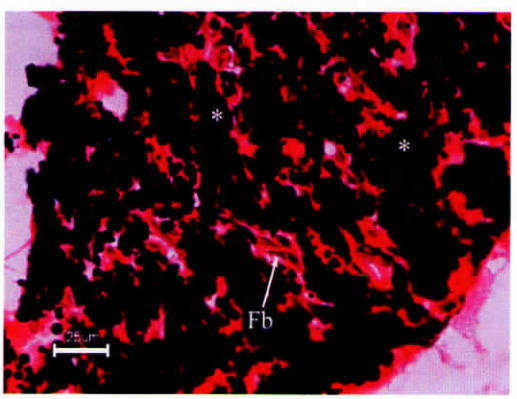

E (60 days)

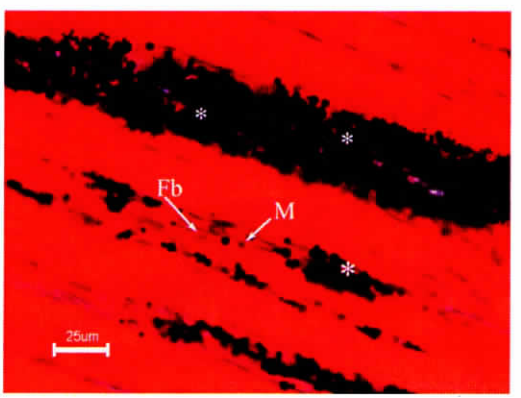

F (60 days)

Figure 6: Light micrographs of H&E stained sections of 30 days (A, B, C); 45 days (D) and 60 days (E, F) muscle with CoCr alloy particles.

(M- macrophage, N- Neutrophils, Fb- Fibroblasts, Fc- Fibrocytes, FBGC- Foreign Body Giant Cells, * - CoCr alloy particles)

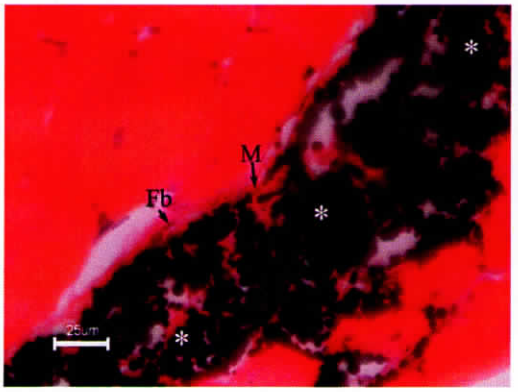

A (75 days)

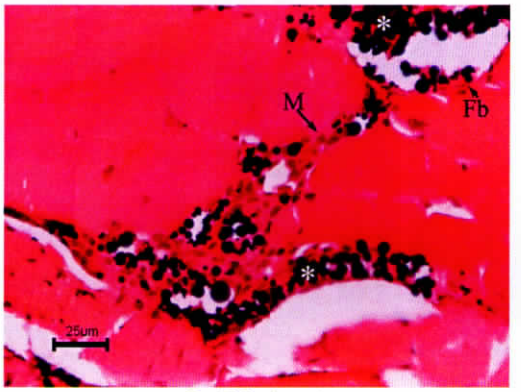

B (90 days)

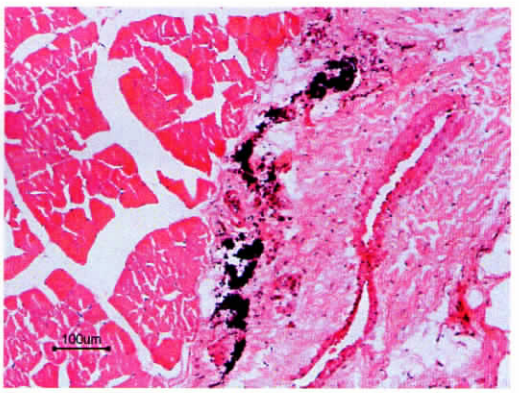

C (120 days)

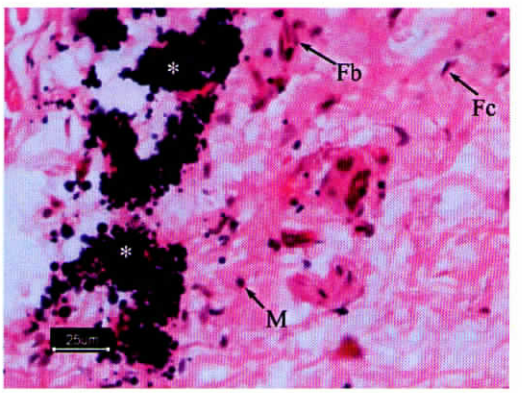

D (120 days)

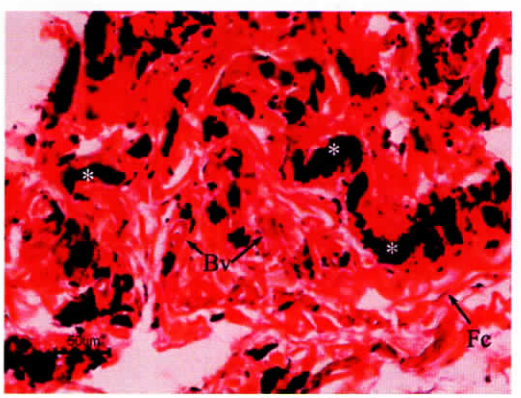

E (150 days)

F (150 days)

Figure 7: Light micrographs of H&E stained sections of 75 days (A); 90 days (B); 120 days (C, D) and 150 days (E, F) muscle with CoCr alloy particles.

(M- macrophage, N- Neutrophils, Fb- Fibroblasts, Fc- Fibrocytes, FBGC- Foreign Body Giant Cells, * - CoCr alloy particles)

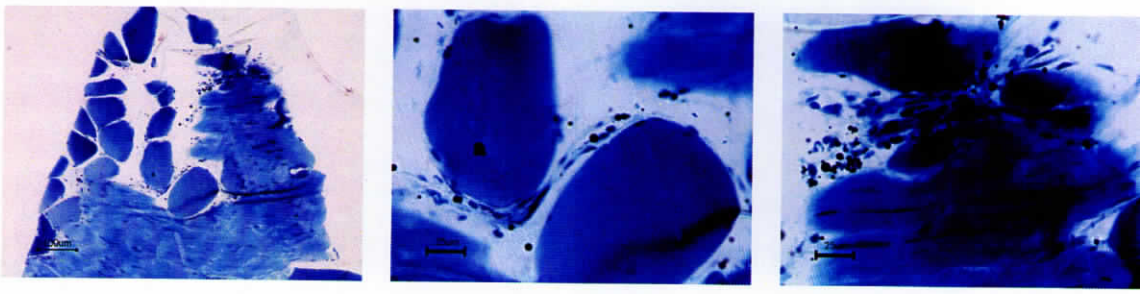

A

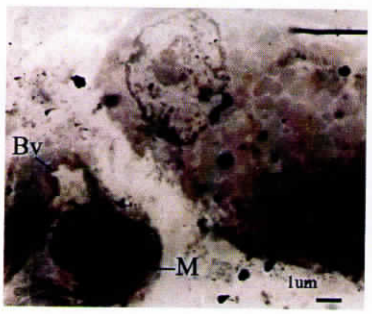

B

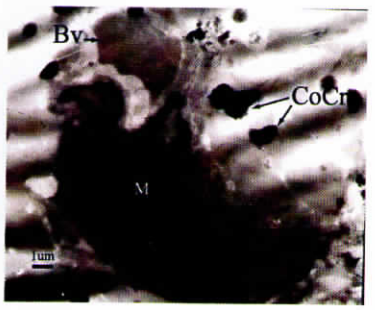

C

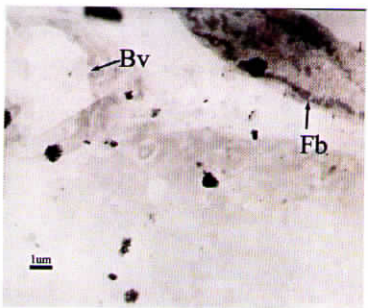

D

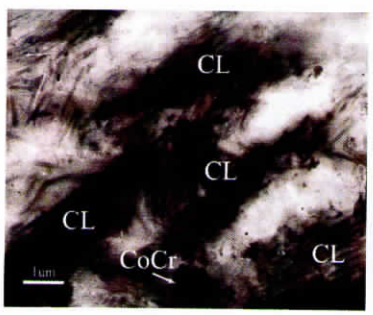

E

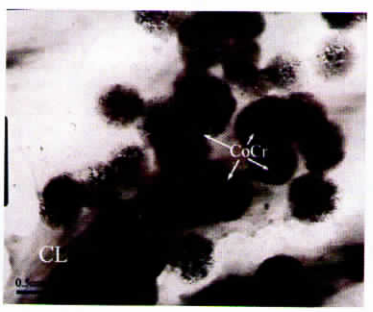

F

G

Figure 8: Light micrographs of toluidine blue stained sections of 5 days (A) muscle with CoCr alloy particles. Transmission electron micrographs showing ultrastructural details of tissue response around CoCr alloy particles (B, C, D, E, F) at 5 days. X ray diffraction pattern of the CoCr alloy particles in tissue (G).

(M- macrophage, Bv- Blood vessels, CL- collagen, Fb- Fibroblasts, CoCr-cobalt chromium metal alloy particles)

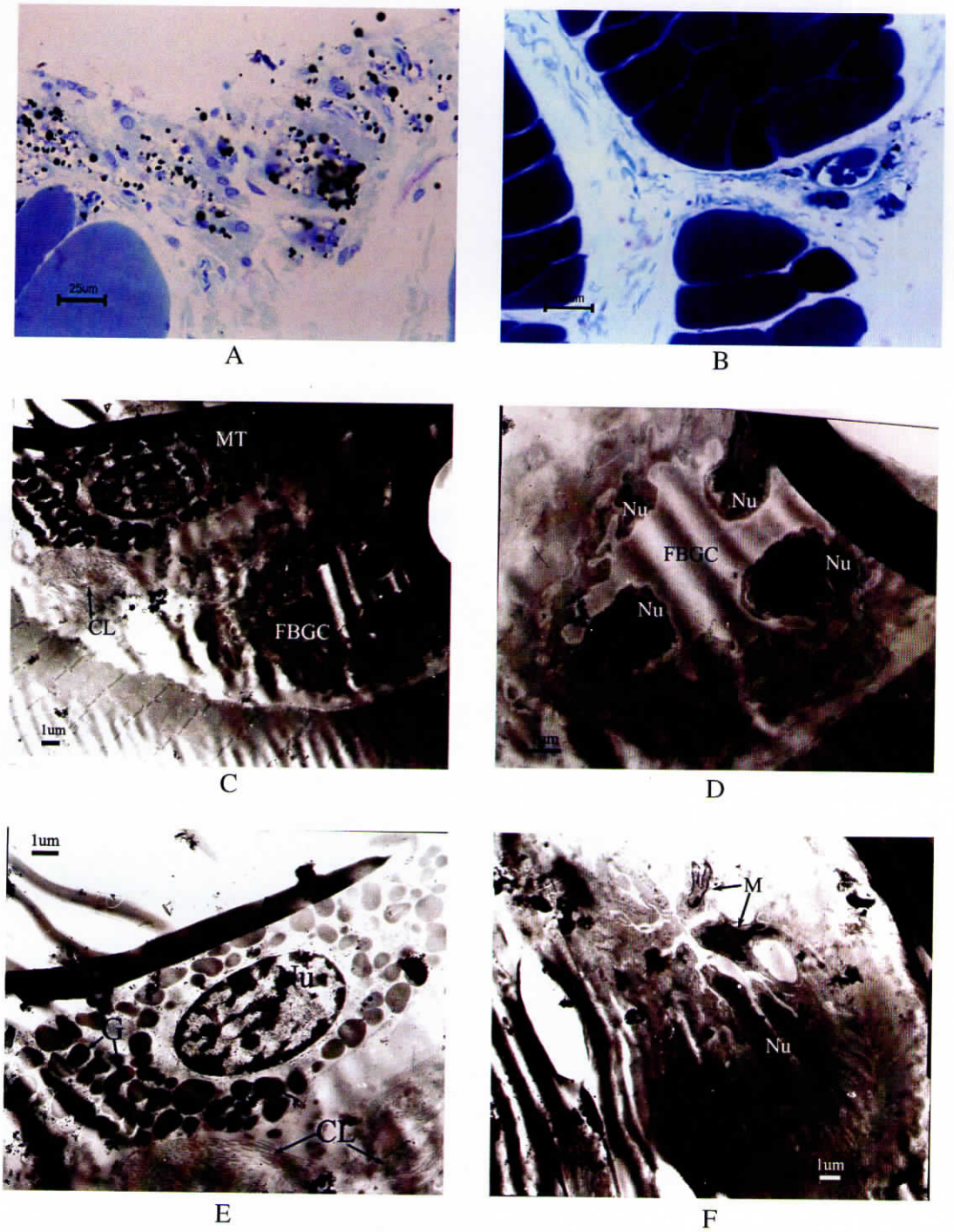

Figure 9: **Light micrographs of toluidine blue stained sections of 45 days (A, B) muscle with CoCr alloy particles. Transmission electron micrographs showing ultrastructural details of tissue response around CoCr alloy particles (C, D, E, F) at 45 days.**

(M- macrophage, MT- mast cells, CL- collagen, FBGC- Foreign Body Giant Cell, Nu- Nucleus, G- granules)

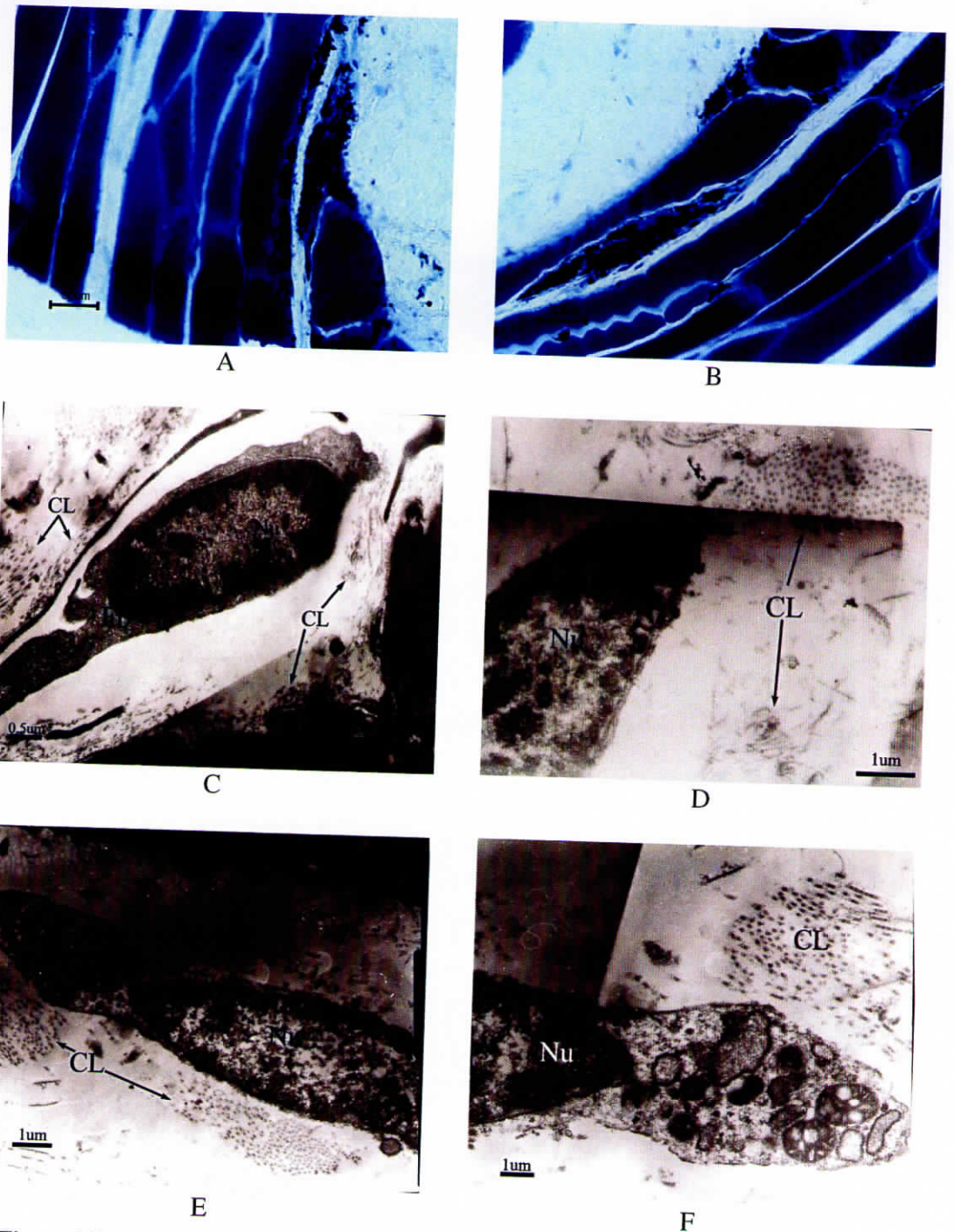

Figure 10: Light micrographs of toluidine blue stained sections of 90 days (A, B) muscle with CoCr alloy particles. Transmission electron micrographs showing ultrastructural details of tissue response around CoCr alloy particles (C, D, E, F) at 90 days.

(CL- collagen, Fb- Fibroblasts, Nu- Nucleus)

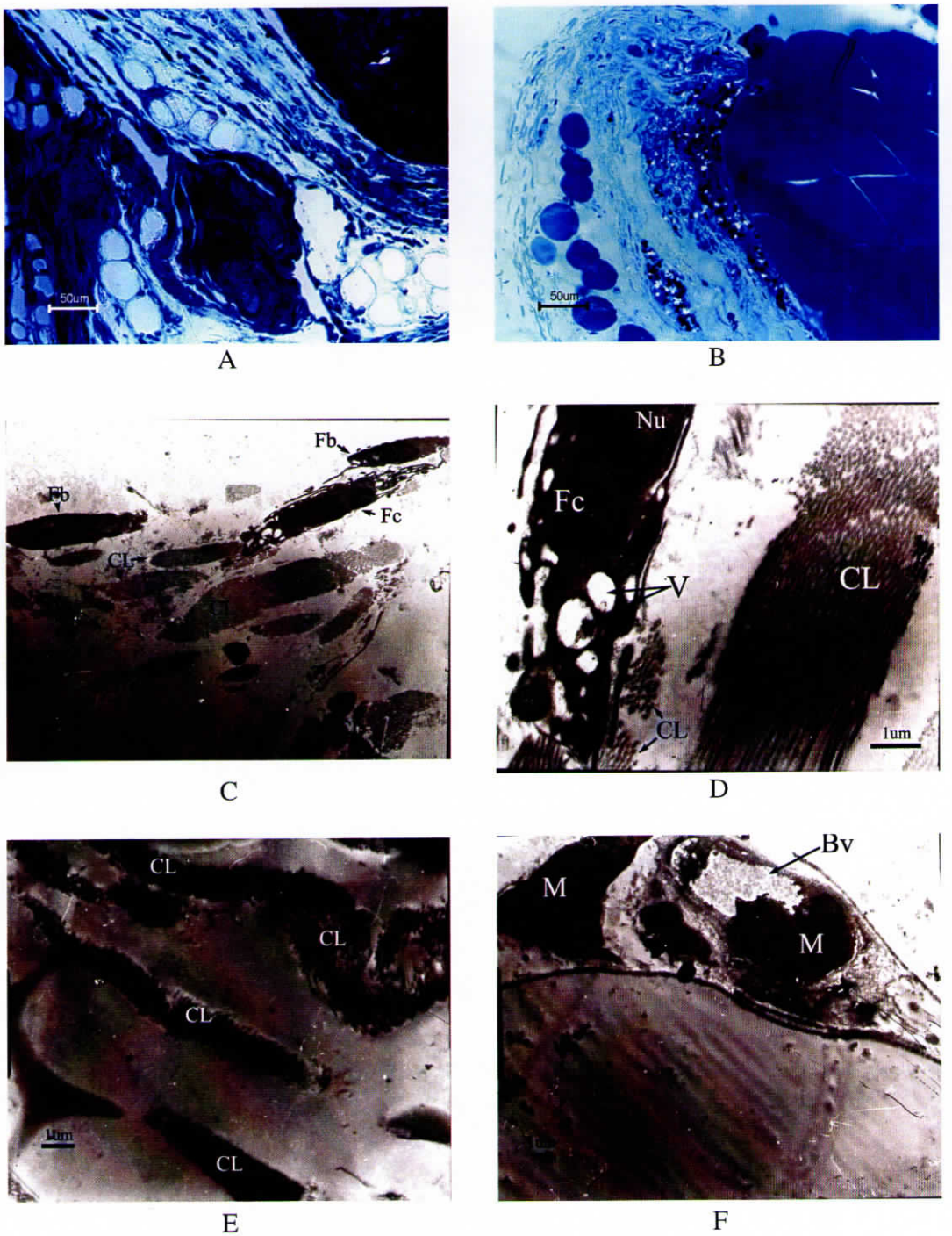

Figure 11: Light micrographs of toluidine blue stained sections of 120 days (A, B) muscle with CoCr alloy particles. Transmission electron micrographs showing ultrastructural details of tissue response around CoCr alloy particles (C, D, E, F) at 120 days.

(M- macrophage, CL- collagen, Fb- Fibroblasts, Fc- Fibrocytes, Nu- Nucleus, Bv- Blood vessels, V- vacuoles)

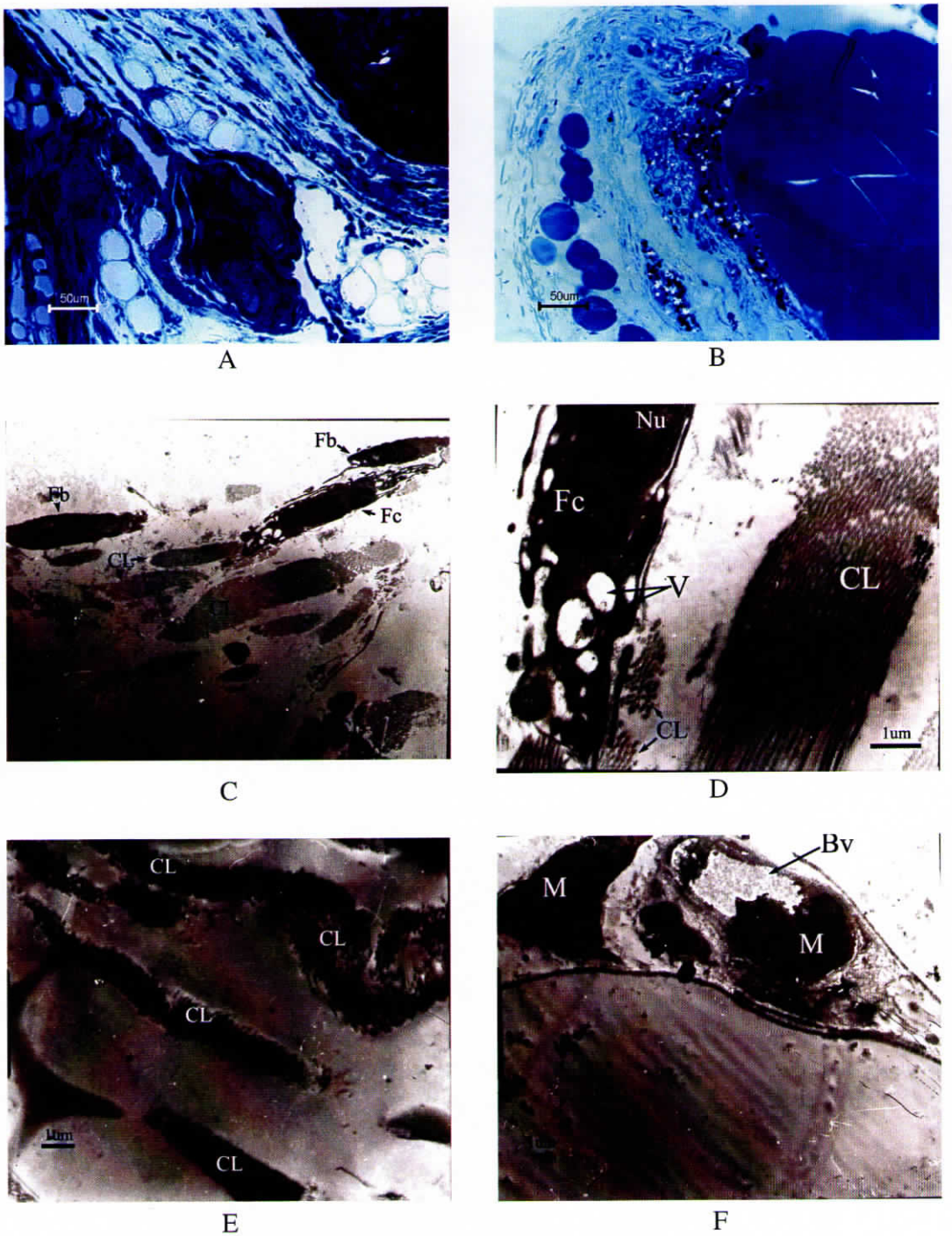

Figure 11: Light micrographs of toluidine blue stained sections of 120 days (A, B) muscle with CoCr alloy particles. Transmission electron micrographs showing ultrastructural details of tissue response around CoCr alloy particles (C, D, E, F) at 120 days.

(M- macrophage, CL- collagen, Fb- Fibroblasts, Fc- Fibrocytes, Nu- Nucleus, Bv- Blood vessels, V- vacuoles)

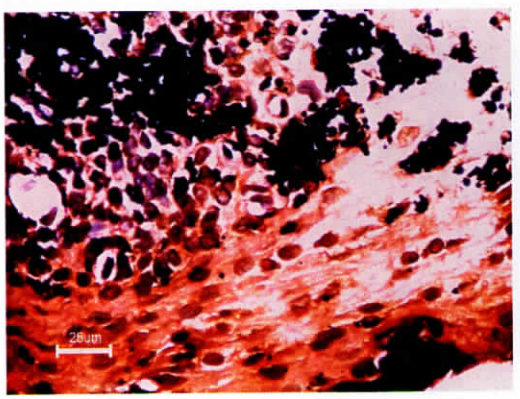

A (5 days)

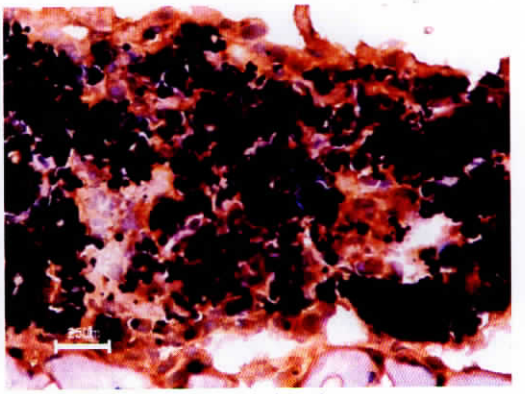

B (45 days)

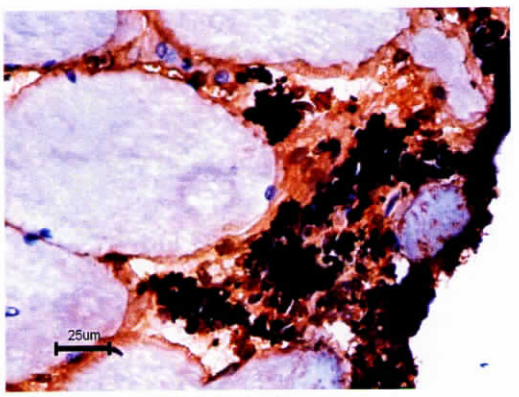

C (90 days)

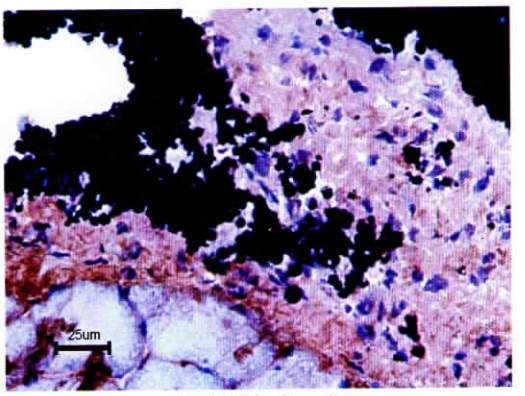

D (120 days)

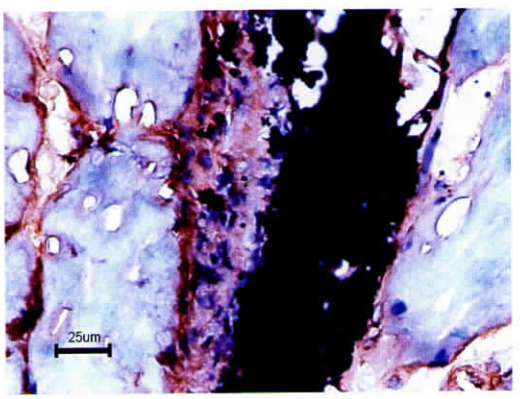

E (150 days)

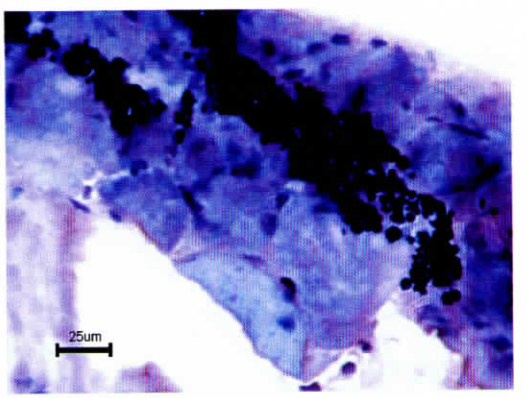

F (negative control)

Figure 12: Light micrographs of IHC, ED1 stained sections of 5 days (A); 45 days (B); 90 days (C); 120 days (D); 150 days (E) and negative control (F).

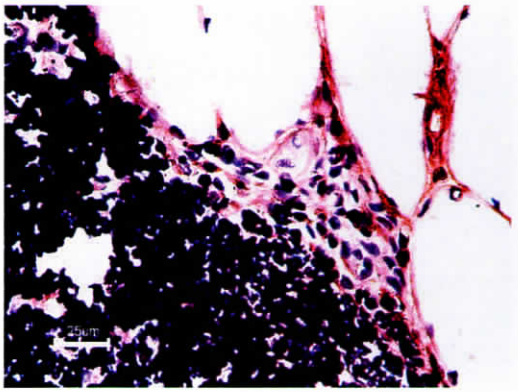

A (5 days)

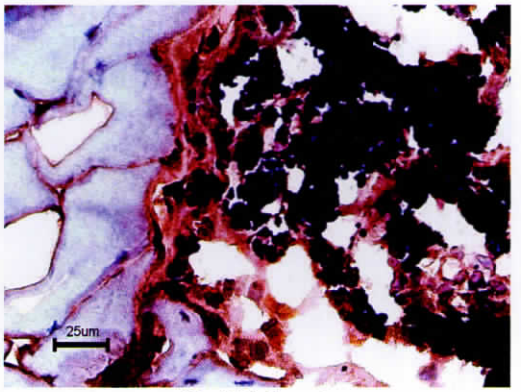

B (45 days)

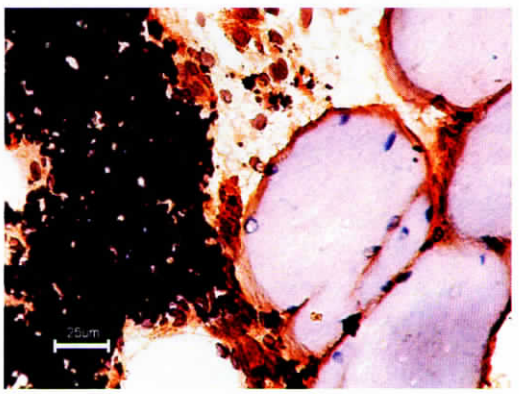

C (90 days)

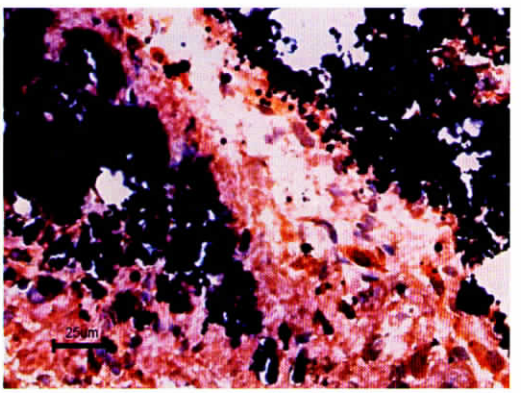

D (120 days)

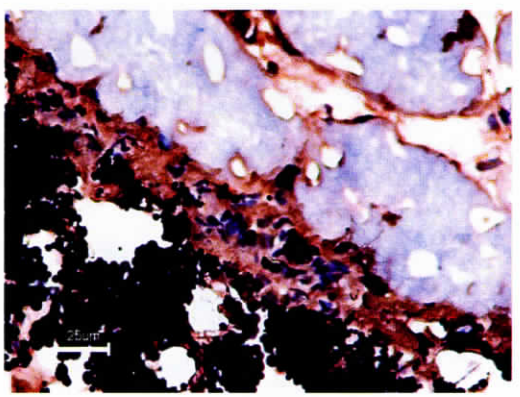

E (150 days)

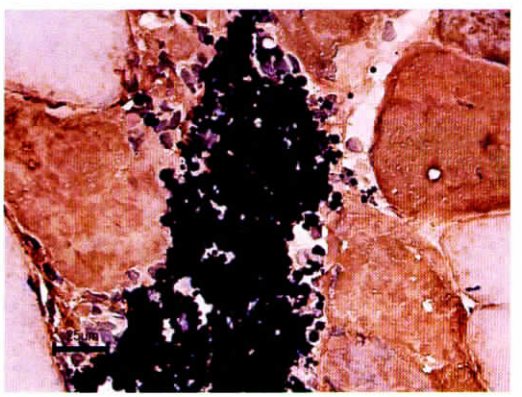

F (negative control)

Figure 13: Light micrographs of IHC, ED2 stained sections of 5 days (A); 45 days (B); 90 days (C); 120 days (D); 150 days (E) and negative control (F).

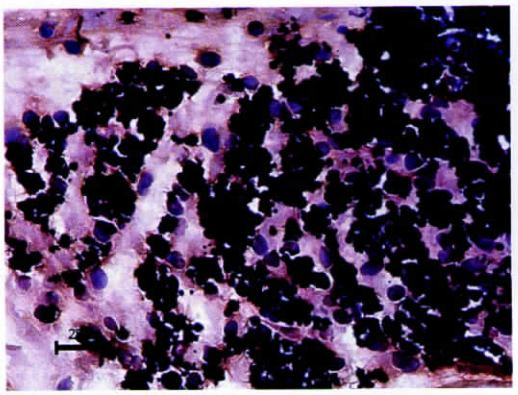

A (5 days)

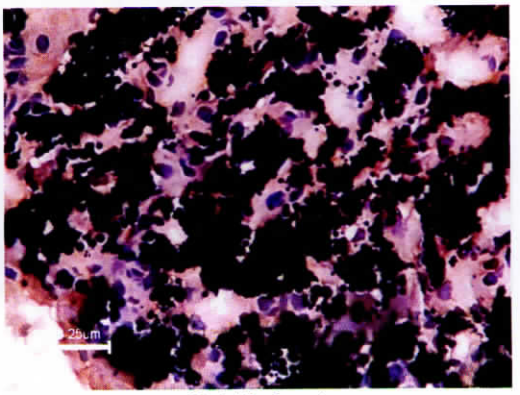

B (45 days)

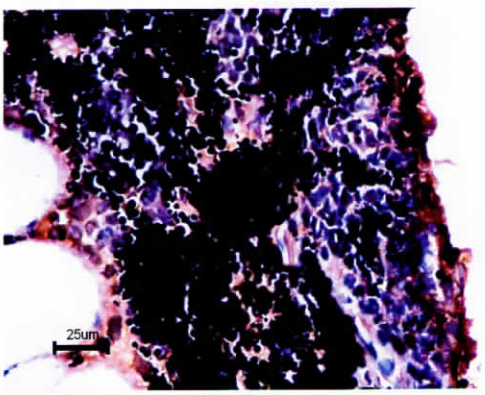

C (90 days)

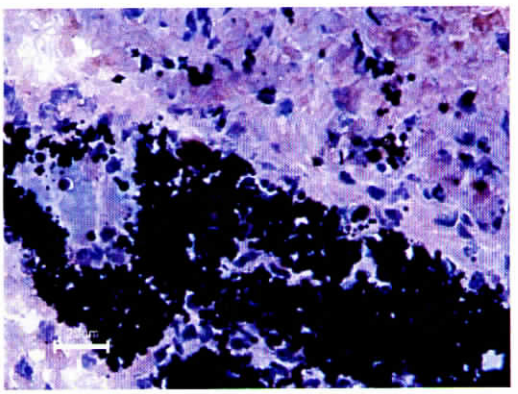

D (120 days)

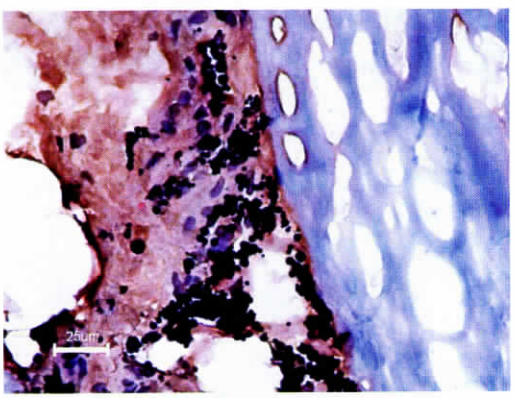

E (150 days)

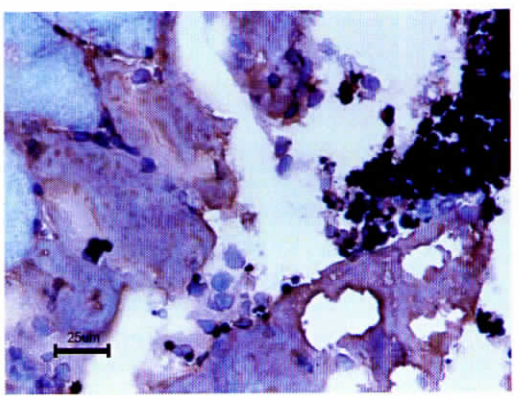

F (negative control)

Figure 14: Light micrographs of IHC, IL-1β stained sections of 5 days (A); 45 days (B); 90 days (C); 120 days (D); 150 days (E) and negative control (F).

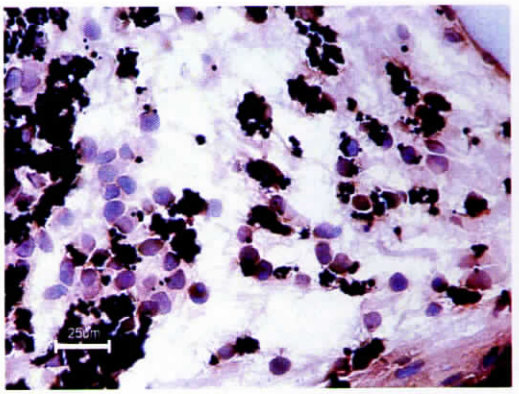

A (5 days)

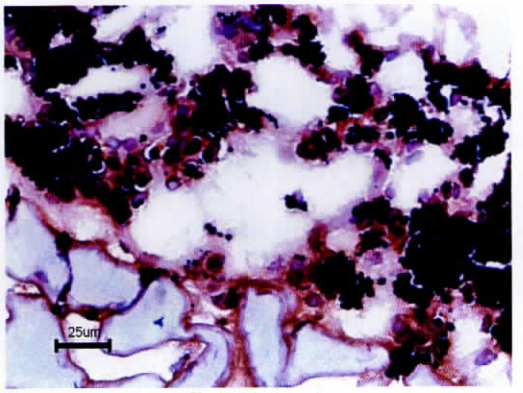

B (45 days)

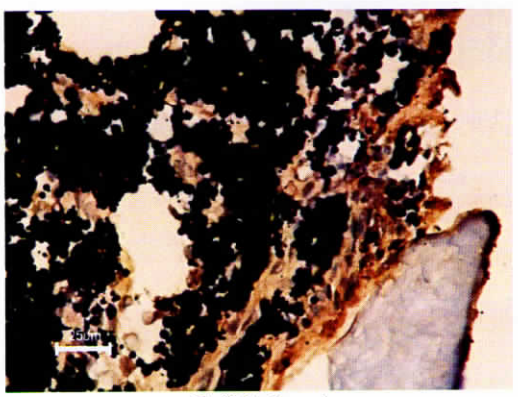

C (90 days)

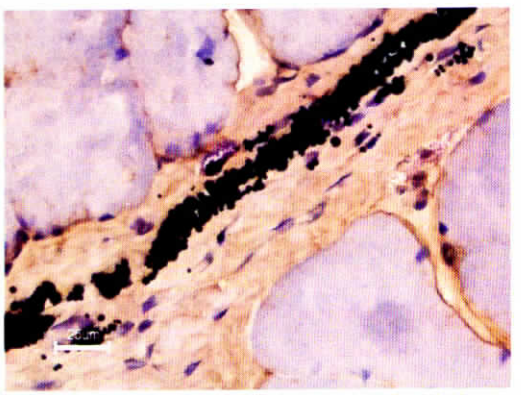

D (120 days)

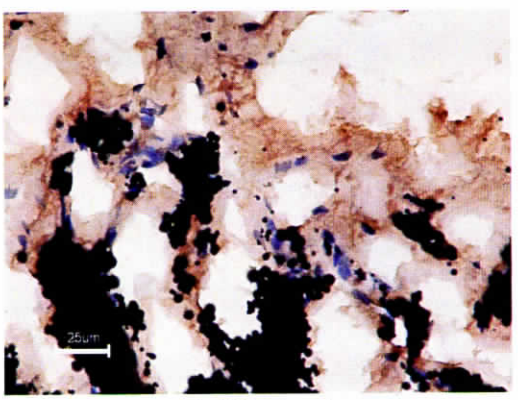

E (150 days)

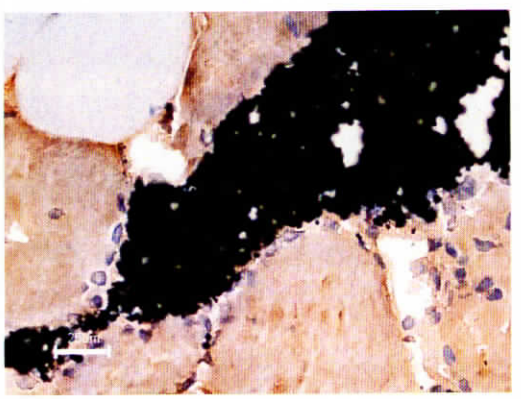

F (negative control)

Figure 15: Light micrographs of IHC, IL-1α stained sections of 5 days (A); 45 days (B); 90 days (C); 120 days (D); 150 days (E) and negative control (F).

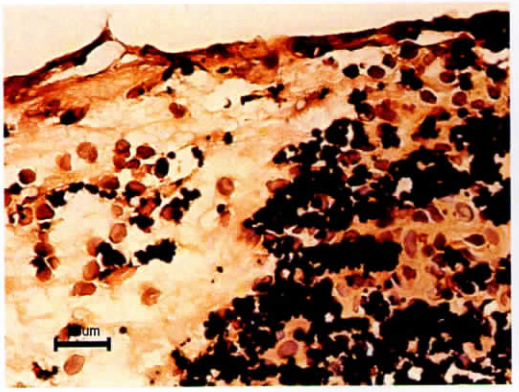

A (5 days)

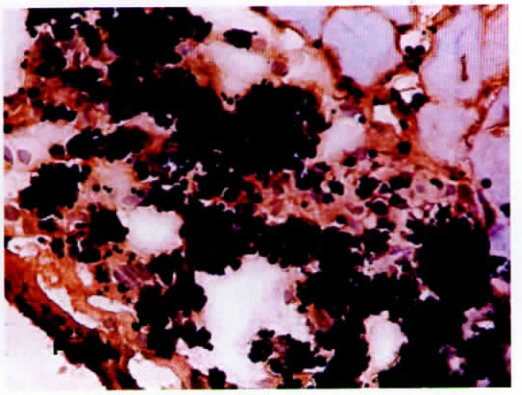

B (45 days)

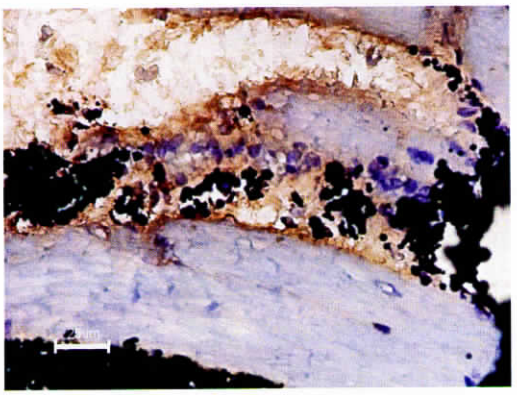

C (90 days)

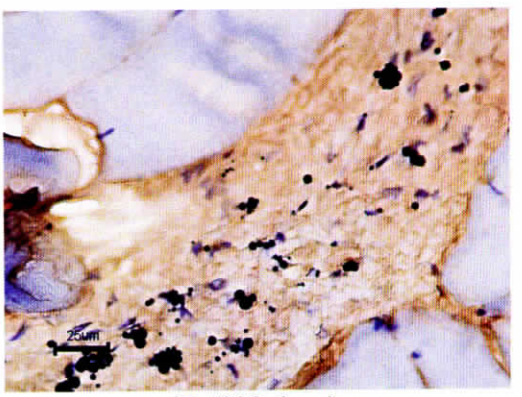

D (120 days)

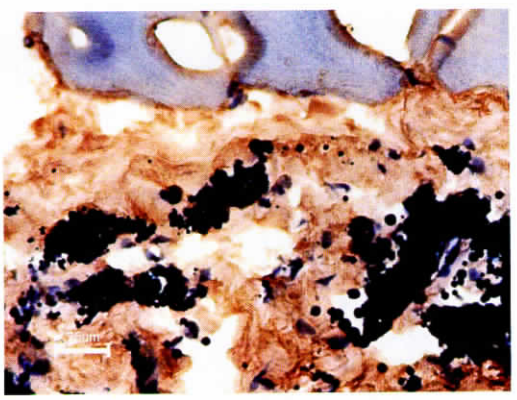

E (150 days)

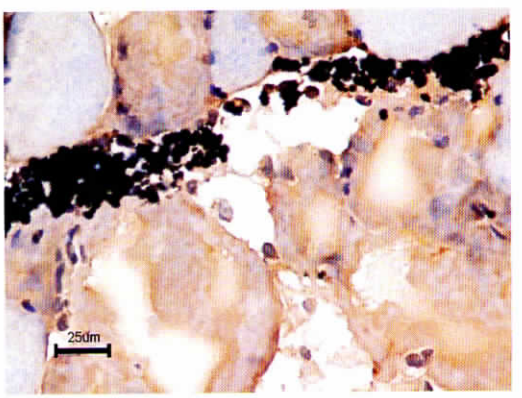

F (negative control)

Figure 16: Light micrographs of IHC, IL-6 stained sections of 5 days (A); 45 days (B); 90 days (C); 120 days (D); 150 days (E) and negative control (F).

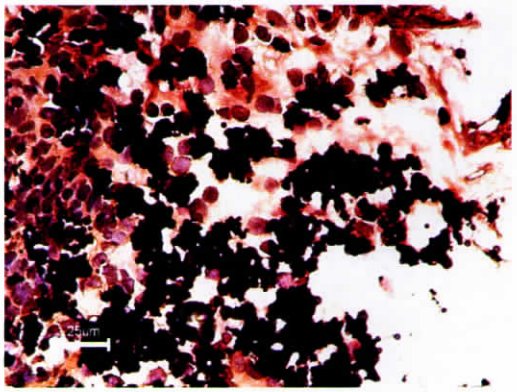

A (5 days)

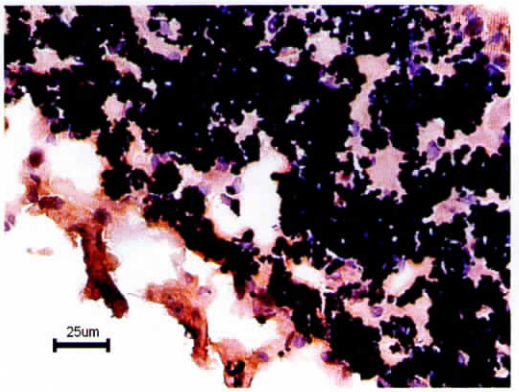

B (45 days)

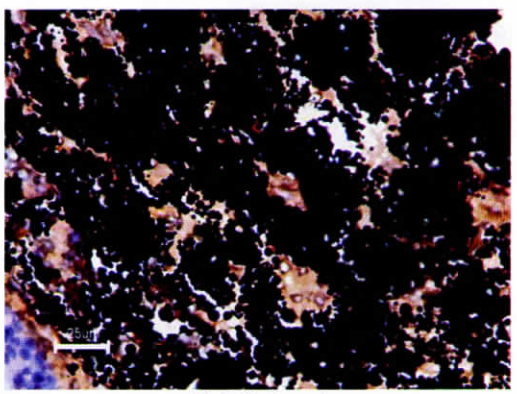

C (90 days)

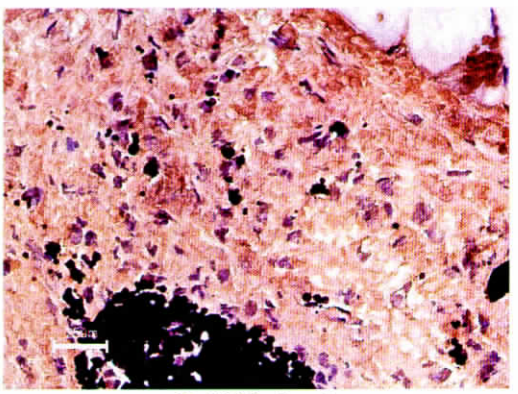

D (120 days)

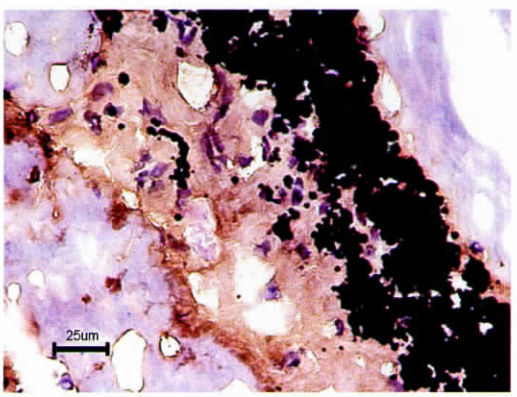

E (150 days)

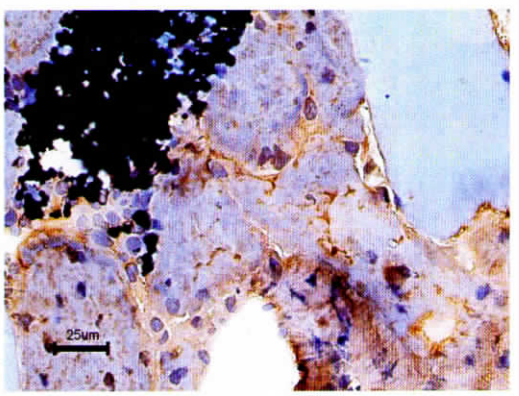

F (negative control)

Figure 17: Light micrographs of IHC, TNF-α stained sections of 5 days (A); 45 days (B); 90 days (C); 120 days (D); 150 days (E) and negative control (F).

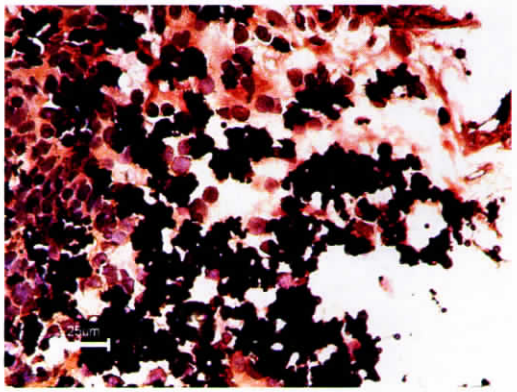

A (5 days)

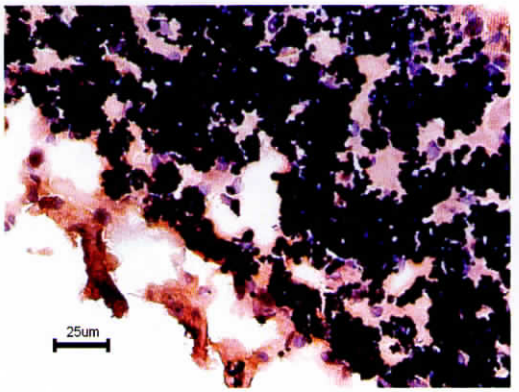

B (45 days)

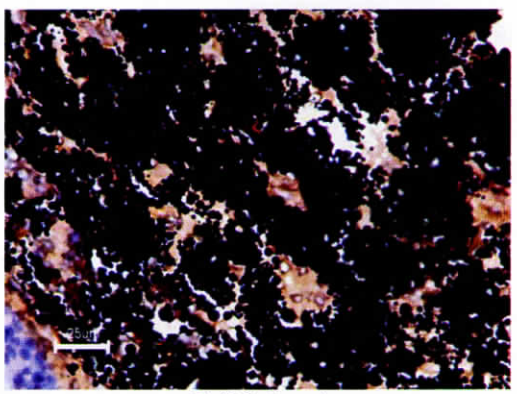

C (90 days)

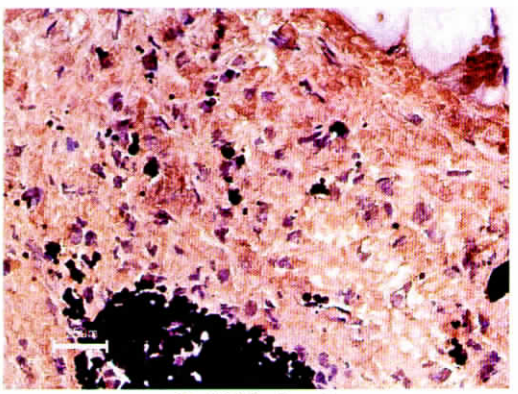

D (120 days)

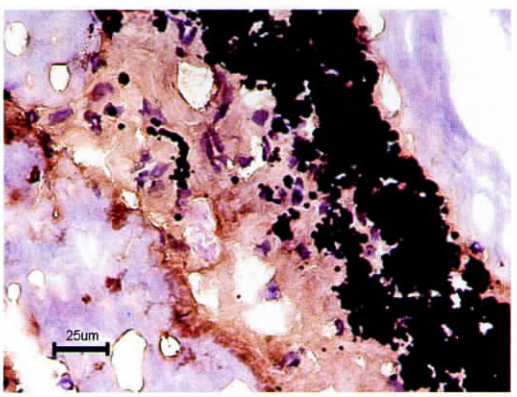

E (150 days)

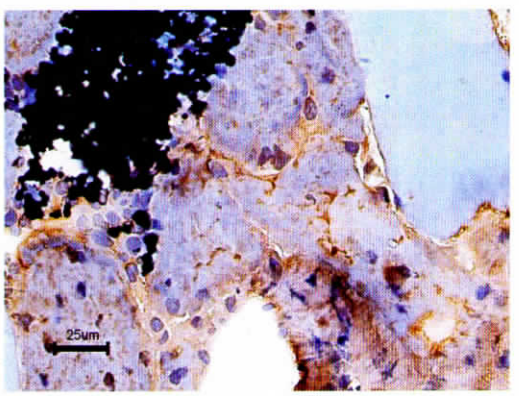

F (negative control)

Figure 17: Light micrographs of IHC, TNF-α stained sections of 5 days (A); 45 days (B); 90 days (C); 120 days (D); 150 days (E) and negative control (F).

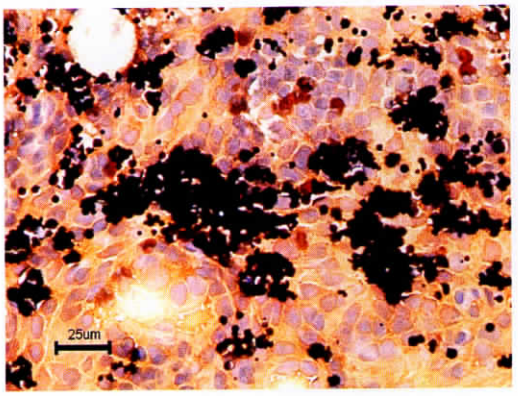

A (5 days)

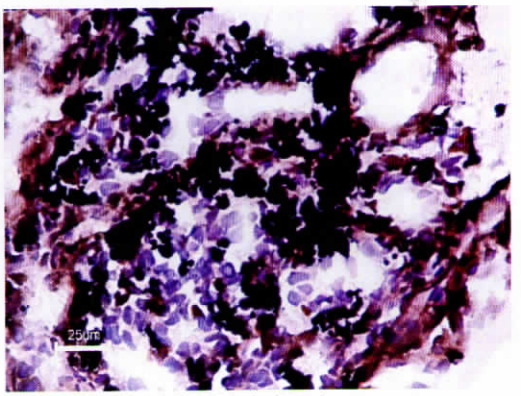

B (45 days)

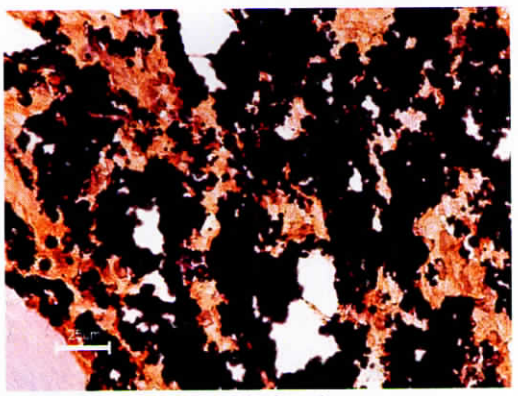

C (90 days)

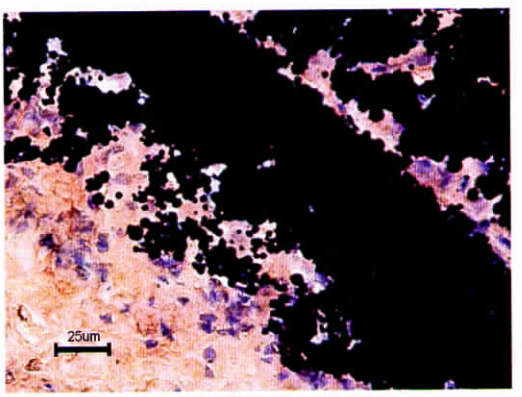

D (120 days)

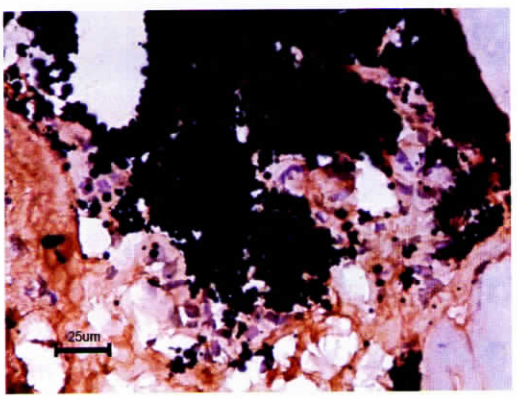

E (150 days)

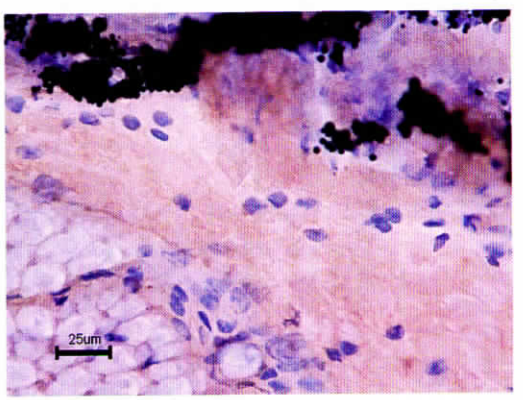

F (negative control)

Figure 18: Light micrographs of IHC, smooth muscle-actin, stained sections of 5 days (A); 45 days (B); 90 days (C); 120 days (D); 150 days (E) and negative control (F).

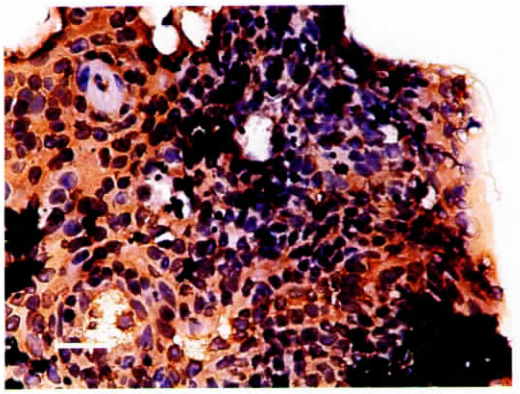

A (5 days)

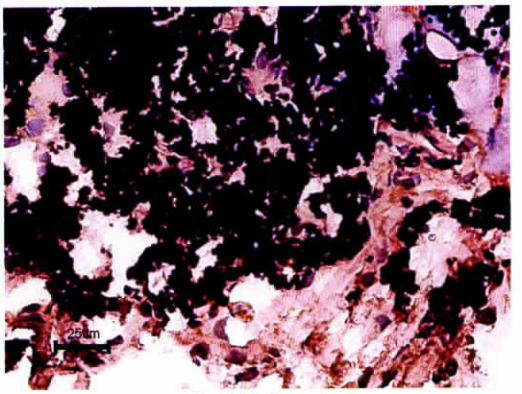

B (45 days)

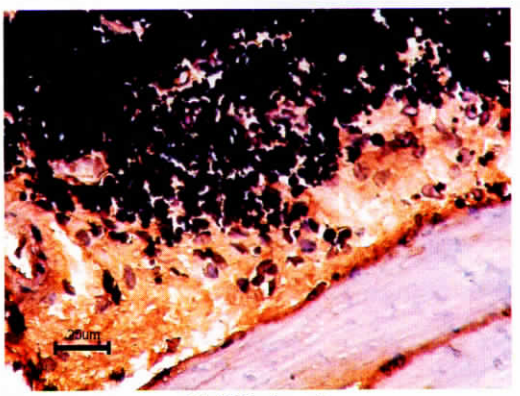

C (90 days)

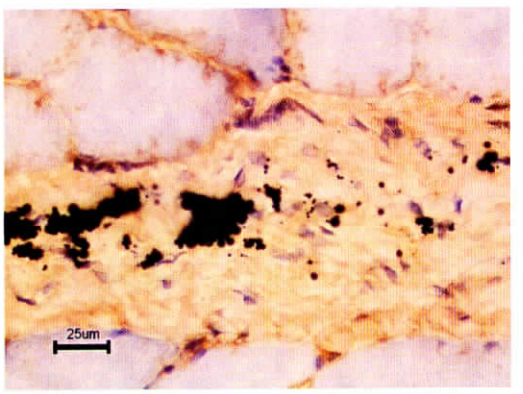

D (120 days)

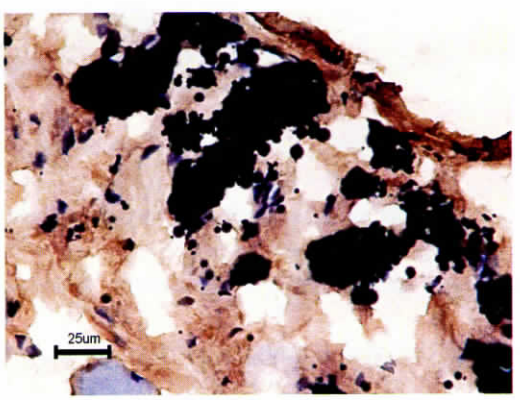

E (150 days)

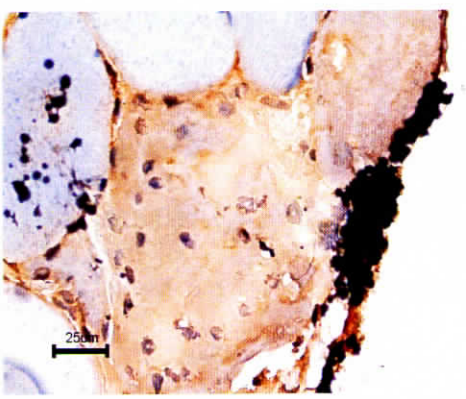

F (negative control)

Figure 19: Light micrographs of IHC, vimentin, stained sections of 5 days (A); 45 days (B); 90 days (C); 120 days (D); 150 days (E) and negative control (F).

The biological response to particulate materials involves a myriad of cells and their cytokines which act via autocrine and paracrine mechanisms to modulate the inflammatory response. The acute inflammatory response takes place seconds or minutes after an injury occurs. The neutrophils are the first cells to arrive at the onset of the inflammatory response. These cells are distinguished by their characteristic multilobed nuclei. The macrophages come in as a second wave to complete what the neutrophils have started and by 2-3 days the monocytes outnumber the neutrophils. If the causative agent persists, the inflammation becomes chronic. Histological evidences of chronic inflammation include the predominance of macrophages and lymphocytes and the formation of granulation tissue. The granulation tissue comprises mainly of fibroblasts, macrophages and new blood vessels. The inner layer of the granulation tissue is highly cellular and vascular, while the outer layer comprises more collagen and acts as a fibrous capsule (Majno *et al*, 1996).

Light microscopical evaluation of Haematoxylin and Eosin stained sections of all fourteen different time periods revealed the persistence of a chronic inflammatory response to the CoCr particles, with time. Acute inflammatory response was noted at early time periods from one to five days. The early inflammatory response could be directed towards both the metal particles as well as to injury caused by the implantation process, the latter being minimal as the procedure followed was an injection mode. By two to three days, the inflammatory response to the implantation procedure itself would decline and any persistent local inflammatory response would be towards the implant (Woodward SC, 1986). Foreign body giant cells were observed as early as one week indicating a transition from acute to chronic inflammatory phase. As early as fifteen days the metal particles tend to cluster together into clumps, which

are surrounded by fibroblasts like cells. The chronic inflammatory phase appears to persist with time. This inflammatory response is characterised by the presence of macrophages, fibroblasts and numerous new blood vessels. A characteristic difference in host response to the CoCr alloy particles implanted within the muscle fibres and within the endomysium was noted. In muscle fibres inflammatory response to the CoCr particles was mild but persistent even at longer time periods. In endomysium the inflammatory response was more pronounced. With time excessive fibrosis with large number of fibroblasts and fibrocytes and scant macrophages was noted. Presence of numerous new blood vessels was also noted. At longer time periods clumping of particles within the fibrous tissue was observed. Fibrosis is the response of fibroblasts to stimulation by cytokines; typically produced in chronic inflammation. The main cell types in fibrotic tissue are fibroblasts, fibrocytes and myofibroblasts and in chronic inflammation contributes to walling off of the infected area or foreign body (Majno *et al*, 1996). This difference in response could be attributed to the variation in cellular constituents between the muscle fibre and the endomysium. The latter comprising mainly of collagenous connective tissue and fibroblasts and in the context of cellular constituents would resemble the fibrous capsule that forms around the implant. It is of interest to note that Doorn *et al*, (1998) have reported on lower histiocytic response around metal on metal prosthesis as compared to metal on polyethylene. The presence of densely textured fibrous tissue with only moderate inflammatory and granulomatous changes in the interfacial membrane of long term surviving prostheses as compared to macrophagic sheets in the periprosthetic membranes around short surviving prosthesis has also been reportedly observed by Boss *et al*, (1996).

Transmission electron microscopic studies were used to further the investigations of cellular response to CoCr alloy particles at the ultrastructural level.

Acute inflammation at five days was indicated by the presence of a large number of macrophages as identified by their large bean shaped nuclei. The area appears to be highly regenerative as evidenced by the presence of a large number of blood vessels and short collagen fibrils and strands that are randomly dispersed. The presence of a chronic inflammatory phase at forty five days was substantiated in the electron micrographs which showed a large number of macrophages most of them coalescing probably in an attempt to form foreign body giant cells. Giant cells are an outcome of frustrated phagocytosis and are a characteristic inflammatory response to foreign bodies. However no metal particles within the giant cell were observed. The presence of numerous blood vessels and collagen fibrils were also noted. At this time period mast cells were also observed. These cells are highly granular and contain heparin, histamine and serotonin in their granules. Degranulation of mast cells causes increased vascular permeability. The presence of mast cells in the pseudocapsule and periprosthetic tissue around failed total hip replacements have been reported by Solovieva *et al*, (1996). Histamine is a proinflammatory mediator. It is known to promote rapid diapedesis of inflammatory cells and upregulates the expression of phagocyte adhesion molecules. Thus mast cells may play a possible role in the recruitment of phagocytes. The role of mast cells in mediating the recruitment of neutrophils and monocytes/macrophages around intraperitoneally and subcutaneously implanted polyethylene terephthalate disks was experimentally proved by Tang *et al*, (1998). The excessive fibrosis observed via light microscopy at longer time periods of ninety days and four months, was confirmed via TEM. The electron micrographs revealed the presence of large amounts of collagen arranged in parallel bundles. The characteristic banding pattern of collagen bundles were visible. Presence of both fibrocytes and fibroblasts adjacent to the collagen bundles were observed. The cells

and the collagen bundles appeared to be arranged parallel to each other. Most of the fibroblasts were hypertrophied with an increased nuclear to cytoplasm ratio, which is indicative of an active state. The occasional presence of collagen as short fibrils and short bundles was also noted.

Results obtained from immunohistochemical studies confirmed the specificity of the inflammatory cells. Subpopulations of macrophages were phenotyped using antibodies to ED1 and ED2. CD 68 or ED1 is a single chain glycoprotein of 110KD that is expressed on the lysosomal membranes of myeloid cells. The antigen is expressed by the majority of newly recruited macrophages. CD 163 or ED2 is a cell surface glycoprotein of 175KD. It is expressed by approximately 50% of peritoneal macrophages, a subset of splenic macrophages and by resident mature macrophages in most other tissues. It is not expressed by monocytes. Positive staining for macrophage marker ED1, ED2 was observed at 5, 45 and 90 days only. The results obtained suggest the predominance of macrophages in the inflammatory response. These IHC results corroborate with those of TEM and histology. The presence of positive staining for macrophages at 45 and 90 days substantiates the presence of a chronic inflammatory response to CoCr alloy particles. The biological response to CoCr alloy particles at later time periods of 120 and 150 days is mainly one of fibrosis characterised by the presence of dense connective tissue, numerous fibroblasts and fibrocytes. This is evidenced by the absence of positive staining for macrophages at these time periods. Immunohistochemical staining for myofibroblasts via antibodies to α- smooth muscle actin and vimentin was also positive at time periods of 5, 45 and 90 days. Myofibroblasts have been reported in wound tissue to be observed on the fourth to sixth day remaining active till the second to third week. The presence of occasional myofibroblasts along with fibroblasts in fibrosis has also been reported (Kuhn C *et al*,

1991), which explains the presence of positive staining at 45 and 90 days. However, positive staining at longer time periods of 120 and 150 days was not observed, indicating a predominance of fibroblasts and fibrocytes in the dense connective tissue.

The proinflammatory mediators produced at the implant-tissue interface have been implicated as casual agents of periprosthetic osteolysis and are known to modulate the inflammatory response to particulate debri. In this study the *in vivo* expression of IL-1, 1L-6 and TNF-α around CoCr alloy particles were evaluated by immunohistochemistry. IL-1 plays a critical role in the regulation of immune response and inflammation acting as an activator of T and B lymphocytes and natural killer (NK) cells. IL-1exsists in two different forms IL-1α and IL-1β that are encoded by distinct genes. Both however bind to the same receptor and elicit similar biological responses. TNF-α also known as cachectin, is a cytokine with a molecular weight of 17KD. Both, IL-1 and TNF-α, are potent stimulators of bone resorption. IL-6 is a 21KD multifunctional protein, which plays a critical role in host defence, immune response and haematopoiesis. IL-6 is also known to be a major promoter of osteoclastogenesis. Data obtained from this study shows the presence of IL-1α at 5, 45 and 90 days only. IL-1β expression was not detected at any time period. A similar trend in the expression of IL-6 and TNF-α was noted with positive staining being observed at 5 and 45 days only. The expression of all four cytokines IL-1β, IL-1α, IL-6 and TNF-α was absent at longer time periods of 120 and 150 days. Since serial sections were used for IHC evaluation, cells that stained positive for macrophages were also positive for cytokines. These results suggest that it is the macrophages at early time periods that are responsible for secretion of the proinflammatory cytokines. These proinflammatory cytokines are known to be key regulators of bone resportion and play a dynamic role in aseptic loosening seen around clinically failed implants.

The biological response seen in clinical failure of THR may be a prolongation of this chronic inflammation and fibrotic response; the inflammatory response being sporadically exacerbated with each set of particulate debri released from the surface of the articulating prosthesis.

Scant macrophage response and excessive fibrosis at long term implantation prompted further investigative studies *in vitro* into CoCr alloy particle-fibroblast interactions at the molecular level.

4.4. *IN VITRO* EXPERIMENTS

4.4.1. Cytoskeletal rearrangements and cytokine profile in murine L929 fibroblasts cultured with CoCr alloy particles.

4.4.1.1. Phase contrast and Scanning Electron Microscopic studies

Phase contrast microscopic evaluation of the L929 fibroblast cultures after 72 hours, showed the control cultures to have attained confluency. The cells had attained their characteristic elongated spindle shaped morphology (Figure 22A). When cultured in presence of 0.3 mg/cm^2 of CoCr alloy particles, the morphology of the cells was similar to that of control (Figure 22B). In presence of 0.5 (Figure 22C) and 1mg/cm^2 (Figure 22D) of CoCr alloy particles, the cellular morphology was quite similar to control. The cells had also attained confluency. It was observed that the CoCr particles tend to cluster and adhere to the fibroblast cells. Changes in cellular morphology were apparent, with the cells appearing narrower at higher concentrations of 5mg/cm^2 of CoCr alloy particles. Cell number was also reduced relative to control (Figure 22E). Exposure to 8mg/cm^2 of CoCr particles caused severe changes in cellular morphology, with cells displaying a necrotic appearance (Figure 22F). The number of cells appeared to be greatly reduced when compared with control.

The scanning electron micrographs corroborated with the findings in phase contrast microscopy. In Figure 23A the characteristic elongated spindle shape of the L929 fibroblasts is clearly observed. The cells appeared to be well adhered to the substratum and good cell spreading was noted. Figure 23B is a higher magnification of the cells. The smooth surface morphology of the cells is noted. In presence of $0.5mg/cm^2$ of CoCr alloy particles the shape and morphology of the fibroblasts was maintained. The metal particles appeared to cluster and adhere to the cells (Figure 23C). This is clearly evinced in Figure 23D, where the metal particles appear to be internalized by the cells. At higher concentrations of $1mg/cm^2$ of metal particles, the shape and morphology of the fibroblasts were maintained (Figure 23E). Cells were attached and spread on the substratum. The metal particles appeared to be bound on the dorsal surface of the cells. In Figure 23F close association of the CoCr alloy particles along the cellular margins of the fibroblasts is clearly evident.

4.4.1.2. Cytoskeletal rearrangement in L929 fibroblasts grown with CoCr alloy particles.

Confocal laser scanning microscopic evaluation of L929 fibroblasts revealed changes in cytoskeletal rearrangement of F-actin and α-actinin molecules following 72 hours culture with low concentrations of CoCr alloy particles.

Even distribution of the F-actin filaments, spanning across the cell body were observed in the control cultures (Figure 24A). The uniform distribution pattern of the F-actin filaments at different planes is better appreciated in the z stack images (Figure 24B). Fibroblasts cultured with $0.5mg/cm^2$ of CoCr alloy particles also displayed an organized arrangement of F-actin filaments. However, voids within the F-actin cytoskeletal framework corresponding to areas occupied by the metal particles were observed (Figure 25A). The close association between the metal particles and the

fibroblast cells are better reflected in the z stack images (Figure 25B), where the presence of the voids are observed even at a plane of focus through the central region of the cell, indicating a possibility of uptake of particles by the fibroblast cells. Similar observations were also made in L929 fibroblasts cultured with 1mg/cm^2 of metal particles (Figure 26A & Figure 26 B).

Confocal laser scanning microscopic evaluation of control fibroblasts cultures revealed an even distribution of α-actinin molecules throughout the cellular body (Figure 27A). The distribution pattern being maintained through the entire thickness of the cell as evinced in the z stack images (Figure 27B). A marked difference in the pattern of α-actinin staining was observed in L929 fibroblasts cultured with CoCr alloy particles. The α-actinin staining was more punctuate, indicating the aggregation of α-actinin into small patches (Figure 28 A & Figure 29A). The aggregation appeared to be more pronounced on the surface of the cell, thinning down to an even distribution of α-actinin from the central region of the cell to the area of cell-substratum interaction. This is clearly revealed in the z stack images of the cells (Figure 28 B & Figure 29 B).

4.4.1.3. Expression profile of IL-6 and IL-1α.

The release of the proinflammatory cytokines IL-6 and IL-1α by L929 fibroblasts following 72 hours culture with CoCr alloy particles was evaluated by ELISA.

Figure 20 reveals a basal secretion of IL-6 (30.025 pg/mL) by control cultures. There appears to be a decrease in IL-6 release in presence of 0.3, 0.5, 1 and 5 mg/cm^2 of metal particles and an increase at higher concentrations of 8 mg/cm^2. However neither the decrease nor the increase was not found to be significant ($P<0.01$).

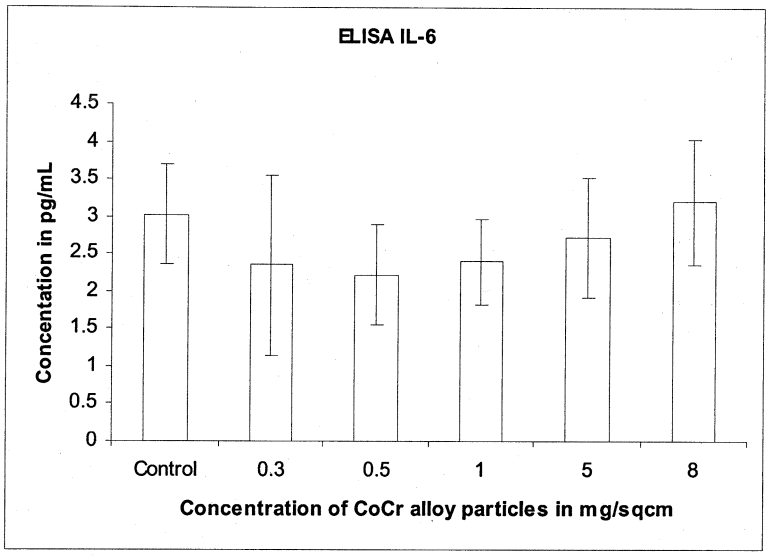

Figure 20: L929 fibroblasts were cultured with CoCr particles at varying concentrations (as indicated in the graph) for 72 hours. Culture medium was harvested and analyzed for released IL-6 by ELISA.

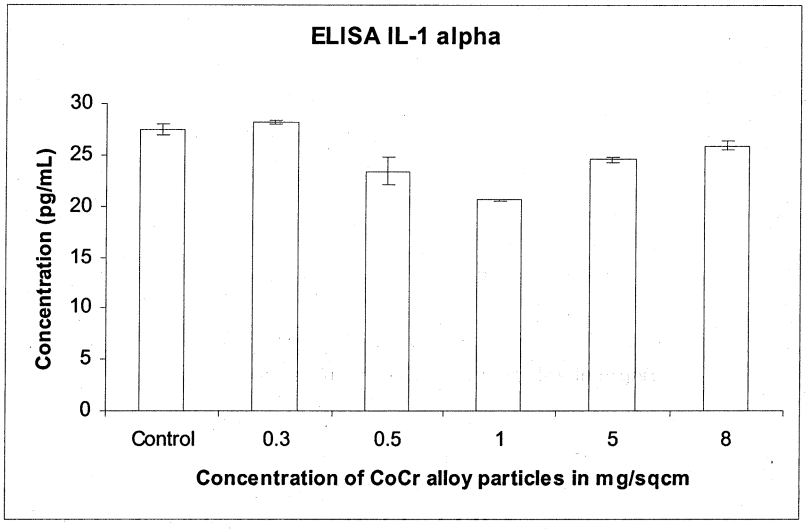

Figure 21: L929 fibroblasts were cultured with CoCr particles at varying concentrations (as indicated in the graph) for 72 hours. Culture medium was harvested and analyzed for released IL-1 α by ELISA.

A basal expression of IL-1 α (27.44pg/mL) was noted in the control fibroblast cultures. The release of IL-1 α appears to increase in presence of 0.3 mg/cm^2 of CoCr alloy particles and decrease with higher concentrations of 0.5, 1, 5 and 8 mg/cm^2 (Figure 21). However neither the decrease nor the increase was found to be significant ($P<0.01$).

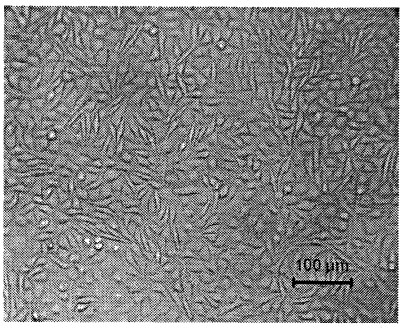

A (Control)

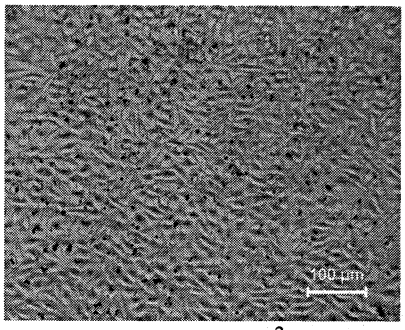

B (0.3 mg/cm^2)

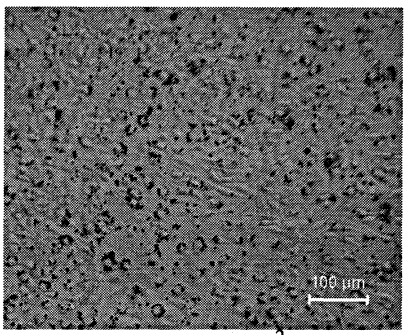

C (0.5 mg/cm^2)

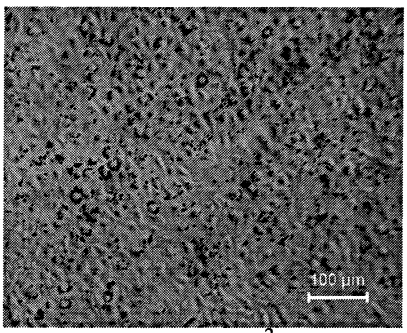

D (1 mg/cm^2)

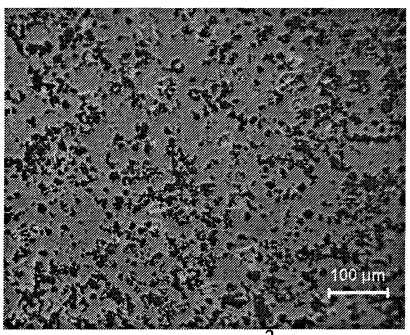

E (5 mg/cm^2)

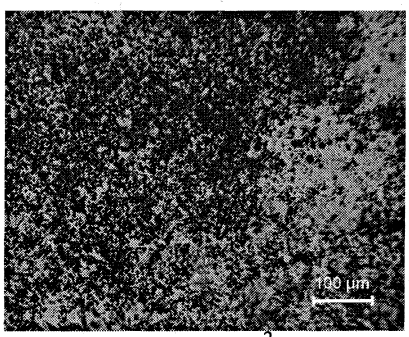

F (8 mg/cm^2)

Figure 22: Phase contrast images of murine L929 fibroblasts following 72 hours culture with CoCr alloy particles at concentrations of 0.3mg/cm^2 (B), 0.5mg/cm^2 (C), 1.0mg/cm^2 (D), 5mg/cm^2 (E)and 8mg/cm^2 (F). Cultures without particles served as control (A).

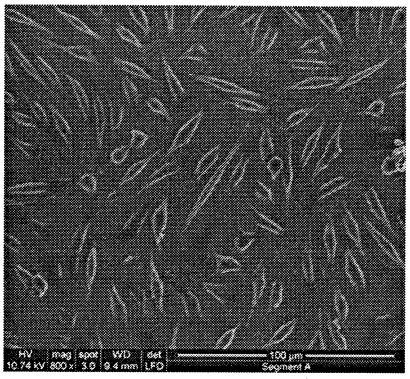

A (Control)

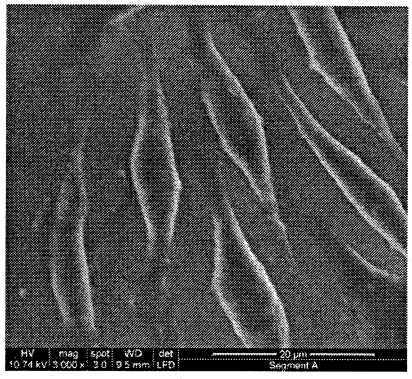

B (Control)

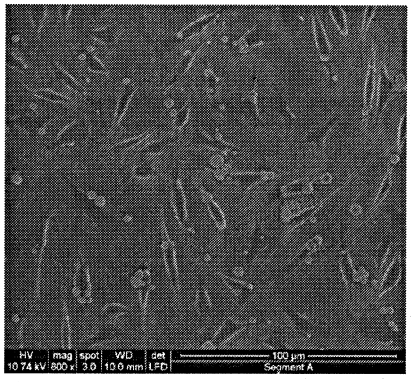

C (0.5 mg/cm^2)

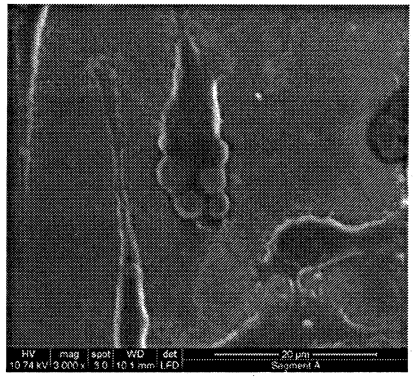

D (0.5 mg/cm^2)

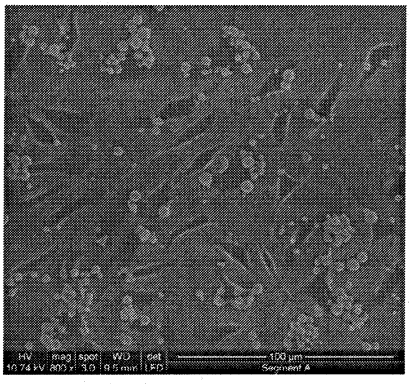

E (1 mg/cm^2)

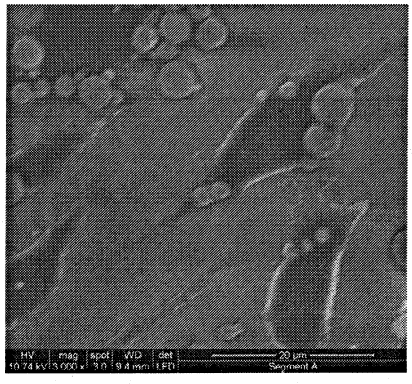

F (1 mg/cm^2)

Figure 23: Environmental Scanning Electron micrographs of murine L929 fibroblasts following 72 hours culture with CoCr alloy particles at concentrations of 0.5mg/cm2 (B, C), 1.0mg/cm2 (D, E). Cultures without particles served as control (A, B).

(A)

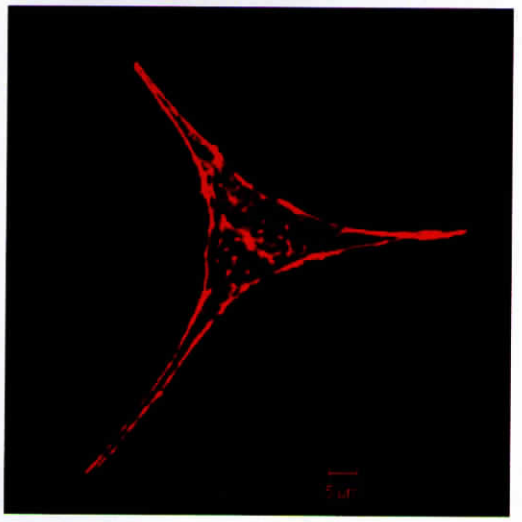

(B)

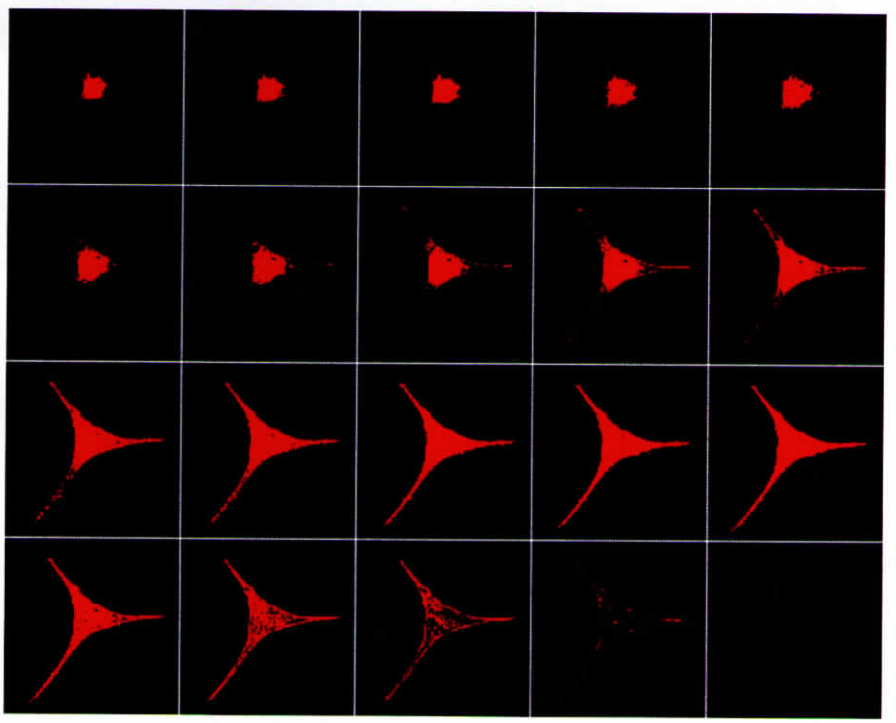

Figure 24: Confocal micrographs of control L929 fibroblasts, stained for F-actin with Phalloidin-TRITC conjugate, following 72 hours culture (A) and Z stack images of the cells (B).

(A)

(B)

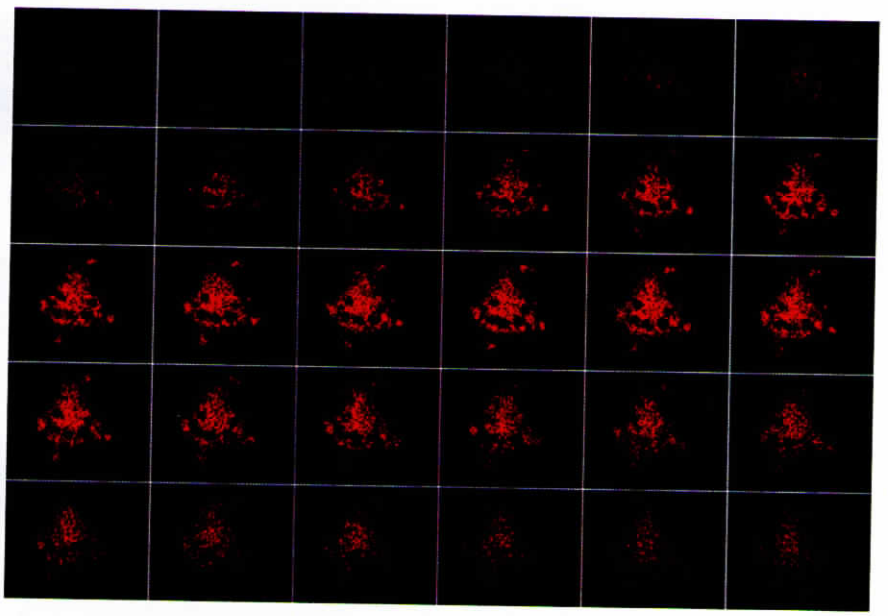

Figure 25: Confocal micrographs of L929 fibroblasts, stained for F-actin with Phalloidin-TRITC conjugate, following 72 hours culture with 0.5mg/cm^2 of CoCr alloy particles (A) and Z stack images of the cells (B).

(A)

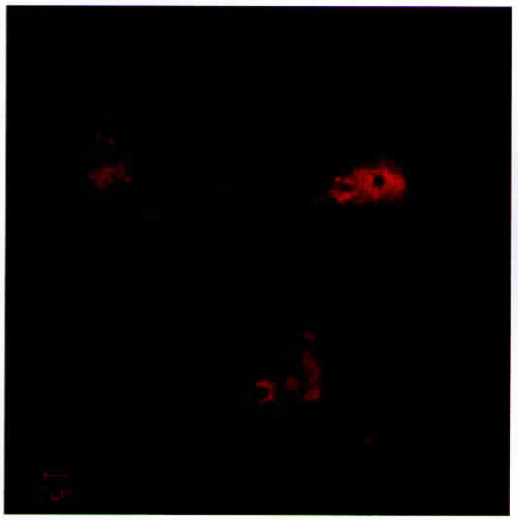

(B)

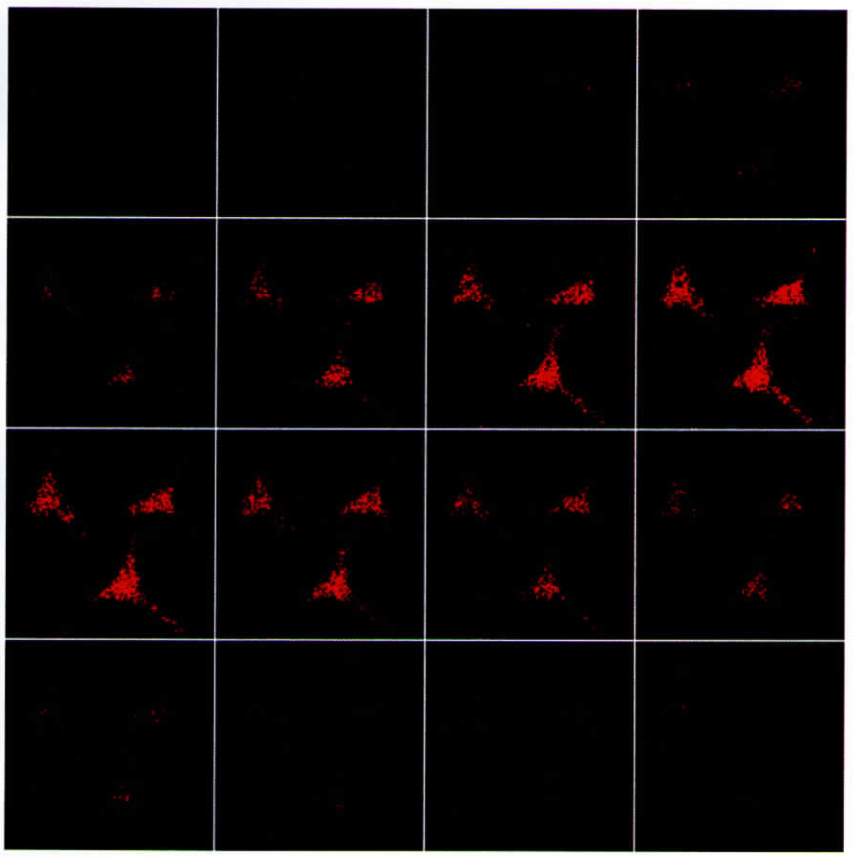

Figure 26: Confocal micrographs of L929 fibroblasts, stained for F-actin with Phalloidin-TRITC conjugate, following 72 hours culture with 1mg/cm^2 of CoCr alloy particles (A) and Z stack images of the cells (B).

(A)

(B)

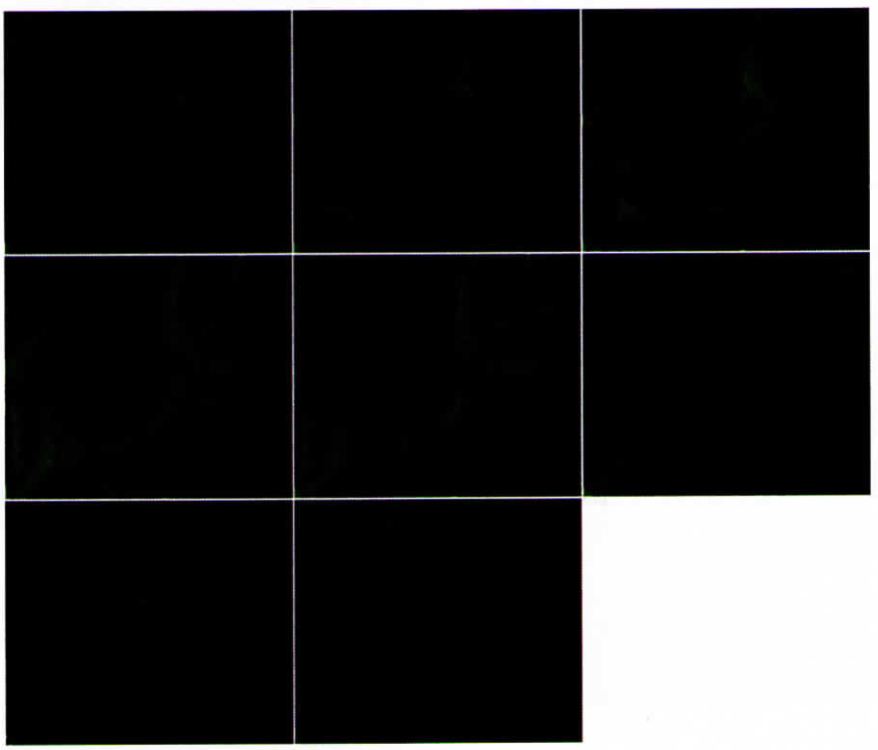

Figure 27: Confocal micrographs of control L929 fibroblasts, stained for α-actinin, following 72 hours culture (A) and Z stack images of the cells (B).

(A)

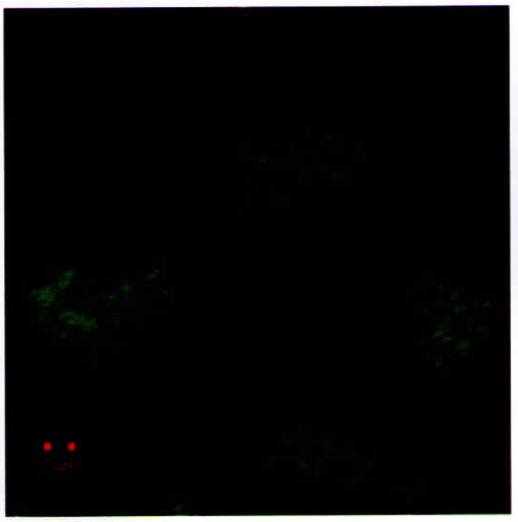

(B)

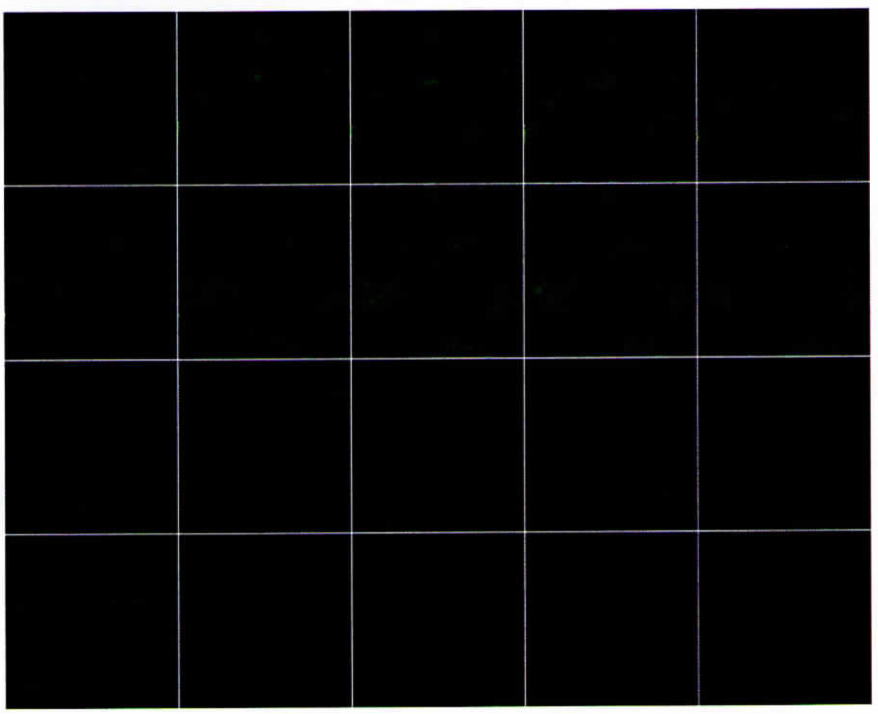

Figure 28: Confocal micrographs of L929 fibroblasts, stained for α-actinin, following 72 hours culture with 0.5mg/cm^2 of CoCr alloy particles (A) and Z stack images of the cells (B).

(A)

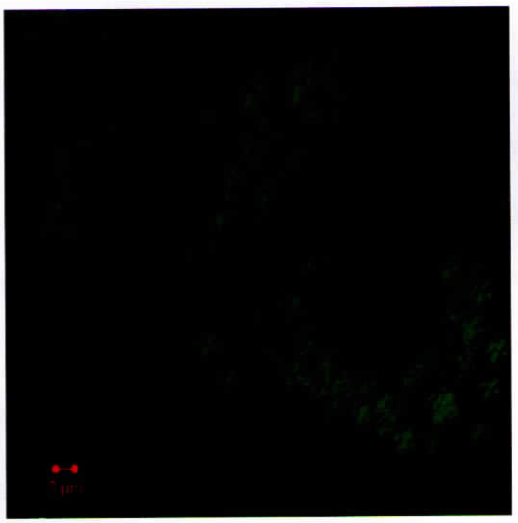

(B)

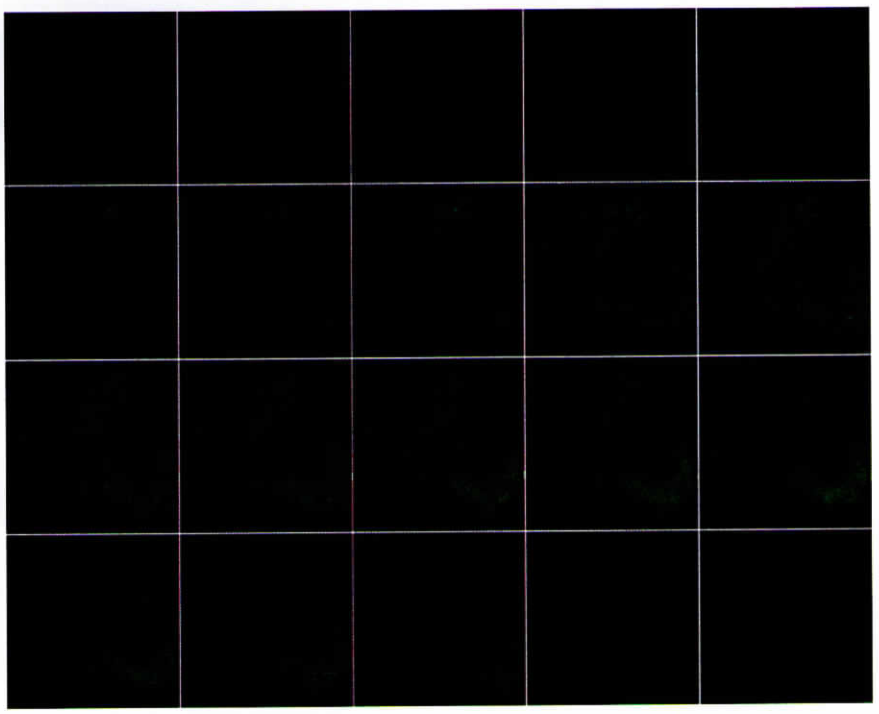

Figure 29: Confocal micrographs of L929 fibroblasts, stained for α-actinin, following 72 hours culture with 1mg/cm^2 of CoCr alloy particles (A) and Z stack images of the cells (B).

In the present study murine L929 fibroblast cells were incubated with CoCr alloy particles at varying concentrations. Phase contrast and Scanning electron microscopy studies reveal the close association of CoCr alloy particles along the cellular margins on the dorsal surface of the fibroblasts. The binding of metal particles does not induce any drastic changes in cellular morphology relative to the controls. This suggests that interactions of metal particles with the cell surface do not lead to changes in cell-substratum interactions occurring on the ventral surface of the cell i.e, no loss of cell attachments with the underlying coverslip occur. Our results are in agreement to those reported by Grinnell *et al*, 1986 who had studied cell surface interactions of fibronectin-coated latex beads with chick embryo fibroblasts and have observed a similar pattern of association of the beads with fibroblast membranes. The fibroblasts have been reported to have phagocytic activity. Findings that fibroblasts phagocytose collagen fibrils (Yajima T, 1988) and latex particles (Mishima H *et al*, 1987) in *in vitro* support this idea.

Changes in cytoskeletal rearrangement of F-actin filaments and α-actinin moieties in fibroblasts cultured with the metal particles were studied by confocal laser scanning microscopy. The cytoskeleton is composed of three fundamental types of filamentous proteins and their associated proteins and are termed as microfilaments, intermediate filaments and microtubules. The microfilaments represent the various forms of actin and their associated proteins. The structural state of these cytoskeletal elements have a direct bearing on cell adhesion, growth, differentiation, cell mobility and nearly all cellular processes are influenced by changes in the state of these ultrastructural elements (Gwynn API *et al*, 1994). Results obtained in this study show the presence of voids within the F-actin framework corresponding to areas occupied by

the CoCr alloy particles. These voids were observed even at plane of focuses within the central region of the cell, indicating the possibility of an uptake of the particles. The remodeling of the actin cytoskeleton is known to be a major requirement for phagocytosis. Filament remodeling could involve several mechanisms (1) an increase in the filament number through the formation of new filaments (nucleation); (2) an increase in the average filament length by the uncapping of established filaments to allow the addition of new monomers; (3) a reduction in the number or length of filaments by severing and/or of sequestering actin monomers; (4) alterations in the structure of the actin network, without a net change in F-actin content, made by bundling or cross linking filaments. Phagocytosis is usually accompanied by the local recruitment of α-actinin, a protein that can bundle actin filaments and link them to integrins (May RC *et al*, 2001). Results from our study show a change in the distribution pattern of α-actinin in the presence of CoCr alloy particles. A punctate staining was observed indicating the aggregation of α-actinin into small patches. These patches were more concentrated on the dorsal surface of the cell, were close interactions with the metal particles occurred. The patchy appearance thinned down with an even distribution being noted from the central regions to the ventral surface of the fibroblast cells. Our results corroborate with those reported by Grinnell *et al*, 1986, who had observed small patches of α-actinin at areas of cell-bead interface. The reorganization of the α-actinin in response to 6-μm and 16-μm fibronectin coated beads was observed after fifteen minutes incubation.

Fibroblasts are primarily thought to be responsible for the synthesis of type 1 collagen, which forms a structural component of tissues. However in addition to this traditional role, fibroblasts also produce cytokines and enzymes that influence tissue remodeling. Results from this study however indicate a lack of increased cytokine

IL-6 and IL-1α secretion in response to CoCr alloy particles. These results are similar to those reported by Papageorgiou *et al*, (2007) who had found a lack of cytokine expression in human dermal fibroblasts when exposed to nano and micron sized CoCr particles *in vitro*. Similar results wherein exposure to varying concentrations of 0.45 and 3.5 micron sized polystyrene beads, did not lead to increased production of IL-6 by L929 fibroblasts have been reported by Olivier *et al*, 2003. Contradictory reports indicating an increase of IL-6 expression in human dermal and foreskin derived fibroblasts following direct stimulation with Ti alloy particles, have been published by Manlapaz *et al*, 1996. Ninomiya *et al*, 2001 had also reported on increased of IL-6 production in human neonatal fibroblasts following stimulation with HA, Ti, CoCr and HA/TCP

To supplement these results, further investigative studies employing the proteomic platforms of 2Dimensional electrophoresis and Mass spectrometry were undertaken.

4.4.2. Proteomic profile of human fibroblasts cultured with CoCr alloy particles and effect of the conditioned media on human monocyte cultures.

4.4.2.1. Effect of CoCr particles on fibroblast viability

4.4.2.1.1 Microscopic examination

Examination of the fibroblast cultures after 24 hours revealed that at a particle concentration of 0.05mg/cm^2 (Figure 31B) the cellular morphology was similar to the control (Figure 31A). At 0.5 (Figure 31C) and 1mg/cm^2 (Figure 31D) of CoCr particles, changes in cellular morphology were apparent, with the cells appearing narrower. Exposure to 5mg/cm^2 of CoCr particles caused drastic changes in cellular morphology, with cells displaying a necrotic appearance (Figure 31E).

At 72 hours the cells in the control culture (Figure 32A) and those exposed to 0.05mg/cm^2 of CoCr particles had attained confluency (Figure 32B). The cells grew in swirl patterns which is a characteristic growth pattern of MRC-5 fibroblasts. In the presence of 0.5mg/cm^2 the cell numbers were reduced relative to the controls (Figure 32C). At this concentration the morphology and swirl pattern of the cells were maintained. At 1mg/cm^2 the swirl pattern was lost and changes in cellular morphology were observed, with cells appearing narrower (Figure 32D). It was observed that the CoCr particles tend to cluster and adhere to the fibroblast cells. The presence of the metal particles in the intercellular spaces was minimal. High dosage of 5mg/cm^2 of CoCr particles appeared to be toxic to the cells as seen by the morphological changes (Figure 32E). When compared to control the number of cells appeared to be greatly reduced.

4.4.2.1.2 MTS-assay

The viability of the MRC-5 fibroblasts in presence of varying concentrations of CoCr particles was evaluated using the MTS assay. Cultures without metal particles served as control. The MTS tetrazolium compound [3-(4,5-dimethylthiazol-2-yl)-5-(3-carboxymethoxyphenyl)-2-(4-sulfophenyl)-2H-tetrazolium, inner salt], is bioreduced by cells into a colored formazan product that is soluble in tissue culture medium. This conversion is presumably accomplished by NADPH or NADH produced by dehydrogenase enzymes in metabolically active cells. The quantity of formazan product as measured by the absorbance at 490nm is directly proportional to the number of living cells in culture.

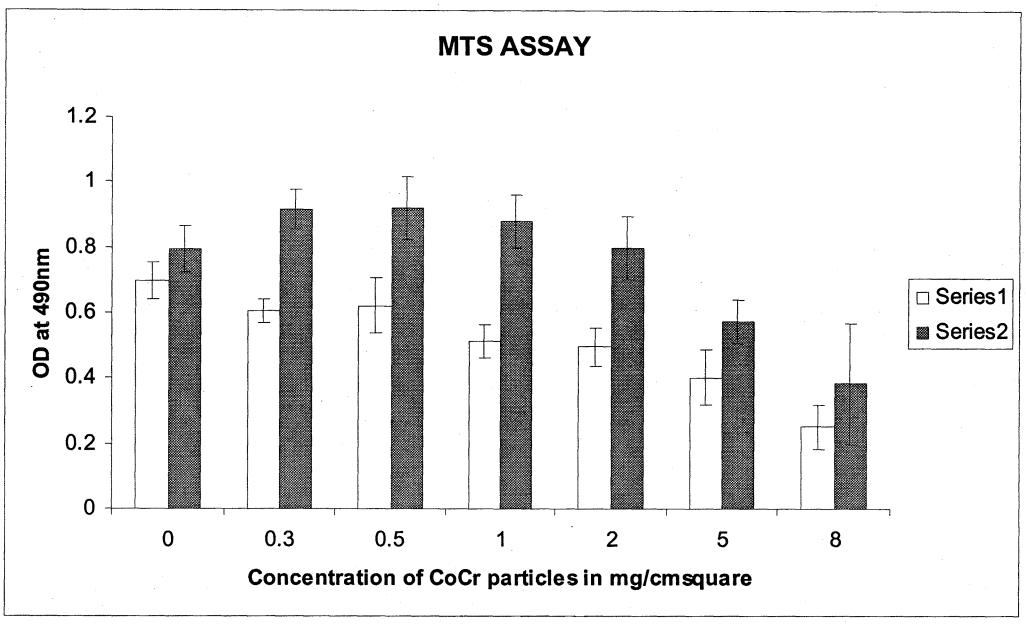

Figure 30: MRC-5 fibroblasts were cultured with CoCr particles at varying concentrations (as indicated in the graph) for 24 hours (Series 1) and 72 hours (Series 2). Viability of MRC-5 fibroblasts was studied via MTS assay.

Our results indicate that there is a gradual but significant ($P<0.05$) decrease in the viability of the fibroblasts, following a 24 hour culture with increasing concentrations of CoCr particles. At high concentrations of 5mg/cm^2 of metal particles, the percentage viability of the cells dropped to 56.43% relative to control.

Results obtained after 72 hours culture, revealed a significant increase ($P<0.05$) in cellular viability relative to control at lower concentrations of metal particles. At higher concentrations of metal particles the relative percentage viability decreases significantly ($P<0.05$) to as low as 48.45% on exposure to 8mg/cm^2 of CoCr particles.

4.4.2.2. Proteomic analysis of fibroblast cultured with CoCr particles.

Total cellular protein profile of fibroblasts cultured with CoCr particles was initially screened via 2D gel electrophoresis using 17cm IPG strips of pH 3-10, linear (Figure 33). For better separation of the proteins further 2DGE experiments were done

using 17cm IPG strips of pH 4-7, linear (Figure 34). At least two gels from each biological replicate were run.

4.4.2.3. Proteomic analysis of monocytes cultured in 40% conditioned medium

Total cellular protein profile of monocytes cultured in 40% conditioned medium from fibroblast CoCr cultures was studied via 2D gel electrophoresis using 17cm IPG strips of pH 4-7, linear (Figure 35). At least two gels from each biological replicate were run.

4.4.2.4. PDQuest analysis

Quantitative and qualitative differences between the 2Delectrophoretic patterns of cellular proteins of control and experiment from the fibroblast and macrophage cultures were investigated by in silico analysis using PDQuest software. PDQuest analysis using the Boolean analysis set for 2 fold increase and significance level of 90% revealed, 13 spots in 72 hour culture of fibroblast with CoCr particles. No spots were detected in 48 hour culture of monocytes with conditioned medium from the fibroblast cultures.

4.4.2.5. Protein identification by MALDI-TOF TOF MS and Mascot protein database search engine

PDQuest analysis revealed 13 spots as showing a 2 fold increases after 72 hour culture of the fibroblast with CoCr particles. The spots were eluted, trypsin digestion performed along with desalting. MS analyses via MALDI TOF TOF MS lead to the identification of only four protein spots. Figure 36 is the representative gel showing the four spots identified. The results of the same are summarized in Table 2. Figure 37 is the peptide mass fingerprint of spot 1, Figure 38 of spot 2, Figure 39 of spot 3 and Figure 40 of spot 4.

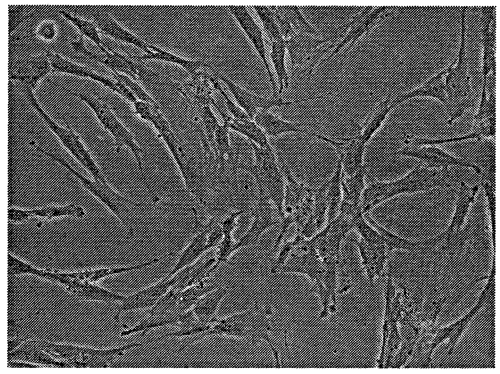

A (Control)

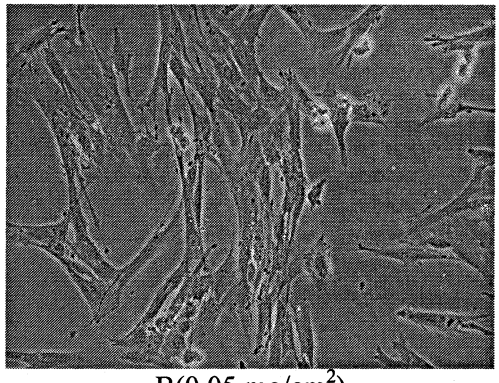

B(0.05 mg/cm^2)

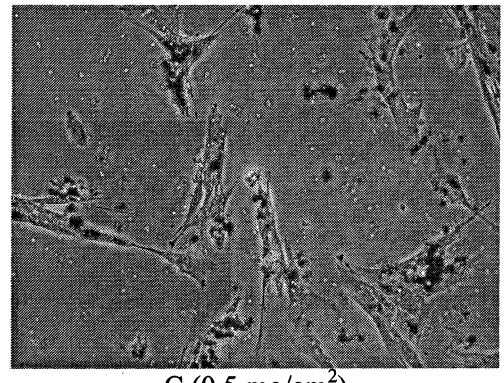

C (0.5 mg/cm^2)

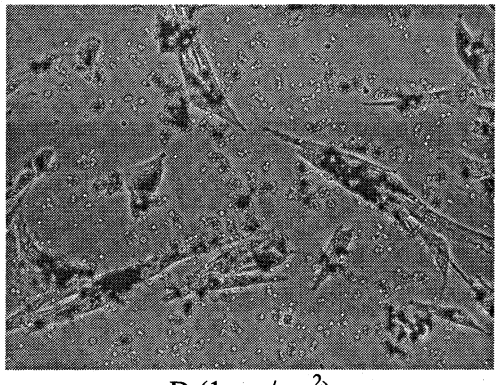

D (1 mg/cm^2)

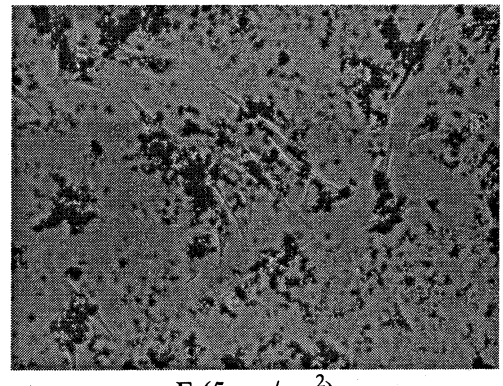

E (5 mg/cm^2)

Figure 31: Light micrographs of human MRC-5 fibroblasts following 24 hours culture with CoCr alloy particles at concentrations of 0.05mg/cm^2 (B), 0.5mg/cm^2 (C), 1mg/cm^2 (D) and 5mg/cm^2 (E). Cultures without particles served as control (A).

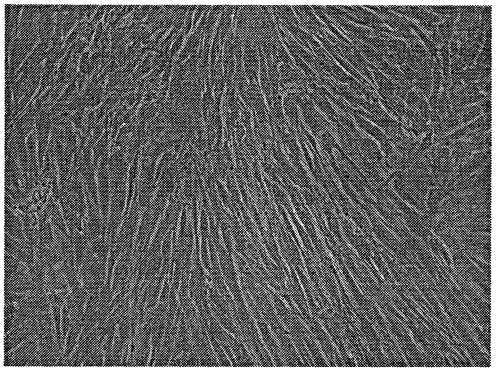

A (Control)

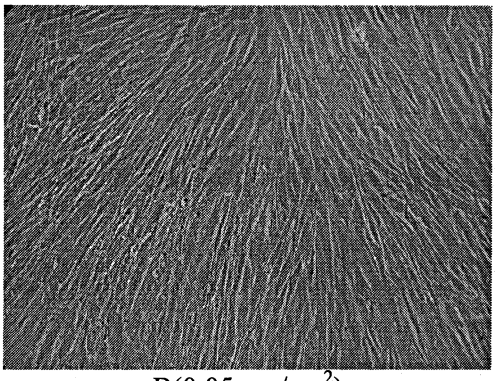

B(0.05 mg/cm^2)

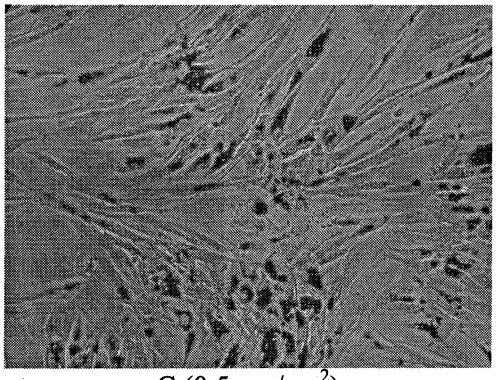

C (0.5 mg/cm^2)

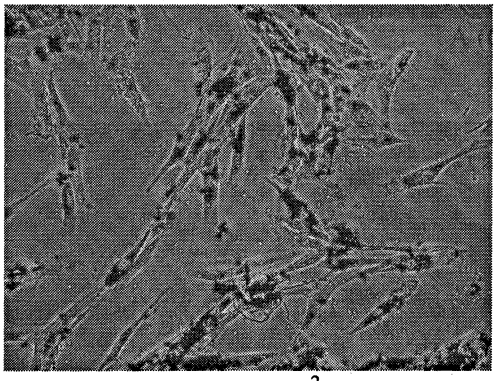

D (1 mg/cm^2)

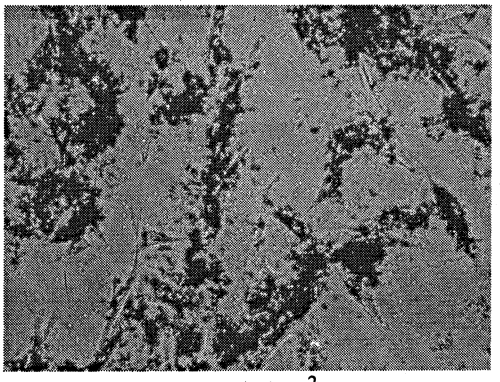

E (5 mg/cm^2)

Figure 32: Light micrographs of human MRC-5 fibroblasts following 72 hours culture with CoCr alloy particles at concentrations of 0.05mg/cm^2 (B), 0.5mg/cm^2 (C), 1mg/cm^2 (D) and 5mg/cm^2 (E). Cultures without particles served as control (A).

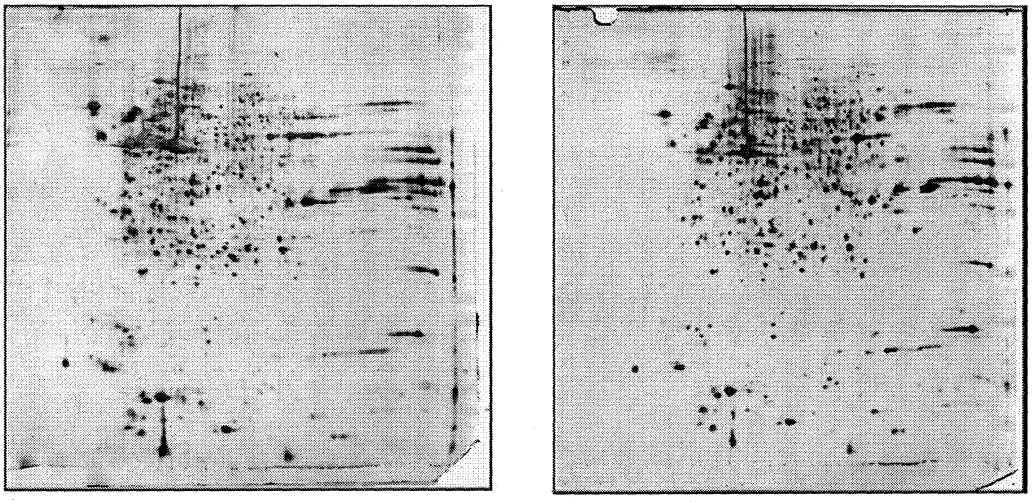

A B

Figure 33: Representative analytical 2D maps of total fibroblast cellular proteins, 72 hours after culture with (A) and without (B) 0.5mg/cm^2 of CoCr particles. 100µg of proteins were loaded onto each 17cm IPG strip of pH 3-10.

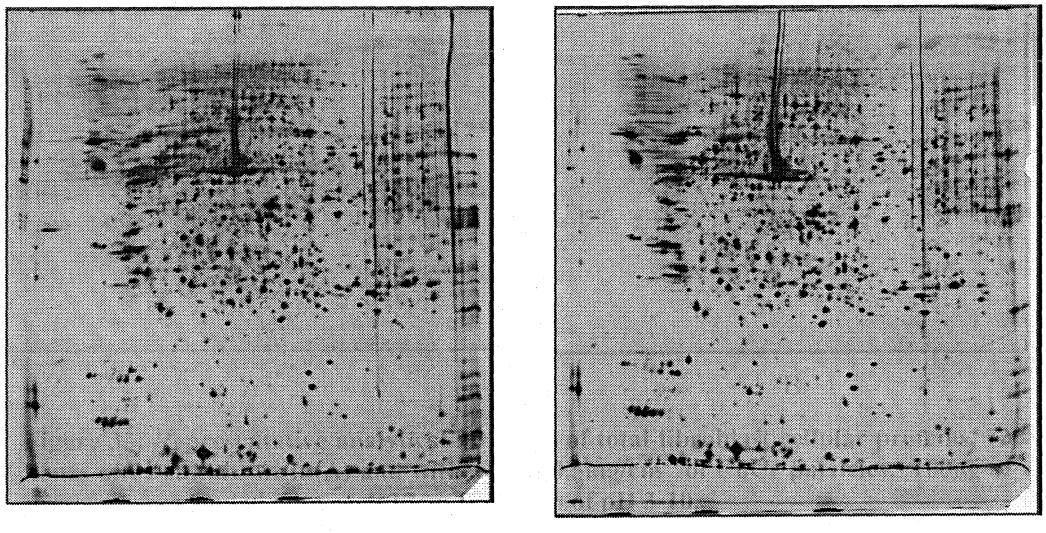

A B

Figure 34: Representative analytical 2D maps of total fibroblast cellular proteins, 72 hours after culture with (A) and without (B) 0.5mg/cm^2 of CoCr particles. 100µg of proteins were loaded onto each 17cm IPG strip of pH 4-7.

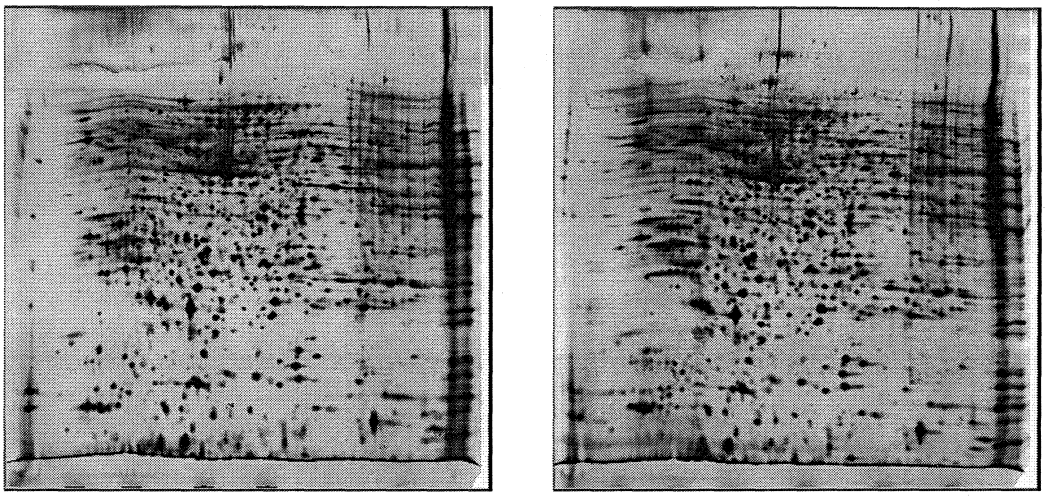

A B

Figure 35: Gel images comparing analytical 2D maps of total monocytes cellular proteins, 48 hours after culture with (A) and without (B) 40% conditioned medium from fibroblast-CoCr cultures. 100µg of proteins were loaded onto each 17cm IPG strip of pH 4-7.

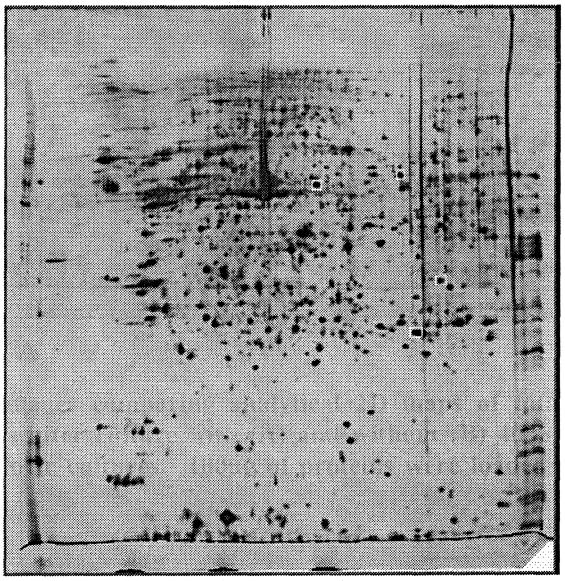

Figure 36: Representative 2D map of total fibroblast cellular proteins, 72 hours after culture with 0.5mg/cm^2 of CoCr particles. 100µg of proteins were loaded onto each 17cm IPG strip pH4-7. Protein spots identified by MALDI TOF TOF MS are represented on the gel image by their serial number.

Table 2: Human MRC-5 fibroblast cellular proteins, identified by MALDI TOF TOF MS, which were found to have two fold increase in expression following a 72 hour culture with CoCr particles.

Serial number	Protein database accession number	Experimental Mass (Da)	Protein Description
1	gi 67464329	60277	Chain A, structure of human muscle pyruvate kinase
2	gi 37655183	43264	N-myc downstream regulated gene 1
3	gi 50845388	40671	Annexin A2 isoform 1
4	gi 999893	26807	Chain B, Triosephoshate Isomerase

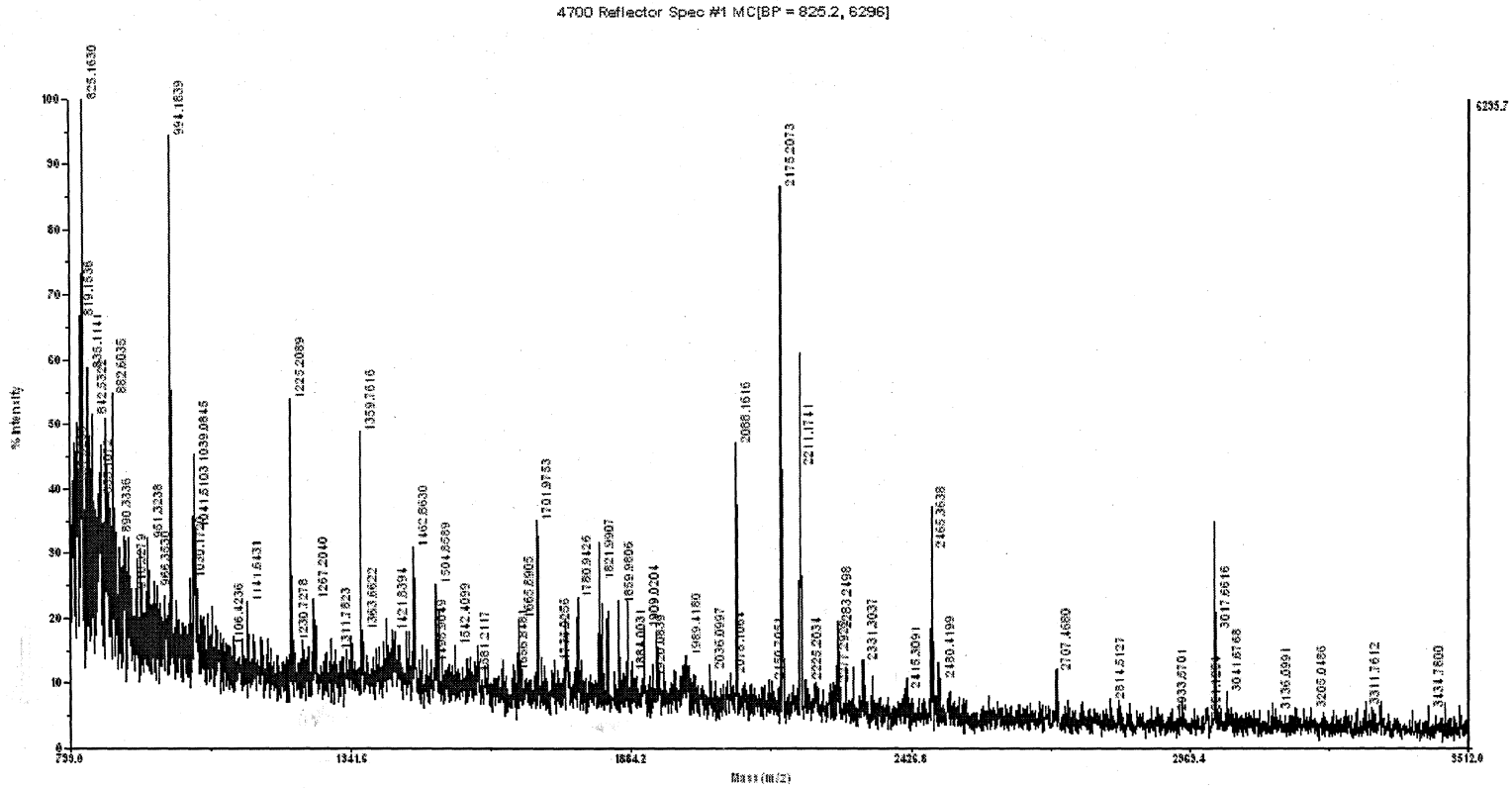

Figure 37: Peptide Mass Fingerprint of Spot 1

PEPTIDE MASS SUMMARY OF SPOT 1

{MATRIX SCIENCE} Mascot Search Results

```
User           :
Email          :
Search title   : SampleSetID: 2822, AnalysisID: 6488, MaldiWellID: 142044, SpectrumID: 890675, Path=\
Database       : NCBInr 060105 (3157245 sequences; 1086037599 residues)
Timestamp      : 16 Jan 2006 at 12:50:43 GMT
Warning        : A Peptide summary report will usually give a much clearer picture of MS/MS search re
Top Score      : 142 for gi|67464392, Chain A, Structure Of Human Muscle Pyruvate Kinase (Pkm2)
```

Probability Based Mowse Score

Ions score is -10*Log(P), where P is the probability that the observed match is a random event.
Protein scores greater than 78 are significant (p<0.05).

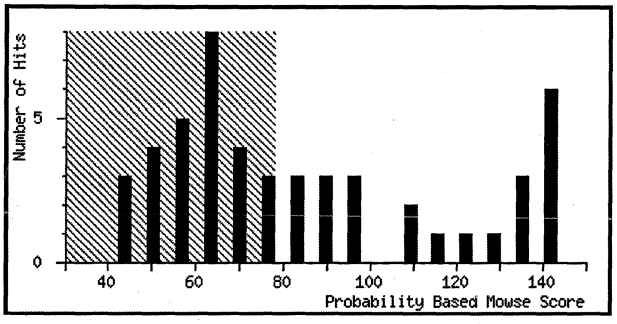

Protein Summary Report

Switch to Peptide Summary Report

To create a bookmark for this report, right click this link: Protein Summary Report (SampleSetID: 2822, AnalysisID: 6488, MaldiWellID: 142044, SpectrumID: 890675, Path=\WXH 2006\060113_6481_99\MS_msms)

Re-Search All | Search Unmatched

Index

	Accession	Mass	Score	Description
1.	gi|67464392	60277	142	Chain A, Structure Of Human Muscle Pyruvate Kinase (Pkm2)
2.	gi|35505	58411	140	pyruvate kinase [Homo sapiens]
3.	gi|14043291	58470	140	Pyruvate kinase 3, isoform 1 [Homo sapiens]
4.	gi|33303751	58583	140	pyruvate kinase, muscle [synthetic construct]
5.	gi|62897413	58517	140	pyruvate kinase 3 isoform 1 variant [Homo sapiens]
6.	gi|31416989	58512	139	Pyruvate kinase 3, isoform 1 [Homo sapiens]
7.	gi|33870117	62046	137	Unknown (protein for IMAGE:2958817) [Homo sapiens]
8.	gi|33873708	62025	137	Unknown (protein for IMAGE:4299213) [Homo sapiens]
9.	gi|33875497	62082	137	Unknown (protein for IMAGE:2964687) [Homo sapiens]
10.	gi|189998	58447	129	M2-type pyruvate kinase
11.	gi|73535281	62570	121	Chain D, Human Pyruvate Kinase M2
12.	gi|34782802	37595	116	PKM2 protein [Homo sapiens]
13.	gi|338827	58534	111	cytosolic thyroid hormone-binding protein (EC 2.7.1.40)
14.	gi|74198829	58390	108	unnamed protein product [Mus musculus]
15.	gi|74221210	58379	97	unnamed protein product [Mus musculus]
16.	gi|74196318	58377	96	unnamed protein product [Mus musculus]
17.	gi|16741633	58378	96	Pyruvate kinase 3 [Mus musculus]
18.	gi|2117873	58479	88	pyruvate kinase (EC 2.7.1.40), muscle splice form M1 - human
19.	gi|33286422	58538	88	pyruvate kinase 3 isoform 2 [Homo sapiens]
20.	gi|74222653	58320	87	unnamed protein product [Mus musculus]

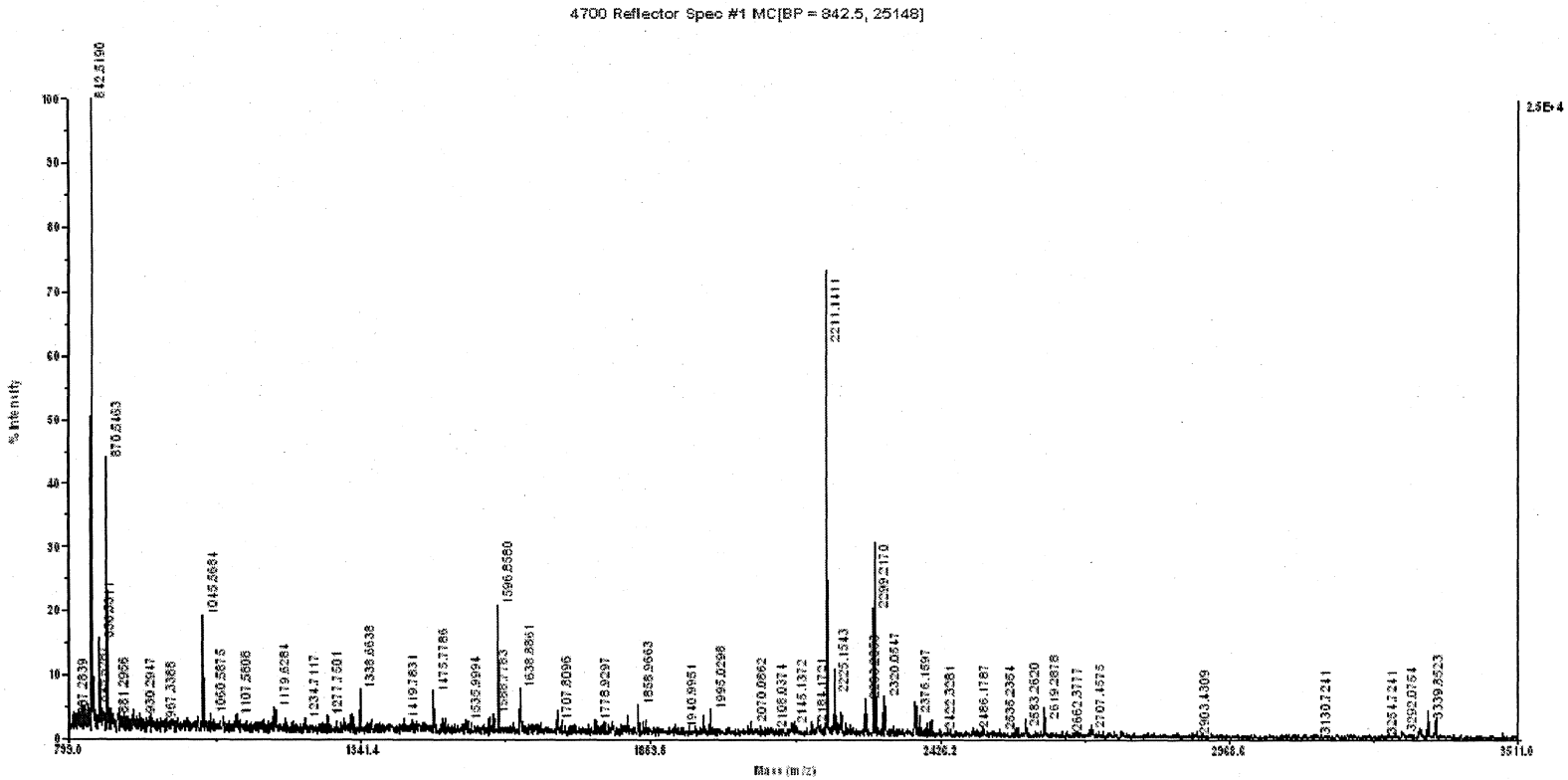

Figure 38: Peptide Mass Fingerprint of Spot 2

PEPTIDE MASS SUMMARY OF SPOT 2

Mascot Search Results

```
User            :
Email           :
Search title    : SampleSetID: 2842, AnalysisID: 6569, MaldiWellID: 143027, SpectrumID: 901269, Path=\
Database        : NCBInr 060105 (3157245 sequences; 1086037599 residues)
Timestamp       : 10 Feb 2006 at 02:13:17 GMT
Warning         : A Peptide summary report will usually give a much clearer picture of MS/MS search re
Top Score       : 100 for gi|37655183, N-myc downstream regulated gene 1 [Homo sapiens]
```

Probability Based Mowse Score

Ions score is -10*Log(P), where P is the probability that the observed match is a random event.
Protein scores greater than 78 are significant (p<0.05).

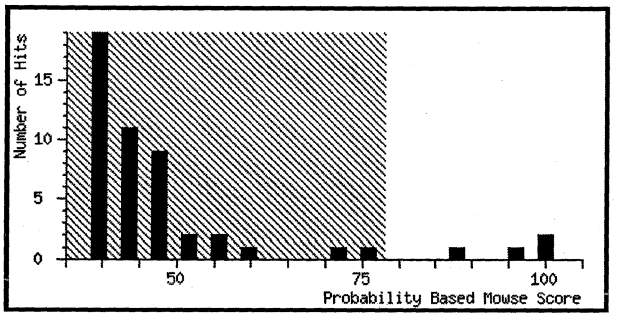

Protein Summary Report

Switch to Peptide Summary Report

To create a bookmark for this report, right click this link: Protein Summary Report (SampleSetID: 2842, AnalysisID: 6569, MaldiWellID: 143027, SpectrumID: 901269, Path=\WXH 2006\060209_4468_56\all)

Re-Search All | Search Unmatched

Index

	Accession	Mass	Score	Description
1.	gi|37655183	43264	100	N-myc downstream regulated gene 1 [Homo sapiens]
2.	gi|33415057	43248	100	transformation-related protein 14 [Homo sapiens]
3.	gi|21754953	35602	97	unnamed protein product [Homo sapiens]
4.	gi|2344812	43252	88	Drg1 [Homo sapiens]
5.	gi|62898816	43292	78	N-myc downstream regulated gene 1 variant [Homo sapiens]
6.	gi|67971160	43330	73	unnamed protein product [Macaca fascicularis]
7.	gi|13623315	11491	58	NDRG1 protein [Homo sapiens]
8.	gi|17741185	24972	57	ABC transporter, nucleotide binding/ATPase protein [Agrobacterium tumef
9.	gi|73974634	42165	56	PREDICTED: similar to N-myc downstream regulated gene 1 [Canis familia
10.	gi|76649697	25477	53	PREDICTED: similar to keratin 17 isoform 3 [Bos taurus]
11.	gi|23612135	41623	50	ST kinase, putative [Plasmodium falciparum 3D7]
12.	gi|27696230	50066	49	MGC52862 protein [Xenopus laevis]
13.	gi|71913740	31541	49	conserved hypothetical protein [Mycoplasma hyopneumoniae 7448]
14.	gi|22778535	36411	48	2-ketogluconate reductase [Oceanobacillus iheyensis HTE831]
15.	gi|77738709	53576	48	Chlorophyllide reductase subunit Z [Rhodopseudomonas palustris BisA53]
16.	gi|76634732	40977	48	PREDICTED: similar to developmentally regulated GTP binding protein 1
17.	gi|47218506	39057	48	unnamed protein product [Tetraodon nigroviridis]
18.	gi|46447886	40299	46	efflux transporter, RND family, MFP subunit [Desulfovibrio vulgaris sub
19.	gi|76649255	54836	46	PREDICTED: similar to 6-phosphofructo-2-kinase/fructose-2,6-biphosphat
20.	gi|13620690	37819	46	hypothetical protein [Streptomyces coelicolor A3(2)]

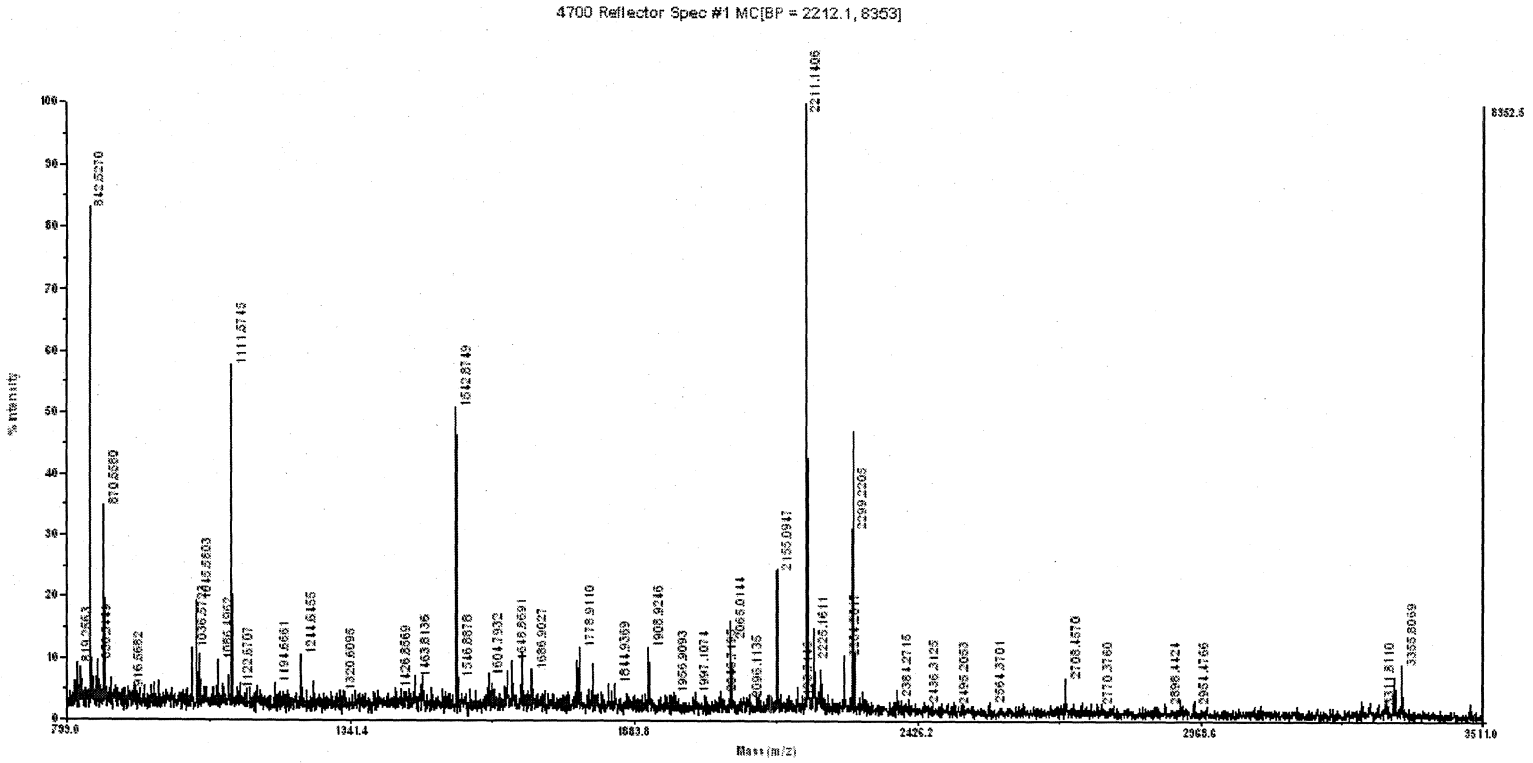

Figure 39: Peptide Mass Fingerprint of Spot 3

{MATRIX SCIENCE} Mascot Search Results

```
User           :
Email          :
Search title   : SampleSetID: 2842, AnalysisID: 6569, MaldiWellID: 143031, SpectrumID: 901295, Path=\
Database       : NCBInr 060105 (3157245 sequences; 1086037599 residues)
Timestamp      : 10 Feb 2006 at 02:23:35 GMT
Warning        : A Peptide summary report will usually give a much clearer picture of MS/MS search re
Top Score      : 190 for gi|50845388, annexin A2 isoform 1 [Homo sapiens]
```

Probability Based Mowse Score

Ions score is -10*Log(P), where P is the probability that the observed match is a random event.
Protein scores greater than 78 are significant (p<0.05).

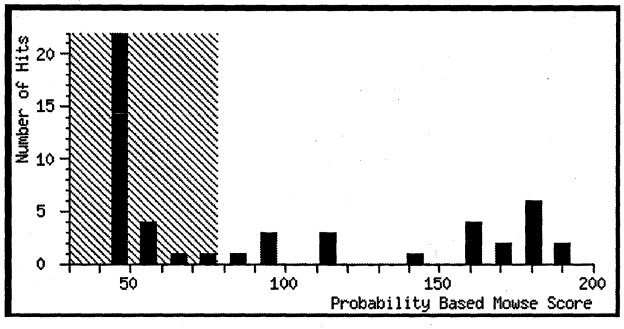

Protein Summary Report

Switch to Peptide Summary Report

To create a bookmark for this report, right click this link: Protein Summary Report (SampleSetID: 2842, AnalysisID: 6569, MaldiWellID: 143031, SpectrumID: 901295, Path=\WXH 2006\060209_4468_56\all)

Re-Search All | Search Unmatched

Index

	Accession	Mass	Score	Description
1.	gi|50845388	40671	190	annexin A2 isoform 1 [Homo sapiens]
2.	gi|34364597	40613	190	hypothetical protein [Homo sapiens]
3.	gi|16306978	38822	185	Annexin A2, isoform 2 [Homo sapiens]
4.	gi|12655075	38808	185	Annexin A2, isoform 2 [Homo sapiens]
5.	gi|18645167	38780	185	ANXA2 protein [Homo sapiens]
6.	gi|62896643	38792	185	annexin A2 isoform 2 variant [Homo sapiens]
7.	gi|30584373	38921	184	Homo sapiens annexin A2 [synthetic construct]
8.	gi|73909156	40731	182	ANXA2 protein [Homo sapiens]
9.	gi|55642227	52738	175	PREDICTED: similar to annexin A2 isoform 1; lipocortin II; annexin II;
10.	gi|56966699	38866	171	Chain A, Annexin A2: Does It Induce Membrane Aggregation By A New Mult
11.	gi|56967119	36631	161	Chain B, Structure Of Human Annexin A2 In The Presence Of Calcium Ions
12.	gi|73586982	38801	160	Annexin A2 [Bos taurus]
13.	gi|27807289	38873	160	annexin A2 [Bos taurus]
14.	gi|50950177	38915	160	annexin A2 [Canis familiaris]
15.	gi|52631987	38795	146	annexin A2 [Sus scrofa]
16.	gi|9247201	39021	118	annexin II [Rattus sp.]
17.	gi|9845234	38939	118	annexin A2 [Rattus norvegicus]
18.	gi|9247200	39236	118	annexin II; calpactin 1 [Rattus sp.]
19.	gi|13097099	38937	99	Annexin A2 [Mus musculus]
20.	gi|63594732	32864	99	PREDICTED: similar to Annexin A2 (Annexin II) (Lipocortin II) (Calpact

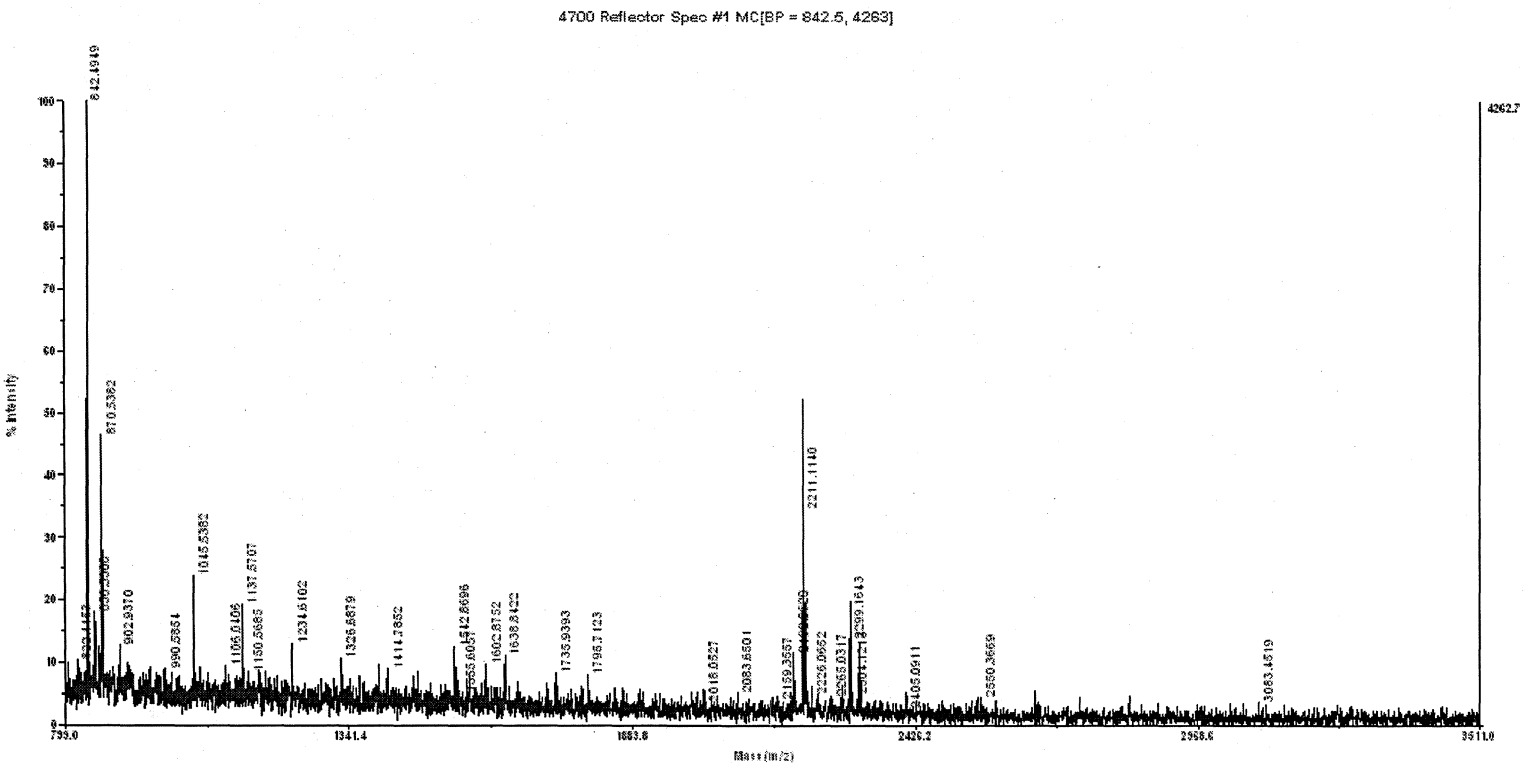

Figure 40: Peptide Mass Fingerprint of Spot 4

PEPTIDE MASS SUMMARY OF SPOT 4

{MATRIX SCIENCE} Mascot Search Results

```
User            :
Email           :
Search title    : SampleSetID: 2842, AnalysisID: 6569, MaldiWellID: 143039, SpectrumID: 901346, Path=\
Database        : NCBInr 060105 (3157245 sequences; 1086037599 residues)
Timestamp       : 10 Feb 2006 at 02:43:56 GMT
Warning         : A Peptide summary report will usually give a much clearer picture of MS/MS search re
Top Score       : 90 for gi|999893, Chain B, Triosephosphate Isomerase (Tim) (E.C.5.3.1.1) Complexed W
```

Probability Based Mowse Score

Ions score is -10*Log(P), where P is the probability that the observed match is a random event.
Protein scores greater than 78 are significant (p<0.05).

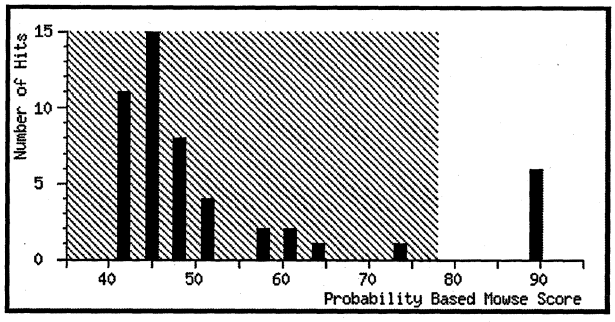

Protein Summary Report

Switch to Peptide Summary Report

To create a bookmark for this report, right click this link: Protein Summary Report (SampleSetID: 2842, AnalysisID: 6569, MaldiWellID: 143039, SpectrumID: 901346, Path=\WXH 2006\060209_4468_56\all)

Re-Search All | Search Unmatched

Index

	Accession	Mass	Score	Description
1.	gi|999893	26807	90	Chain B, Triosephosphate Isomerase (Tim) (E.C.5.3.1.1) Complexed With ;
2.	gi|17389815	26910	90	Triosephosphate isomerase 1 [Homo sapiens]
3.	gi|4507645	26938	90	triosephosphate isomerase 1 [Homo sapiens]
4.	gi|62896835	26981	90	triosephosphate isomerase 1 variant [Homo sapiens]
5.	gi|55730014	26941	90	hypothetical protein [Pongo pygmaeus]
6.	gi|66360366	26951	89	Chain B, Human Triosephosphate Isomerase Of New Crystal Form
7.	gi|83674984	26967	74	rcTPI1 [Gorilla gorilla]
8.	gi|73997314	24638	63	PREDICTED: similar to Triosephosphate isomerase (TIM) (Triose-phosphate
9.	gi|136066	26894	61	Triosephosphate isomerase (TIM) (Triose-phosphate isomerase)
10.	gi|73997318	26983	61	PREDICTED: similar to Triosephosphate isomerase (TIM) (Triose-phosphate
11.	gi|62868677	34125	56	elicitor of the hypersensitivity reaction [Erwinia chrysanthemi]
12.	gi|675519	34253	56	HrpN harpin [Erwinia chrysanthemi]
13.	gi|39647708	28938	52	putative short-chain alcohol dehydrogenase-like protein [Rhodopseudomor
14.	gi|73997316	23182	51	PREDICTED: similar to Triosephosphate isomerase (TIM) (Triose-phosphate
15.	gi|77388600	14590	51	transcriptional regulator, ArsR family [Rhodobacter sphaeroides 2.4.1]
16.	gi|66805707	69721	50	hypothetical protein DDB0188051 [Dictyostelium discoideum]
17.	gi|55637745	23241	49	PREDICTED: similar to Triosephosphate isomerase (TIM) (Triose-phosphate
18.	gi|342348	26979	47	triosephosphate isomerase [Macaca mulatta]
19.	gi|74267824	26901	47	Triosephosphate isomerase [Bos taurus]
20.	gi|47682755	27762	47	TPI1 protein [Homo sapiens]

Fibroblasts are much more than a source of scaffolding. They are key cells in the wound repair process. They participate in the immune response by producing and responding to cytokines and chemokines that initiate the recruitment and retention of bone marrow-derived immune effector cells. The fibrous capsule that forms around joint prosthesis is comprised of mainly collagen along with cells like fibroblasts and fibrocytes. Following initial release of wear debri from the implant, the fibroblast and fibrocytes are the first type of cells to come into contact with these particles. In the present study we have used the proteomic platforms of 2D gel electrophoresis and tandem mass spectrometry to elucidate the molecular changes in specific cell types in response to CoCr alloy particles using *in vitro* models. *The use of these proteomic platforms to study the effects of clinically relevant CoCr particles on fibroblast intracellular proteins has been reported for the first time, through this work.*

Particles of CoCr (Haynes alloy, ASTM F-75), a commonly used constituent of joint prosthesis, were used in this study at clinically relevant sizes of 1-7μm. Human Lung fibroblasts MRC-5 have been used in earlier *in vitro* studies to evaluate biological response to wear debri (Reno F *et al*, 2002). Cobalt is highly toxic and cobalt ions that leach out from CoCr alloys have also been shown to induce cellular damage *in vitro* (Evans EJ *et al*, 1986 and 1994). The toxicity of CoCr being well documented, preliminary experiments were carried using light microscopy evaluation and MTS assay to obtain a concentration of CoCr particles wherein the viability of the fibroblast cells in the experimental cultures was not reduced when compared to the control cultures without CoCr particles. Our results are in agreement with previous studies which show that cobalt and chromium ions induce a dose-dependent cytotoxic effect on MG63 osteoblast like cells (Fluery C *et al*, 2006). Our results also indicate

that following 72 hours incubation, fibroblasts cultured with low concentrations of particles, demonstrated an increase in cell viability as compared to control. Earlier reports have demonstrated an increase in proliferation of bovine synovial fibroblast on exposure to low concentrations of titanium, chromium and titanium-aluminium and a decrease in cellular proliferation even at very low concentrations of cobalt (Maloney WJ *et al*, 1993).

2DE of the cellular proteins extracted from fibroblasts following 72 hour culture with CoCr particles revealed thirteen protein spots to be upregulated. Of these, four proteins were identified by tandem mass spectrometry using MALDI TOF TOF MS. These being, N-myc downstream regulated gene 1 protein, Triose phosphate isomerase, Pyruvate kinase and Annexin II isoform 1.

N-myc downstream regulated gene 1 protein (Ndrg1) is a stress responsive protein that shuttles between cytoplasm and nucleus. This recently discovered protein is also named as Cap 43, Drg1, RTP and rit 42 and is involved in stress response, hormone response, cell growth and differentiation. Research has shown that the expression of NDRG1 gene is induced by nickel, a transition metal sharing similar physical properties to cobalt. Ndgr1 is also known as nickel specific induction protein (Slanikow K *et al*, 2000 (a), 2002 and Li J *et al*, 2004).

Glycolysis is the major metabolic pathway for the utilization of glucose. Triose phosphate isomerase and Pyruvate kinase are vital enzymes in the glycolytic pathway. Triose phosphate isomerase catalyses the reversible conversion of dihydroxyacetone to glyceraldehyde 3-phosphate, the latter proceeding into the glycolytic pathway. Pyruvate kinase catalyses the final step in glycolysis ie., the conversion of phosphoenol

pyruvate to pyruvate with concomitant phosphorylation of ADP to ATP. This step is one of the major regulatory steps of glycolysis.

Annexins are a family of calcium regulated phospholipid binding and membrane binding protein. They function as membrane-membrane or membrane cytoskeletal linkers and have been implicated in Ca^{2+} regulated exocytotic events, certain aspects of endocytosis and stabilization of specific domains of organelle membranes and the plasma membrane. Members of this calcium dependent phospholipids binding protein family play a role in the regulation of cellular growth and in the signal transduction pathways. Annexin II also binds F actin and has a calcium dependent filament bundling activity (Gerke V *et al*, 2002 and 2004). This protein also functions as an autocrine/paracrine factor secreted by osteoclasts that stimulates human osteoclasts formation and bone resorption *in vitro*. Annexin II has been reported to induce GM-CSF expression and RANKL synthesis by bone marrow stromal cells. Both GM-CSF and RANKL are required for Annexin II stimulation of osteoclasts formation (Li F *et al*, 2005 and Menna C *et al*, 1999). Annexins also play a role in adhesion, inflammation and fibrinolysis. Recent research initiatives have also shown Annexin II to be involved in cellular response to oxidative stress.

Earlier reports have demonstrated the ability of Co^{2+} and Cr^{3+} to modify the redox state and cause oxidation of cellular proteins in Human U937 macrophages and MG 63 osteoblasts (Fluery C *et al*, 2006 and Petit A *et al*, 2005). Data obtained from the present study are similar in that CoCr alloy in particulate form evinced a change in the redox state of human fibroblast. Divalent cobalt ions induce the stabilization of HIF-1α under normoxic conditions, thereby mimicking a hypoxia like state (Bunn HF *et al*, 1996). HIF-1α (Hypoxia inducible transcription factor) is a major transcription

factor that regulates hypoxia responsive genes. Peters *et al*, (2005) have shown the stabilization of the HIF-1α in human EC following exposure to divalent cobalt. Hypoxia has been reported to be an inducer of the NDRG1 gene and the hypoxic induction of the NDRG1 gene is proved to be dependent on the transcription factor HIF-1α (Cangul H, 2004). The expression of Ndrg1 protein is also induced by nickel, a transition metal sharing similar physical properties to cobalt. Nickel creates hypoxia like conditions in cells and induces hypoxia responsive genes. Our results indicate an upregulation of both the Ndrg1 protein and major proteins of the glycolytic pathway proteins i.e., Triose phosphate isomerase and Pyruvate kinase. These results are in agreement with previous reports showing the induction of genes involved in glucose transport and glycolysis in mice fibroblast by both hypoxia and the transition metal nickel (Slanikow K *et al*, 2000 (b) and 2002). Upregulation in the glycolytic enzyme triose phosphate isomerase in hypoxygenated tissue has also been demonstrated. RNAs encoding the glycolytic enzyme Aldolase a, Phoshoglycerate kinase 1 and Pyruvase kinase M were found to be induced in Hep3B and HeLa cells on exposure to the hypoxia mimicking agent cobalt chloride (Semenza LG *et al*, 1994). The expression of triose phosphate isomerase has been experimentally proved to be regulated via the HIF pathway (Geiss B *et al*, 2004). Data from our experiments also show an upregulation of the protein Annexin 2. There is growing evidence of the role of Annexin II in the cellular response to oxidative stress. The over expression of Annexin II has been demonstrated *in vitro* in porcine renal tubular cell lines LLC-PK1, following treatment with H_2O_2, an inducer of oxidative stress (Tanaka T *et al*, 2004). *In vivo* studies have also shown an upregulation of annexin II at the RNA level in renal proximal tubules of rats that were subjected to oxidative stress via treatment with ferric nitrilotriacetate (Tanaka T *et al*, 2000).

Macrophages, which are key players in the inflammatory response that leads to periprosthetic osteolysis, come into the scenario only at a later stage. Monocytes are released from the bone marrow and circulate in the blood before extravasating into the tissues, where they differentiate into resident macrophages. In order to elucidate the downstream interactions between fibroblasts and monocytes, the effect of conditioned medium from the fibroblast-CoCr cultures on the intracellular protein expression of human monocyte U937 culture was analyzed by 2D gel electrophoresis. Comparing the experimental replicate group with the control via PDQuest analysis however did not reveal any protein spots that exhibited a two fold increase in intensity. These results indicate that the activation of monocytes might not be directly influenced by the fibroblasts and suggest the requirement of other chemokines like M-CSF or other cell types probably endothelial cells.

It is therefore conceivable that the introduction of CoCr debri into the biological milieu influences a change in the redox state of the fibroblasts in the interfacial membrane and induces the transition of the fibroblast cells into a hypoxia like state. The data obtained are results from preliminary experiments that need to be investigated by further experimentation looking at upregulation at the RNA level. The study reflects the possibility of a hypoxic environment in the periprosthetic tissue surrounding metallic implants, an aspect that warrants further investigation. These results find significance in view of the recent comeback of metal on metal joint prosthesis.

Chapter 5

SUMMARY, CONCLUSIONS & FUTURE DIRECTIVES

Artificial joint replacements have provided a new lease of life in many patients, where the function of the normal joint has been compromised as a result of disease or accident. However, asceptic loosening continues to be a vexing problem and the primal reason for failure of the joint prosthesis. Much research is being dedicated to understand the pathomechanisms of asceptic loosening and most of these works have centered on the study of tissue surrounding clinically failed implants and in delineating the role of macrophages, osteoblasts and osteoclasts in asceptic loosening.

5.1. SUMMARY

This work was undertaken with the specific aim of studying the cellular response to particulate material of the orthopedic biomaterial CoCr alloy (ASTM-F75) in soft tissue using an *in vivo* model and in elucidating the molecular changes in specific cell types, in response to these particles using *in vitro* models. To achieve these aims the plan of work was undertaken under three phases with the objectives (i) To study the molecular mechanisms involved in the progress of cellular response to

particulate material in an *in vivo* model (ii) To evaluate cell-material interactions at the molecular level using an *in vitro* model and (iii) To elucidate changes in cellular protein profile, in response to particulate material using an *in vitro* model.

In the *in vivo* experiments CoCr alloy particles were injected into the gluteus muscle of young adult male Wistar rats, using saline as a carrier. Saline alone served as control. The animals were sacrificed and host response to implanted metal particles studied over fourteen different time periods ranging from 1 to 150 days. Results obtained from light microscopical evaluation, transmission electron micrographs and immunohistochemical studies corroborate to reveal a characteristic difference in host response to when particles are implanted in the endomysium and when implanted directly into the muscle fiber. With time excessive fibrosis with aggregation of the metal particles into clumps and presence of dense connective tissue, numerous blood vessels, fibroblasts, fibrocytes and scant macrophages was noted in the endomysium, while mild but persistent chronic inflammation was noted in the muscle fibre. The difference in response could be attributed to the difference in cellular composition of endomysium and muscle fibre. The presence of proinflammatory cytokines IL-1α, IL-6, TNF-α was detected at early time periods. Cells that stained for the macrophage markers ED1 and ED2 were also positive for the cytokines suggesting that it is the macrophages in early time periods that are responsible for the secretion of proinflammatory cytokines.

We hypothesize that since the fibrous capsule that surrounds the prosthesis is mainly composed of collagen and few cells of fibroblasts and fibrocytes, the particulate materials that emanate from the surface of the prosthesis would first come in contact with these cells. In addition, the excessive fibrosis noted at the later time periods of our

in vivo study also promted us to evaluate the interactions of fibroblasts with CoCr alloy particles, using *in vitro* models. Two different *in vitro* models, murine L929 fibroblasts and human MRC-5 fibroblasts were used. The metal particles were observed to be toxic to the fibroblasts at higher concentrations. Close associations of the CoCr alloy particles along the cellular margins on the dorsal surface were noted. Though no drastic changes in cellular morphology was noted, changes in the distribution pattern of F-actin and α-actinin, especially at areas of cell-particle interaction were revealed through confocal laser scanning microscopy. The results obtained also suggest the possibility of uptake of the particles by the L929 fibroblasts. Evaluation via ELISA of the proinflammatory capability of particle stimulated fibroblasts did not show any significant changes in cytokine expression of IL-6 and IL-1α in murine L929 fibroblasts following 72 hours culture with varying concentrations of CoCr alloy particles.

This study has also for the first time evaluated changes in cellular protein profile of fibroblasts grown with CoCr alloy particles using the proteomic platforms of 2DGE and MALDI-TOF TOF MS. Four proteins Annexin II, Pyruvate kinase, Triose phosphate isomerase and N-myc downstream regulated gene 1 protein were found to be upregulated. Cobalt is a hypoxia mimicking agent and N-myc downstream regulated gene 1 protein, Triose phosphate isomerase, Pyruvate kinase and Annexin II are important hypoxia regulated gene products that are found to be over expressed in cellular oxidative stress response. Our data indicates that exposure of fibroblast to CoCr induces the transition of these cells into a state of hypoxia and oxidative stress even in normoxic culture conditions. The study reflects the possibility of a hypoxic environment in the periprosthetic tissue surrounding metallic implants.

The proinflammatory capability of particle stimulated fibroblasts was further probed by evaluating the effect of conditioned medium from these fibroblast-CoCr cultures on protein expression profile of human monocytes U-937. An increase in the expression of intracellular proteins of the U937monocytes was not effected, which indicates that the activation of monocytes might not be directly influenced by the fibroblasts and suggest the requirement of other chemokines like M-CSF or other cell types probably endothelial cells

5.2. CONCLUSIONS

Data obtained from this study show that the cellular response to CoCr alloy particles in soft tissue follows a sequence that culminates in the formation of excessive fibrosis within the endomysium and a persistant chronic inflammation within the muscle fiber. The endomysium mimics the interfacial membrane around implants in its cellular constituents and hence reflects the initial sequence of response once material particles are released into the biological milieu. As evinced by the *in vitro* experiments CoCr alloy particles induce the transition of fibroblast cells into a hypoxia like state, suggesting the possibility of a hypoxic environment in the interfacial membrane. Hypoxia is a known potent inducer of fibrogenesis and angiogenesis and could be responsible for the excessive fibrosis seen at later time periods in our *in vivo* studies. The results of this study draw significance in view of the recent comeback of metal on metal total hip implants.

5.3. FUTURE DIRECTIVES

Insights revealed from this work on the importance of the fibroblasts in material particle-tissue interaction reflect the need to further study the functions of fibroblasts as a major player in the pathomechanisms of periprosthetic osteolysis and

asceptic loosening. Future directives in relation to this work would focus on identifying the role of hypoxic fibroblasts in mediating and promoting osteoclastogenesis especially in relation to wear debri induced periprosthetic osteolysis. The role of endothelial cells in the downstream activation of macrophages, fibroblasts also needs to be further probed. Identifying the key regulators of wear debri induced inflammation, would help in devicing means of preventing periprosthetic osteolysis, which is at present a major setback in older patients who have the added problem of osteoporosis.

BIBLIOGRAPHY

Akisue T, Bauer TW, Farver CF and Mochida Y. The effect of particle wear debris on NF- κB activation and proinflammatory cytokine release in differentiated THP-1 cells. J Biomed Mater Res 2002;59:507-515.

Al Saffar N and Revell PA. Interleukin-1 production by activated macrophages surrounding loosened orthopaedic implants: A potential role in osteolysis. Br J Rheumatol 1994;33:309-316.

Al Saffar N, Revell PA, Khwaja HA and Bonefield W. Assessment of the role of cytokines in bone resorption in patients with total joint replacements. J Mater Sci: Mater in Med 1995;6:762-767.

Algan SM, Purdon M and Horowitz SM. Role of tumor necrosis factor alpha in particulate induced bone resorption. J Orthop Res 1996;14:30-35.

Al-Saffar N. The osteogenic properties of the interface membrane at the site of orthopedic implants: The impact of underlying joint disease. J Long Term Eff. Med Implants. 1999;9:23-45.

Anissian HL, Stark A, Good V, Dahlstand H and Clarke IC. The wear attern in metal on metal hip prosthesis. J Biomed Mater Res (Appl Biomater) 2001;58:673-678.

Archibeck MJ, Jacobs JJ, Roebuck KA and Glant TT. The Basic Science of Periprosthetic Osteolysis. J Bone Joint Surg Am. 2000;82:1478-1489.

Basle MF, Bertrand G, Guyent S, Chappard D and Lesourd M. Migration of metal and polyethylene particles from articular prostheses may generate lymphadenopathy with histiocytosis. J Biomed Mater Res 1996;30:157-164.

Becker S, Soukup JM, Gilmour ML, Delvin RB. Stimulation of human and rat alveolar macrophages by urban air particulates: effects on oxidant radical generation and cytokine production. Toxicol Appl Pharmacol 1996;141:637-48.

Bernd Baumann, Jochen Seufert , Franz Jakob , Ulrich Noth , Olaf Rolf , Jochen Eulert , Christof P. Rader. Activation of NF-KB signalling and TNFa-expression in THP- 1 macrophages by TiAlVa- and polyethylene-wear particles. Journal of Orthopaedic Research 2005;23:1241-1248.

Blaine TA.; Pollice, P. F.; Rosier, R. N.; Reynolds, P. R.; Puzas, J. E.; and O'Keefe, R. J. Modulation of the production of cytokines in titanium-stimulated human peripheral blood monocytes by pharmacological agents. The role of cAMP-mediated signaling mechanisms. J. Bone and Joint Surg., 1997;79-A: 1519-1528.

Blum et al., Improved silver staining of plant proteins, RNA and DNA in polyacrylamide gels. Electrophoresis 1987; 8: 93-99.

Boss JH, Misselevich I, Behar J and Mendes DG. Histological analysis of the periprosthetic tissues of long term surviving cemented total hip arthroplasties. J Long Term Effects of Medical Implants. 1996; 6:73-90.

Bukata SV, Gelinas J , Wei X , Rosier RN , Puzas JE, Zhang X , Schwarz EM, Song XR, Griswold DE , Okeefe RJ. PGE2 and IL-6 production by fibroblasts in response to titanium wear debris particles is mediated through a Cox-2 dependent pathway. Journal of Orthop Res 2004; 22: 6–12.

Bunn HF, Poyton RO. Oxygen sensing and molecular adaptation to hypoxia. Physiol Rev 1996;76:839-885.

Cangul H. Hypoxia ugregulates the expression of the NDRG1 gene leading to its overexpression in various human cancers. BMC Genetics 2004;5:27.

Catelas I, Medley JB, Campell PA, Huk OL and Bobyn JD. Comparison of *In vitro* with *In vivo* characteristics of wear particles from metal-metal hip implants. J Biomed Mater Res Part B: Appl Biomater 2004;70B:167-178.

Catelas I, Petit A, Vali H, Fragiskatos C, Meilleur R, Zukor DJ, Antoniou J and Huk OL. Quantitative analysis of macrophage apoptosis vs necrosis induced by cobalt and chromium ions *in vitro*. Biomaterials 2005;26:2441-2453.

Catelas I, Petit A, Zukor DJ and Huk OL. Cytotoxic and apoptotic effects of cobalt and chromium ions on J774 macrophages-Implication of caspase-3 in the apoptotic pathway. J Mater Sci: Mater in Med 2001;12:949-953.

Catelas I, Petit A, Zukor DJ, Antoniou J and Huk OL. TNF-α secretion and macrophage mortality induced by cobalt and chromium ions in *in vitro* qualitative analysis of apoptosis. Biomaterials 2003;24:383-391.

Clohisy JC, Hirayama T, Frazier E, Han Suk-Ku and Amer YA. NF-kB signaling blockade abolishes implant particle-induced osteoclastogenesis. J Orthop Res 2004;22: 13-20.

Dobbs HS and Minski MJ. Metal ion release after total hip replacement. Biomaterials 1980;1:193-198.

Doorn PF, Campbell PA, Worrall J, Benya PD and Mckellop HA. Metal wear particle characterization from metal on metal total hip replacements: Transmission electron microscopy study of periprosthetic tissues and isolated particles. J Biomed Mater Res 1998;42:103-111.

Eriksson AS and Thomsen P. Leukotriene B4, interleukin 1 and leucocyte accumulation in titanium and PTFE chambers after implantation in the rat abdominal wall. Biomaterials 1991;12:827-830.

Evans EJ and Thomas IT. The in-vitro toxicity of cobalt-chrome-molybdenum alloy and its constituent metals. Biomaterials 1986;7:25-29.

Evans EJ. Cell damage *in vitro* following direct contact with fine particles of titanium, titanium alloy and cobalt- chrome-molybdenum alloy. Biomaterials 1994;15:713-717.

Fleury C, Petit A, Mwale F, Antoniou J, Zukor DJ, Tabrizian M and Hul OL. Effect of cobalt and chromium ions on human MG-63 osteoblasts *in vitro*: Morphology, cytotoxicity and oxidative stress. Biomaterials 2006;27:3351-3360.

Fritz EA, Jacobs JJ, Glant TT and Roebuck KA. Chemokine IL-8 induction by particulate wear debris in osteoblasts is mediated by NF-κB. J Orthop Res 2005;23(6):1249-57.

Garrigues GE, Cho DR, Rubash HE, Goldring SR, Herndon JH and Shanbhag AS. Gene expression clustering using self-organizing maps: analysis of the macrophage response to particulate biomaterials. Biomaterials 2005;26:2933-2945.

Geiss Bernhard, Hofbauer KH, Deutzmann R and Kurtz A. Hypoxia up regulates triose phosphate isomerase expression via a HIF dependent pathway. Eur J Physiol 2004;448:175-180.

Gerke V, Moss SE. Annexins: From structure to function. Physiol Rev 2002;82: 331-371.

Gerke Volker, Rescher U. Annexins-unique membrane binding proteins with diverse function. J Cell Science 2004;117:2631-2639.

Germain MA, Hatton A, Williams S, Mathews JB, Stone MH, Fisher J and Ingham E. Comparison of the cytotoxicity of clinically relevant cobalt chromium and alumina ceramic wear particles *in vitro*. Biomaterials 2003; 24: 469-479.

Goodman S, Trindade M, Ma T, Lee M, Wang N, Ikenou T, Matsuura I, Miyanishi K, Fox N, Regula D, Genovese M, Klein J, Bloch D and Smith RL. Modulation of bone ingrowth and tissue differentiation by local infusion of interleukin-10 in the presence of ultra-high molecular weight polyethylene (UHMWPE) wear particles. J Biomed Mater Res 2003 65A:43-50.

Goodman SB, Knoblich G, O'Connor M, Song Y, Huie P and Sibley R. Heterogeneity in cellular and cytokine profiles from multiple samples of tissue surrounding revised hip prostheses. J Biomed Mater Res 1996;31:421-428.

Grinnell F and Geiger B, Interaction of fibronectin coated beads with attached and spread fibroblasts. Exp Cell Res 1986;162:449-461.

Gwynn API. Cell biology at interfaces. J Mater Sci: Mater in Med 1994;5:357-360.

Hagerty DR, Salzmann DL, Kleinert LB and Williams SK. Cellular proliferation and macrophage populations associated with implanted expanded polytetrafluoroethylene and polyethyleneterephthalate. J Biomed Mater Res 2000;49:489-497.

Hallab NJ, Mikecz K, Vermes C, Skipor A, Jacobs JJ. Differential lymphocyte reactivity to serum-derived metal–protein complexes produced from cobalt-based and titanium-based implant alloy degradation. J Biomed Mater Res 2001; 56: 427–436.

Hallab NJ, Skipor A, Jacobs JJ. Interfacial kinetics of titanium- and cobalt-based implant alloys in human serum: Metal release and biofilm formation. J Biomed Mater Res 2003; 65A: 311–318

Hatton A, Nevelos JE, Mathews JB, Fischer J and Ingham E. Effects of clinically relevant alumina ceramic wear particles on TNF-α production by human peripheral blood mononuclear phagocytes. Biomaterials 2003;24:1193-1204.

Henderson B. Therapeutic modulation of cytokines. Annals of the Rheumatic Diseases 1995;54:519-523.

Hercus B and Revell PA. Phenotypic characteristics of T lymphocytes in the interfacial tissue of asceptically loosened prosthetic joints. J Mater Sci: Mater in Med 2001;12:1063-1067.

Hercus B, Saed S and Revell PA. Expression profile of Tcell associated molecules in the interface tissue of aseptically loosened prosthetic joints. J Mater Sci: Mater in Med 2002;13:1153-1156.

Hirakawa K, Bauer TW, Stulberg BN and Wilde AH. Comparison and quantification of wear debris of failed total hip and knee arthroplasty. J Biomed Mater Res 1996;31:257-263.

Hooper KA, Nickolas TL, Yurkow EJ, Kohn J and Laskin DL. Characterization of the inflammatory response to biomaterials using a rodent air pouch model. J Biomed Mater Res 2000;50:365-374.

Horowitz SA and Gonzales JB. Effects of polyethylene on macrophages. J Orthop Res 1997;15:50-56.

Horowitz SM and Purdon MA. Mechanisms of cellular recruitment in asceptic loosening of prosthetic joint implants. Calcif Tissue Int 1995;57:301-305.

Horowitz SM, Algan SA and Purdon MA. Pharmacologic inhibition of particulate-induced bone resorption. J. Biomed. Mater. Res. 1996; 31: 91-96.

Horowitz SM, Rapuano BP, Lane JM and Burstein AH. The interaction of the macrophage and the osteoblast in the pathophysiology of asceptic loosening of joint replacements. Calcif Tissue Int 1994;54:320-324.

Huk OL, Zukor DJ, Ralston W and Lisbona A. Apoptosis in interface membranes of aseptically loose total hip arthroplasty. J Mater Sci: Mater in Med 2001;12:653-658.

Ichinose S, Muneta T, Aoki H and Tagami M. TEM observations of seven retrieved total knee joints made of Co-Cr-Mo and Ti-Al-V alloys. Bio-Medical Materials and Engineering 2003;13:125-134.

Im GL and Han JD. Suppressive effects of interleukin-4 and interleukin-10 on the production of proinflammatory cytokines induced by titanium alloy particles. J Biomed Mater Res(Appl Biomater) 2001;58:531-536.

Ingham E and Fisher J. The role of macrophages in the osteolysis of total joint replacement. Biomaterials 2005; 26:1271-1286

Ishiguro N, Kojima T, Ito T, Saga S, Anma H, Kurokouchi K, Iwahori Y, Iwase T and Iwata H. Macrophage activation and migration in interface tissue around loosening total hip arthroplasty. J Biomed Mater Res 1997;35:399-406.

Jiranek W, Jasty M, Wang JT, Bragdon C, Wolfe H, Goldberg M and Harris W. Tissue response to particulate polymethylmethacrylate in mice with various immune deficiencies. J Bone Joint Surg. 1995;77-A:1650-166.

Kadoya Y, Revell PA, Al-Saffar N, Kobayashi A, Scott G and Freeman MAR. Bone formation and bone resorption in failed total joint arthroplasties: Histomorphometric analysis with histochemical and immunohistochemical technique. J Orthop Res 1996;14:473-482.

Kinov P, Leithner A, Radl R, Bodo K, Khoschsorur GA, Schauenstein K and Windhager R. Role of free radicals in aseptic loosening of hip arthroplasty. J Orthop Res 2006;24:55-62.

Knoch FV, Heckelei A, Wedemeyer C, Saxler G, Hilken G, Henschke F, Loer F and Knoch MV. The effect of simvastatin on polyethylene particle-induced osteolysis. Biomaterials 2005;26:3549-3555.

Knoch MV, Wedemeyer C, Pingsmann A, Knoch FV, Hilken G, Sprecher C, Henschke F, Barden B and Loer F. The decrease of particle-induced osteolysis after a single dose of bisphosphonates. Biomaterials 2005;26:1803-1808.

Kuhn C and McDonald JA. The roles of the myofibroblast in idiopathic pulmonary fibrosis. Ultrastructure and immunohistochemical features of sites of active extracellular matrix synthesis. Am J of Pathol 1991;138:1257-1265.

Lalor PA and Revell PA. The Presence of a Synovial Layer at the Bone-Implant Interface: An Immunohistological Study Demonstrating the Close Similarity to True Synovium. Clinical Materials 1993;14:91-100.

Langkamer VG, Case CP, Heap P, Taylor A, Collins C, Pearse M and Solomon L. Systemic distribution of wear debris after hip replacement. A cause for concern? J Bone Joint Surg (Br) 1992;74-B:831-839.

Laquerriere P, Laquerriere AG, Jallot E, Balossier G, Frayssinet P and Guenounou M. Importance of hydroxyapaptite particles characterictics on cytokines production by human monocytes *in vitro*. Biomaterials 2003;24:2739-2747.

Lewis JB, Randol TM, Lockwood PE and Wataha JC. Effect of subtoxic concentrations of metal ions on NF-κB activation in THP-1 human monocytes. J Biomed Mater Res 2003;64A:217-224.

Li F, Chung H, Reddy SV, lu G, Kurihara A, Zhao AZ and Roodman GD. Annexin II stimulates RANKL expression through MAPK. Bone Miner Res 2005;20:1161-7.

Li J, Davidson G, Huang Y, Jiang BH, Shi x, Costa M and Huang C. Nickel compounds act through phosphatidylinositol-3- kinase/Akt-Dependent, P70 S6k- independent pathway to induce hypoxia inducible factor transactivation and Cap 43 expression in mouse epidermal C141 cells. Cancer Res 2004;64:94-101.

Li TF, Santavirta S, Waris V, Lassus J, Lindroos L, Xu JW, Virtanen I and Konttinen Y. No lymphokines in T cells around loosened hip prostheses. Acta Orthop Scand 2001;72(3):241-247.

Lind M, Trindade MCD, Yasay B, Goodman SB and Smith RL. Effect of particulate debri on macrophage dependent fibroblast stimulation in coculture. J Bone Joint Surg [Br] 1998;80-B: 924-30.

Liu HC, Chang WH, Lin FH, Lu KH, Tsuang YH and Sun JS. Cytokine and Prostaglandin E2 release from leukocytes in response to metal ion derived from different prosthetic materials: An *in vitro* study. Artif Org 1999;23(12):1099-1106.

Lynne CJ, Frondoza C and Hungerford DS. Immunohistochemical evaluation of interface membranes from failed cemented and uncemented acetabular components. J Biomed Mater Res (Appl Biomater) 1999;48:889-898.

Majno and Joris. Cells, Tissues and Diseases: Principles of General Pathology. Blackwell Sciences, 1996.

Maloney WJ, Smith RL, Castro Frank and Schurman DJ. Fibroblast response to Metallic Debris *in vitro*. J Bone and Joint Surg 1993; 75-A (6): 835-844.

Manlapaz M, Maloney WJ and Smith RL. *In vitro* activation of human fibroblasts by retrieved titanium alloy wear debris. J Orthop Res 1996;14:465-472.

Masse A, Bosetti M, Buratti C, Visentin O, Bergadano D and Cannas M. Ion release and chromosomal damage from total hip prostheses with metal on metal articulation. J Biomed Mater Res Part B: Appl Biomater 2003;67B:750-757.

Masui T, Sakano S, Hasegawa Y, Warashina H and Ishiguro N. Expression of inflammatory cytokines, RANKL and OPG induced by titanium, cobalt-chromium and polyethylene particles. Biomaterials 2005;26:1695-1702.

May RC and Machesky LM. Phagocytosis and the actin cytoskeleton. J Cell Science 2001;114:1061-1077.

Menna C, Devlin RD, Reddu SV, Gazitt Y, Choi SJ and Roodman GD. Annexin II increases osteoclast formation by stimulating the proliferation of osteoclast precursors in human marrow cultures. J Clin Invest 1999;103:1605-1613.

Mishima H, Yasumata K, Nishida T and Otori T. Fibronectin enhances the phagocytic activity of cultured rabbit keratocytes. Invest Ophthalmol Vis Sci 1987;28:1521-1526.

Mitchell W, Mathew JB, Stone MH, Fisher J and Ingham E. Comparison of the response of human peripheral blood mononuclear cells to challenge with particles of three bone cements *in vitro*. Biomaterials 2003;24:737-748.

Miyaguchi M, Kobayashi A, Iwaki H, Ohashi H, Kadoya Y and Yamano Y. Human monocyte response to retrieved polymethylmethacrylate particles. J Biomed Mater Res 2002;62:331-337.

Nakashima Y, Sun DH, Trindade MCD, Maloney WJ, Goodman SB, Schurman DJ and Smith RL. Signaling pathways for tumor necrosis factor-α and interleukin-6 expression in human macrophages exposed to titanium alloy particulate debris *in vitro*. J Bone Jt Surg 1999;81:603-15.

Ninomiya JT, Struve JA, Stelloh CT, Toth JA, Crosby KE. Effect of hydroxyapatite particulate debris on the production of cytokines and proteases in human fibroblast. Journal of Orthop Res 2001; 19: 621-628.

Oliver V, Dual JL, Hindie M, Pouletaut P and Nagel MD. Comparative particle induced cytotoxicity towards macrophages and fibroblast. Cell Biology and Toxicology 2003; 19: 145-159.

Olmedo D, Guglielmotti MB, Cabrini RL. An experimental study of the dissemination of titanium and zirconium in the body. J Mater Sci: Mater in Med 2002;13:793-796

Olmedo DG, Tasat D, Guglielmotti MB, Cabrinin RL. Titanium transport through the blood stream. An experimental study on rats. J Mater Sci: Mater in Med 2003;14;1099-1103.

Pandey R, Quinn J, Joyner C, Triffitt JT, Athanasou NA. Arthroplasty implant biomaterial particle associated macrophages differentiate into osteoclastic bone resorbing cells. Ann Rheum Dis 1996;55:388-395.

Papageorgiou I, Brown C, Schins R, Singh S, Newson R, Davis S, Fisher J, Ingham E and Case CP. The effect of nano and micron sized particles of cobalt chromium alloy on human fibroblasts *in vitro*. Biomaterials 2007;28:2946-2958.

Pap T, Claus A, Ohtsu S, Hummel KM, Schwartz P, Drynda S, Pap G, Machner A, Stein B, George M, Gay RE, Neumann W, Gay S and Aicher WK. Osteoclast independent bone resorption by fibroblast like cells. Arthritis Res Ther 2003; 5: R163-R173.

Park YS, Moon YW, Lim SJ, Yang JM, Ahn G, Choi YL. Early osteolysis following second generation metal on metal hip prosthesis. J Bone Joint Surg Am 2005; 87: 1515-1521.

Peters K, Schmidt Harald, Unger ER, Kamp G, Prols F, Berger BJ and Kirkpatrick CJ. Paradoxical effects of hypoxia mimicking divalent cobalt ions in human endothelial cells *in vitro*. Mol Cell Biochem 2005;270:157-166.

Petit A, Mwale F, Tkaczyk C, Antoniou J, Zukor DJ and Huk OL. Induction of protein oxidation by cobalt and chromium ions in human U937 macrophages. Biomaterials 2005;26:4416-4422.

Petit A, Mwale F, Zukor DJ, Catelas I, Antoniou J and Hulk OL. Effect of cobalt chromium ions on bcl-2, bax, caspase-3 and caspase-8 expression in human U937 macrophages. Biomaterials 2004;25:2013-2018.

Pioletti DP, Leoni L, Genini D, Takei H, Du P and Corbeil J. Gene expression analysis of osteoblastic cells contacted by orthopedic implant particles. J Biomed Mater Res 2002;61:408-420.

Prabhu A, Shelburne CE, Gibbons DF. Cellular proliferation and cytokine responses of murine macrophage cell line J774A.1 to polymethylmethacrylate and cobalt-chrome alloy particles. J Biomed Mater Res 1998;15(42);665-673.

Rae T. The biological response to titanium and titanium-aluminium-vanadium alloy particles. II Long term animal studies. Biomaterials 1986;7:37-40.

Rae T. The biological response to titanium and titanium-alumminium-vanadium alloy particles. I Tissue culture studies. Biomaterials 1986;7:30-36.

Ratner BD, Hoffman AS, Schoen FJ and Lemmons JE. Editors. Application of materials in Medicine, Biology and Artificial Organs.In: Biomaterials science: An introduction to materials in medicine. 2nd Edition, Elsvier Academic Press, 2004.

Ren W, Li XH, Chen BD and Wooley PH. Erythromycin inhibits wear debris induced osteoclastogenesis by modulation of murine macrophage NF-κB activity. J Orthop Res. 2004;22(1):21-9.

Reno F and Cannas M. UHMWPE oxidation increases matrix metalloproteinase-2 (MMP-2) release in human fibroblasts. J Mater Sci: Mater in Med 2002;13:403-406.

Reno F, Sabbatini M, Masse A, Bosetti M and Cannas M. Fibroblast apoptosis and caspase-8 activation in asceptic loosening. Biomaterials 2003;24:3941-3946.

Rosengren A, Bjursten LM and Danielsen N. Analysis of the inflammatory response to titanium and PTFE implants in soft tissue by macrophage phenotype quantification. J Mater Sci: Mater in Med 1998;9:415-420.

Sakai H, S Jingushi, T Shuto, K Urabe, T Ikenoue, K Okazaki, T Kukita, A Kukita and Y Iwamoto. Fibroblasts from the inner granulation tissue of the pseudocapsule in hips at revision arthroplasty induce osteoclast differentiation, as do stromal cells. Ann. Rheum. Dis, 2002;61;103-109.

Savio JA, Overcamp LM and Black J. Size and shape of biomaterial wear debris. Clin Mater 1994; 15:101-14.

Savrino L, Granchi D, Ciapeti G, Cenni E, Pantoli AN, Rotini R, Veribesu CA, Baldini N and Giunti A. Ion release in patients with metal-on-metal hip bearings in total joint replacements: A comparison with metal-on polyethylene bearings. J Biomed Mater Res (Appl Biomater) 2002;63:467-474.

Schelde A, Samorapoompichit P, ausch-Fan XH, Franz A, Fureder W, Sperr WR. Response of L929 fibroblasts, human gingival fibroblast and human mast cells to various metal cations. J Dent Res 1995;74:1513-1520.

Schmalzried TP and Callaghan JJ. Current Concepts Review - Wear in Total Hip and Knee Replacements. J Bone Joint Surg Am. 1999; 81: 115-136.

Schmidt C, Steinbach G, Deckling R,Claes LE, Ignatius AA. IL-6 and PGE2 release by human osteoblasts on implant materials. Biomaterials 2003;24:4191-4196.

Schwarz EM, Looney RJ, O'Keefe RJ. Anti-TNFalpha therapy as a clinical intervention for periprosthetic osteolysis. Arthritis Res 2000;2:165.

Schwarz EM, Lu AP, Goater JJ, Benz EB, Kollias G, Rosier RN, Puzas JE and O'Keefe RJ. Tumor necrosis factor alpha/ nuclear transcription factor-kappaB signaling in periprosthetic osteolysis. J Orthop Res 2000; 18:472-80.

Semenza LG, Roth PH, Fang HM and WangGL. Transcriptional regulation of genes encoding glycolytic enzymes by hypoxia inducible factor-1. J Biol Chem 1994;269:23757-23763.

Shanbhag A, Jacobs JJ, Black J, Galante JO and Glant TT. Macrophage/particle interactions: Effect of size, composition and surface area. J Biomed Mater Res 1994;28:81-90.

Shanbhag AS, Hasselman CT, Rubash HE. Inhibition of wear debris mediated osteolysis in a canine total hip arthroplasty model. Clin Orthop 1997; 344:33.

Slanikow K, Blagosklonny MV, Ryan H, Johnson R and Costa M. Carcinogenic nickel induces genes involved with hypoxic stress. Cancer Res 2000 60;38-41.

Slanikow K, Davidson T and Costa M. The role of hypoxia inducible signaling pathway in nickel carcinogenesis. Enviornmental Health Perscpectives 2002;110;831-834.

Slanikow K, Su W, Bolgosklonny MV and Costa M. Carcinogenic metals induce hypoxia inducible factor stimulated transcription by reactive oxygen species-independent mechanism. Cancer Res 2000;60:3375-3378.

Soloviev A, Schwarz EM, Kuprash DV, Nedospasov SA, Puzas EJ, Rosier RN and Keefe RJO. The role of p105 protein in NF κB activation in ANA-1 murine macrophages following stimulation with titanium particles. J Orthop Res 2002;20(4):714-22.

Solovieva SA, Ceponis A, Konttinen YT, Takagi M, Suda A, Eklund KK, Sorsa T and Santavirta S. Mast cells in loosening of totally replaced hips. Clin Orthop Rel Res. 1996;225:171-191.

Stea S, Visentin M, Granchi D, Cenni E, Ciapetti G, Sudanese A and Toni A. Apoptosis in peri-implant tissue. Biomaterials 2000;21:1393-1398.

Sujata VB. Biomaterials. Narosa Publishing House, 2002.

Sun DJ, Trindade MCD, Nakashima Y, Maloney WJ, Goodman SB, Schurman DJ, Smith RL. Human serum opsonization of orthopedic biomaterial particles: Protein-binding and monocyte/macrophage activation *in vitro*. J Biomed Mater Res 2003; 65A: 290–298.

Suska F, Esposito M, Gretzer C, Kalltrop M, Tengvall P and Thomsen P. IL-1α, IL-1β and TNF-α secretion during *in vivo*/ex vivo cellular interactions with titanium and copper. Biomaterials 2003;24:461-468.

Suska F, Gretzer C, Esposito M, Emanuelsson L, Wennerberg A, Tengvall P and Thomsen P. *In vivo* cytokine secretion and NF- κB activation around titanium and copper implants. Biomaterials 2005;26:519-527.

Tanaka T, Akatsuka S, Ozeki M, Shirase T, Hiai H and Toyakuni S. Redox regulation of annexin 2 and its implication for oxidative stress-induced renal carcinogenesis and metastasis. Oncogene 2004;23:3980-3989.

Tanaka T, Kondo S, Iwasa Y, Hiai H and Toyokuni S. Expression of stress response and cell proliferation genes in renal cell carcinoma induced by oxidative stress. Am J Pathol 2000;156:2149-2157.

Tang L, Jennings TA and Eaton JW. Mast cells mediate acute inflammatory responses to implanted biomaterials. Proc. Natl. Acad. Sci, USA. 1998;95:8841-8846.

Thomas IT and Evans EJ. The effect of cobalt chromium-molybdenum powder on collagen formation by fibroblasts *in vitro*. Biomaterials 1986; 7:301-304.

Tripathi P and Aggarwal A. NF-κB transcription factor: a key player in the generation of immune response. Current Science 2006;90(4):519-531.

Udagawa N, Takahashi N, Akatsu T, Tanaka H, Sasaki T, Nishihara T, Koga T, Martin TJ, Suda T. Origin of osteoclasts: mature monocytes and macrophages are capable of differentiating into osteoclasts under a suitable microenvironment prepared by bone marrow-derived stromal cells. Proc Natl Acad Sci USA 1990;87:7260–4.

Urban RM, Jacobs JJ, Tomlinson MJ, Garvrilovic J, Black J and Peoc'h M. Dissemination of wear particles to the liver, spleen and abdominal lymph nodes of patients with hip or knee replacements. J Bone Joint Surg 2000;82-A:457-477

Wang JY, Wicklund BH, Gustilo RB and Tsukayama DT. Titanium, chromium and cobalt ions modulate the release of bone-associated cytokines by human monocytes/macrophages *in vitro*. Biomaterials 1996;17(23):2233-2240.

Wang ML, Hauschka PV, Tuan RS and Steinbeck MJ. Exposure to particles stimulates superoxide production by human THP-1 macrophages and avian HD-11EM osteoclasts activated by tumor necrosis factor alpha and PMA. Arthroplasty 2002;17(3):335-346.

Wang ML, Sharkey PF, Tuan RS. Particle bioreactivity and wear mediated osteolysis. J Arthroplasty 2004;19(8):1028-1038.

Warme BA, Epstein NJ, Trindade MCD, Miyanishi K, Ma T, Saket RR, Regula D, Goodman SB and Smith RL. Proinflammatory mediator expression in a novel murine model of titanium-particle-induced intramedullary inflammation. J Biomed Mater Res Part B:Appl Biomater 2004;71B:360-366.

Williams PL, Warwick R, Dyson M, Bunnister LH. Editors. Grays Anatomy. 37th Edition. Churchill Livingston, Longman group UK limited, 1989.

Wilson CJ, Clegg RE, Leavesley DI and Pearcy MJ. Mediation of biomaterial-cell interactions by adsorbed proteins: a review. Tissue Engineering 2005; 11: 1-18.

Woodward SC. Evaluation by light microscopy. In: Handbook of Biomaterials Evaluation. Scientific, Technical and Clinical testing of Implant materials. Macmillan Publishing Company, 1986.

Wooley P, Morren R, Andary J, Sud S, Yang SY, Mayton L, Markel D, Sieving A and Nasser S. Inflammatory response to orthopedic biomaterials in the murine air pouch. Biomaterials 2002;22:517-526.

Yajima T. Collagen remodeling in wound healing by gingival fibroblasts *in vitro*. Adv Dent Res 1988;2:228-233.

APPENDIX

Sorenson's Phosphate Buffer
0.1 M of Sorenson's Phosphate Buffer pH 7.4 was prepared by mixing 40.5ml of 0.2M disodium hydrogen phosphate with 0.2M of sodium dihydrogen phosphate.

Phosphate Buffered Saline
Dissolved 8g of Sodium Chloride, 1.15g of Disodium hydrogen phosphate, 0.2 g of Potassium Chloride, 0.2g of Potassium dihydrogen phosphate in 700ml of distilled water. the pH was adjusted to 7.4±0.2. The solution was made up to 1Litre with distilled water.

Meyers Egg Albumin
50ml of egg white was made up to 100ml with glycerine. Mixed well using magnetic stirrer. Added 100mg Thymol and stored at 4°C.

Harris Haematoxylin
Dissolved 5g of Haematoxylin powder in 25ml of absolute alcohol. Dissolved 50g of ammonia or potassium alum in water by gently heating. Mixed the two solutions by pouring the haematoxylin solution into the alum solution while hot. Brought to boil rapidly while continuously stirring the solution. Added 1.25g of mercuric oxide or 0.5 g of sodium iodate slowly. Plunged the vessel into a basin of cold water. Added 20ml of glacial acetic acid. The solution was filtered and stored.

0.1% Water Soluble Eosin
Dissolved 10g of eosin in 700ml of distilled water. The solution was made up to 1Litre with distilled water. Added 0.5ml of acetic acid and a pinch of thymol. Filtered and stored.

Acid Alcohol
700 ml of isopropyl alcohol is made up to 1Litre with distilled water. 10mL of this solution is pipetted out and discarded. 10ml of Con.HCl is slowly added to the remaining alcohol solution.

Scotts Tap Water
Dissolved 2g of potassium bicarbonate in a beaker with a little water. Dissolved 20g of magnesium sulphate with distilled water is a separate beaker. Poured the dissolved bicarbonate into the magnesium sulphate solution and missed well. The solution was made up to 1Litre with distilled water.

10% Neutral Buffered formalin
Dissolved 6.5g of Disodium hydrogen phosphate (anhydrous), 4g of Sodium dihydrogen phosphate monohydrate, 100ml of Formalin in 900ml of distilled water. Adjusted the pH of the solution to 7. The solution was made up to 1Litre with distilled water.

Toludine blue-O
Dissolved 0.25g of toludine blue-o in 1% solution of sodium borate.
4% Paraformaldehyde
Dissolved 4g of paraformaldehyde in 100ml of PBS. Solution was heated to 56°C to dissolve the paraformaldehyde crystals. Aliquoted and stored at -80°C. Thawed to RT before use.

Rehydration Base Buffer
(This protocol is for 400mL)

7M Urea---------- 42.02g
2M Thiourea---------- 15.244g
4% CHAPS---------- 3.9g
NOTE: Add thiourea and urea first and a half amount of water. On dissolving add CHAPS. On dissolution make up to 100mL with MQ water.

Equilibration Base Buffer
(This protocol is for 400mL)

6M Urea----------144.4g
1.5M Tris pH 8.8 (50mM) ----------13.13mL
2% (W/V) SDS----------8g
30% Glycerol----------120ml
MQ water ----------155mL
NOTE: Add less amount of water first and then finally after complete dissolution add remaining.

DTT Equilibration buffer 1 (reduction)

200mg of DTT per 10ml of equilibration buffer

Iodoacetamide Equilibration buffer 2 (Alkylation)

250mg of IAA per 10ml of equilibration buffer

10x Running Buffer
(This protocol is for 2Litre)

Glycine----------288g
Tris----------60g
SDS----------20g
On dissolving make up to 21Litre with MQ water
NOTE: for running buffer prepare 1X by taking 200mL of 10X running buffer and making up to 2Litre with MQ water.